FIRE RESISTANCE TESTS ON CROSS-LAMINATED TIMBER FLOOR PANELS:

AN EXPERIMENTAL AND NUMERICAL ANALYSIS

A thesis submitted to
the Faculty of Graduate and Postdoctoral Affairs
in Partial Fulfillment of the requirements for the degree

Master of Applied Science

by

Marc Aguanno

BEng

Department of Civil and Environmental Engineering
Carleton University

Ottawa-Carleton Institute of Civil and Environmental Engineering

January 2013

Your file Votre référence
ISBN: 978-0-494-94254-3

Our file Notre référence
ISBN: 978-0-494-94254-3

Abstract

Cross-laminated timber (CLT) is an innovative wood technology currently gaining popularity in Canada. However, there is little published information available regarding its performance in fire. The focus of this research is on a series of eight medium-scale, fire-resistance CLT floor tests. Parameters such as charring rate, temperature profile, deflection, gypsum protection and adhesive performance, as well as the overall fire resistance of the floors when subjected to both standard and non-standard fire exposures were evaluated. The results, which compare favourably to past standard full-scale CLT floor tests, were used to develop a numerical model capable of predicting the performance of various CLT floor configurations exposed to any possible fire or load. The experiments demonstrate that CLT panel constructions can be designed to possess a fire-resistance that complies with building code requirements. The additional fire performance data provided from the results of these tests will help facilitate the incorporation of CLT into design standards and building codes.

Acknowledgements

First and foremost, I would like to thank both my supervisors, Professor George Hadjisophocleous and Dr. Steven Craft for their encouragement, direction, and teachings throughout my research and period in the Fire Safety Engineering program at Carleton University. I would also like to thank Ba Lamthien and Arthur Turcot for the months of work they put into helping me prepare and conduct the experiments involved in this thesis at the Carleton University fire research facility in Carleton Place. In addition, I would like to express my gratitude to the entire staff at the Canadian National Fire Laboratory in Carleton Place for their friendly advice and assistance throughout the construction of our testing equipment.

I would like to thank Lindsay Osborne at FPInnovations for inviting me to witness a full-scale CLT testing series and providing me with the information from those tests necessary to complete this research. I would also like to thank Julie Frappier at Nordic Engineered Wood for supplying all of the test floors and material data used in the experiments.

Finally I would like to thank Ying Hei Chui, Kenneth Koo and the entire NEWBuildS Research Network, as well as Carleton University for providing the necessary funding, without which, none of this research would have been possible.

Table of Contents

List of Tables

List of Figures and Illustrations

List of Appendices

Nomenclature

A	Surface area, m^2
A_n	Net area of cross-section, mm^2
c	Specific heat capacity, J kg^{-1} K^{-1}
F_b	Factored bending strength, MPa
F_v	Factored shear strength, MPa
f_b	Specified strength in bending, MPa
Fo	Fourier number
h_f	Convective heat transfer coefficient in fire, W m^{-2} K^{-1}
h_∞	Convective heat transfer coefficient in ambient air, W m^{-2} K^{-1}
k	Thermal conductivity, W m^{-1} K^{-1}
K_D	Load duration factor
K_H	System factor
K_L	Lateral stability factor
K_{Sb}	Service condition factor
K_T	Treatment factor
K_{zb}	Size factor in bending
K_{zv}	Size factor in shear
m	Mass, kg
M_f	Bending moment resistance, N m
M_r	Factored bending moment resistance, N m

q''_{fire} Heat flux from fire, W m^{-2}

$\dot{q}_G$ Internal heat generation, W m^{-3}

S Section modulus, m^3

t Time, s

Δt Time step duration, s

T Temperature, °C

T_f Temperature of the fire, °C

T_∞ Temperature of ambient air, °C

Δx Control volume size, m

Greek Letters

α Specified load factor

β_0 Charring rate for one-dimensional charring under standard fire exposure, mm/min

β_n Design notional charring rate under standard fire exposure, mm/min

ϵ Emissivity

ϕ Resistance factor

ρ Density, kg m^{-3}

σ Stefan-Boltzmann constant, 5.67×10^{-8} W m^{-2} K^{-4}

1 Introduction

In the last few years there has been considerable interest in the use of innovative wood technologies from designers, wood and construction industries, and various levels of government to increase the amount of wood used in the construction of residential, office, school and commercial buildings. One such technology is the cross laminated timber (CLT) panel.

CLT is a solid timber panel constructed by gluing or fastening together decks typically made from nominal 2" x 4"s. However, unlike traditional glulam panels, each deck layer is oriented 90° to the previous. The process is repeated in this fashion and panels are constructed with anywhere from 3 to 9, or more layers (see Figure 1-1). Timber used in each layer is composed of softwood, normally spruce, pine, or fir (SPF) and finished panels can provide load distribution and dimensional stability in all directions due to the oppositely oriented ply layers. This allows CLT panels to cover long spans and function as floors, walls, or roof systems. The panels can be used to replace steel and concrete and even act as the entire structure of multi-storey buildings, such as the nine-storey residential building, Stadthaus, in Hackney, London [1].

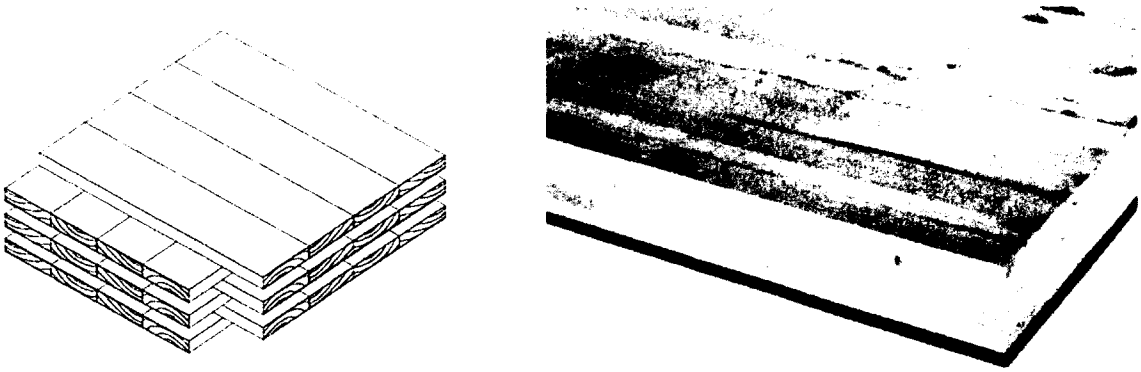

Figure 1-1: Examples of Cross-Laminated Timber Panels

This type of construction was originally invented in the 1970s in Europe and industrial-scale manufacture began in the late 1980s. It has since gained popularity across the UK, and with the introduction of the "Wood First Act" in British Columbia in 2009 [2], stipulating the use of wood as the primary building material in all new provincially funded buildings. CLT has garnered significant attention elsewhere in Canada as well. However, despite its growing popularity, there is currently little information published on the fire performance of CLT panels.

In order to modify Canadian building codes to allow taller mid-rise wood constructions, further research is necessary to demonstrate the safety of such buildings. To facilitate this, a multi-disciplinary NSERC strategic research Network for Engineered Wood-based Building Systems (NEWBuildS) [3] has been established in collaboration with FPInnovations, the Institute for Research in Construction of the National Research Council, the Canadian Wood Council, and 11 universities across Canada. The objective of this network is to advance scientific knowledge and construction technologies that will enable wood-based products to be used in mid-rise and non-residential construction, or integrated into hybridized construction. The research conducted in this thesis is a part of that network and focuses specifically on investigating the fire performance of CLT floors. Using Carleton University's newly constructed furnace, a series of eight medium-scale, fire-resistance tests were conducted on various CLT floor panel configurations. The tests were conducted to evaluate a number of parameters such as the charring rate, temperature profile, deflection, gypsum protection and adhesive performance, as well as the overall fire resistance of the floors when subjected to both standard and non-

standard fire exposures. Four of these experiments were arranged to mirror four full-scale CLT floor tests conducted by FPInnovations and the National Research Council of Canada. The aim of this was to assess whether the results of medium-scale test data was justified for use in gauging full-scale CLT performance.

As Canada, and many other countries around the world, move from prescriptive- to performance-based building codes [4], the use of modelling tools and calculation methods for measuring the performance of various design alternatives against the established safety levels has become increasingly necessary. To contribute to this progress, a numerical model was developed based on information in the literature and the tests conducted in this thesis. The aim of the model was to predict the time that a desired CLT floor assembly can endure when subjected to a defined fire and load. The model was calibrated to match experimental data as close as possible and output was compared with traditional simple calculation methods to evaluate which would be most applicable for design analysis.

It is believed that the results of these tests will demonstrate that CLT panels are a building technology that possesses fire-resistances capable of complying with building code requirements. In addition, this work is hoped to help in the development of new Building Codes that will incorporate CLT in future revisions of the National Building Code of Canada (NBCC).

1.1 Main Objectives

The main objectives of this research are to:

1. Provide a better understanding of the fire performance and characteristics of CLT floors when exposed to both standard and non-standard fires.
2. Compare the performance of CLT panels when tested in medium-scale and full-scale fire resistance tests using standard fire exposures.
3. Develop a numerical model to predict the fire resistance of CLT floors.

2 Literature Review

This chapter provides a summary of the literature referenced in this thesis. Standard fire resistance testing, previous related research on CLT, as well as information regarding the material properties of wood and gypsum at elevated temperatures are covered.

2.1 Standard Fire-Resistance Test for Floors

A standard fire-resistance test for a floor assembly is a test method used as a means of determining whether a particular construction will meet the minimum performance criteria required in a building code or other regulation, usually quantified by a fire resistance rating. The standard fire-resistance test used in Canada is CAN/ULC-S101 [5], the United States uses ASTM E119 [6], and internationally many countries have adopted the standard ISO 834 [7] directly or with some modification. For tests of floors and roofs, an assembly is structurally loaded and a standard fire exposure is subjected to the underside of the specimen.

The CAN/ULC-S101 standard fire-resistance test [5] has three failure criteria; structural, insulation and integrity. The structural criterion states that the assembly must support the applied load. Insulation failure occurs when the unexposed side of the panel exceeds an average temperature increase greater than either 140°C from its original temperature, or 180°C at any one location on the assembly. The integrity of the panel is considered failed if flames or gases hot enough to ignite a cotton pad pass through to the unexposed side. The assembly is given a fire-resistance in the form of a time measured in minutes from the start of the test until one of these failure criteria has occurred. The fire-resistance *rating* is given by this time rounded down to the highest of the following ratings; 30 minutes, 45 minutes, one hour, an hour and a half, two hours, and one hour increments after that.

2.1.1 Fire-Resistance Furnace and Test Assembly

A typical fire-testing furnace consists of a large steel box lined with fire bricks and/or a ceramic fibre blanket. The furnace has a number of burners, most often fuelled by gas or premixed air and gas. There is an exhaust chimney and several thermocouples for measuring furnace temperatures as shown in Figure 2-1. Test specimens are built into a restraining frame, which is lowered onto the top of the furnace to close it off. The desired load is then applied to the top surface of the specimen.

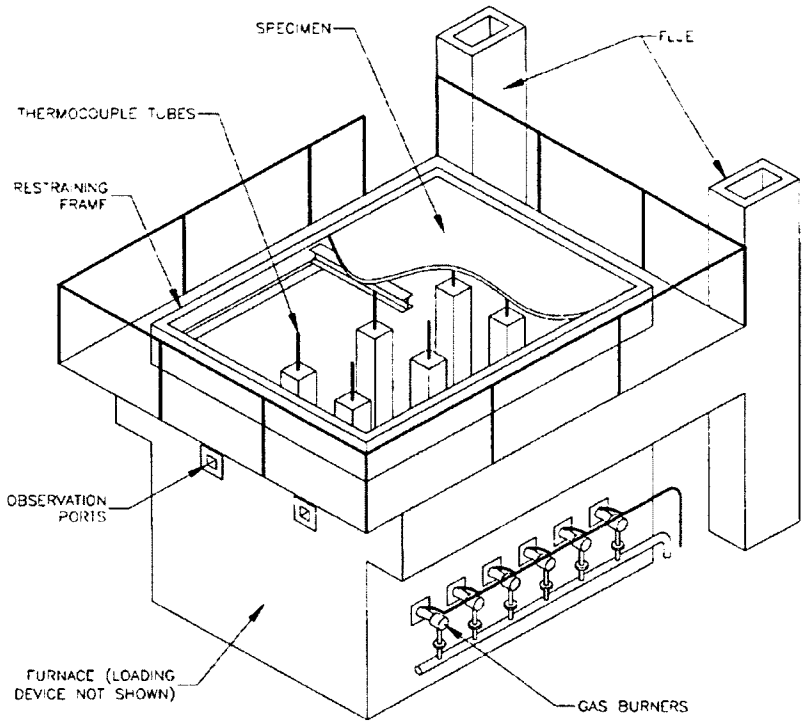

Figure 2-1: Typical floor furnace (reproduced from [5])

There are no international or national standards for the specific dimensions of the furnace; however ASTM E119 [6] specifies a minimum specimen size of 16 m^2 with a span of at least 3.7 m, while ISO 834 recommends measurements of 3 x 4 m [8]. The National Research Council of Canada (NRCC) has a full-scale floor testing furnace that measures 3.96 m x 4.87 m [9]. The loading system at the NRCC consists of a steel frame carrying 30 hydraulic jacks able to apply a uniformly distributed load across the entire surface of the floor specimen. In order to monitor the temperature in the furnace and follow the necessary standard time-temperature curve, burners must be automatically controlled by feedback from nine shielded thermocouples enclosed in sealed porcelain tubes or wrought steel or iron pipe [5].

2.1.2 Standard Fires

The time-temperature curves used in the various standard fire resistance tests are referred to as standard fires and are typically defined by an equation. ASTM E119 [8] and ISO 834 [8] specify the most widely used standard fire curves, and as shown in Figure 2-2, are very similar to each other.

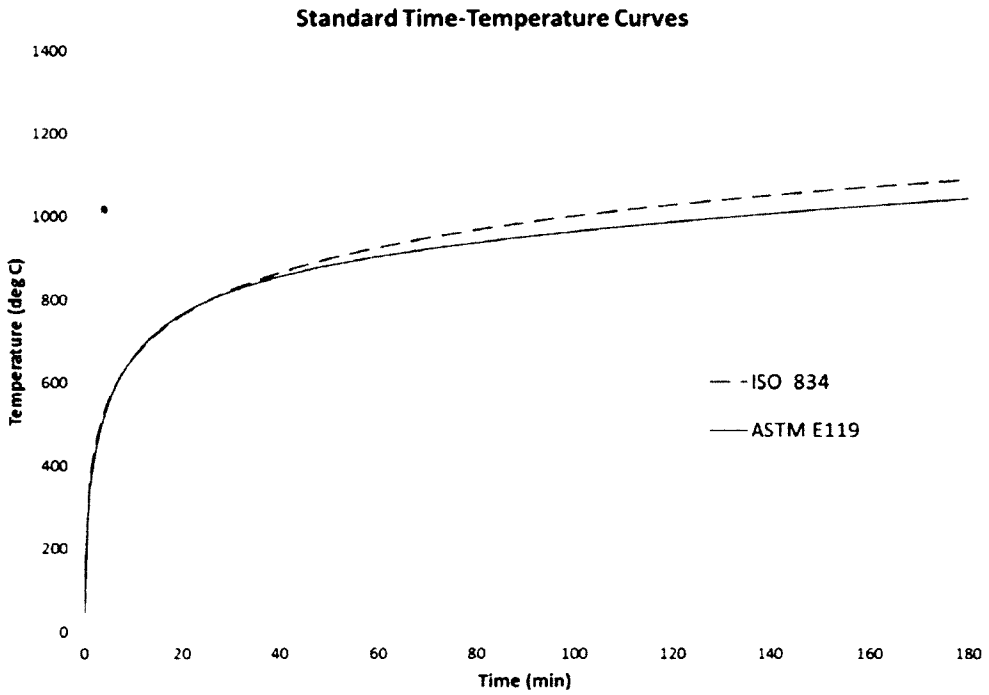

Figure 2-2: Standard time-temperature curves

The standard fire curve in Canada, set out in CAN/ULC-S101 [5], is identical to the ASTM E119 curve. Temperatures in this curve initially increase rapidly to about 765°C after 20 minutes before beginning to level-off. After about an hour, temperatures are nearly 900°C and around 1000°C after two hours. Unlike a real fire, the temperature in the standard fire continues to increase indefinitely to ensure the specimen fails at some point during the test.

2.2 Non-Standard Fires

Non-standard fires, also referred to as a parametric, real, or design fires, are typically used when assessing an assembly's performance in a specific real-fire scenario. These fires are most often replications of compartment fires and typically only focus on the post-flashover stage when temperatures are very high and can be considered uniform throughout the compartment. A variety of models have been developed for design fires, one of the most widely referenced being the 'Swedish curves' of Magnusson and Thelandersson [10] shown in Figure 2-3. The opening factor is the ratio of the ventilation area available to the fire divided by the total enclosure surface area, multiplied by the square root of the opening height. This factor governs the amount of oxygen a fire will receive in a post-flashover case [11]. The fuel load is the amount of combustible energy in the contents of the compartment divided by the floor area of the compartment.

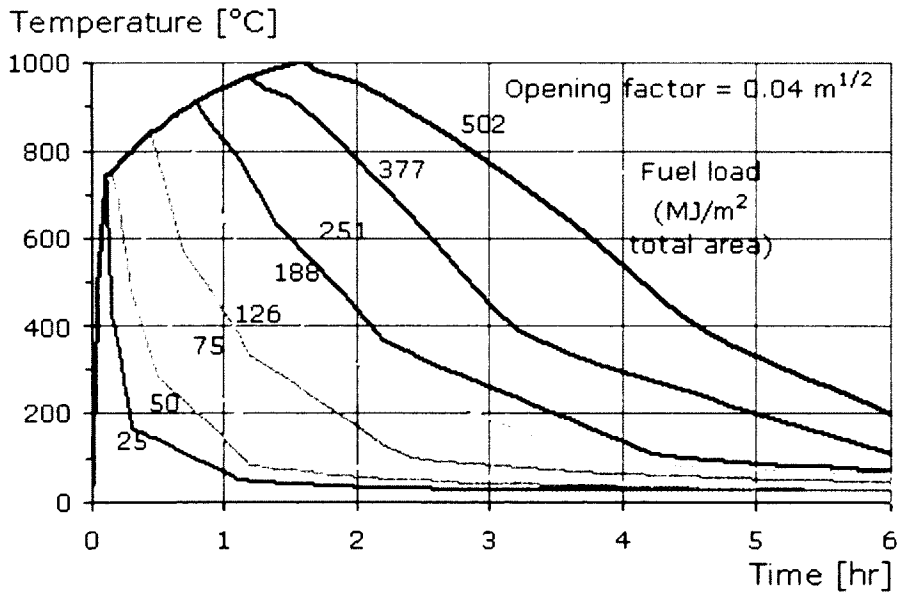

Figure 2-3: Swedish time-temperature curves for different fuel loads (reproduced from [12])

Parametric fire curves take into account compartment size, fuel load, ventilation conditions and thermal properties of the compartment boundaries. They offer a more realistic estimate of the fire severity, which can be significantly worse than equivalent early stages of standard time-temperature relationships. Unlike standard fires, a cooling or 'decay' phase, as shown in Figure 2-4 is often incorporated at the end of the curve.

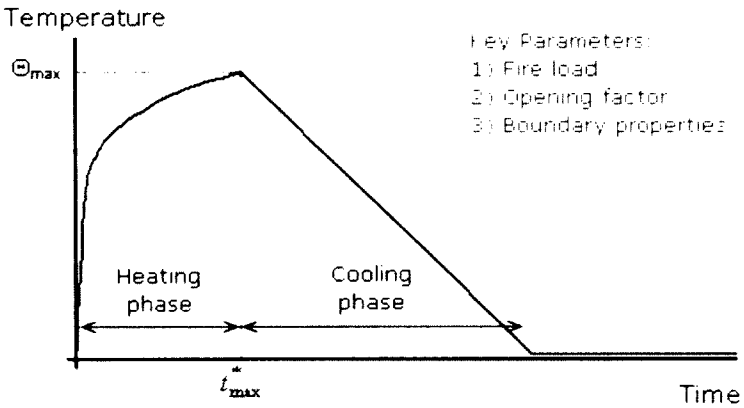

Figure 2-4: A typical parametric fire curve (reproduced from [18])

Tests performed against a non-standard fire are typically uniquely designed for a particular compartment or fire event, and therefore it may sometimes be difficult to find past experiments with a comparable fire. For this reason commercial fire tests more often involve standard fire exposures as their results can be more easily compared to allow different products to be ranked against one another.

2.2.1 Equivalent Fire Severity

The concept of relating the results of a non-standard fire resistance test to a standard fire resistance test is known as equivalent fire severity. It attempts to calculate the time that an assembly subjected to a non-standard fire resistance test would last in a standard fire resistance test. Numerous different methods of evaluating equivalency

have been proposed, one of which of most interest to this study is the 'equal area concept' [8].

2.3 Eurocode – Reduced Cross-Section Method [14]

EN 1995-1-2 (Eurocode 5) [14] outlines a method of calculating the mechanical resistance in timber members exposed to a standard fire. As a member is heated, a heat-affected zone of about 35 to 40 mm [8] develops below to the char layer. Strength properties and the modulus of elasticity in this zone are weakened due to the elevated temperatures. The Eurocode outlines two simplified methods of imitating this behaviour; the reduced properties method and the reduced cross-section method.

The reduced properties method applies to rectangular cross-sections of wood, typically beams, exposed to fire on three or four sides. Since the experiments conducted in this thesis involve a single surface exposed to the fire, this method does not apply and will not be covered.

The reduced cross-section method involves subtracting a specified layer of uncharred wood, which is assumed to possess zero-strength, from the cross-section of the member. Charred sections of the member are also considered to have zero strength. The thickness of the zero-strength layer is defined such that the mechanical strength of the member, based on its total cross-section, minus the zero-strength and char layer, , will theoretically possess an equivalent strength to that of an actual identical member subjected to the standard fire with the same char depth. The zero-strength layer specified in the Eurocode is 7 mm. During the first 20 minutes of heating, this depth is

stipulated to increase linearly from 0 to 7 mm. If gypsum protection is present, the zero-strength layer will increase linearly from 0 to 7 mm from the beginning of the test until the calculated time when charring begins. This calculation is described in the next section.

2.3.1 Eurocode - Charring [14]

In order to determine the reduced cross-section, the char depth must be calculated throughout the fire exposure. This can be taken as the position of the 300°C isotherm in the member. However, barring a method of heat transfer analysis, a more simplified approach is advocated, which is to assume a constant charring rate. Different charring rates are specified in the Eurocode depending on the type of wood (softwood, hardwood, LVL, or paneling). For wood with a density greater than 450 kg/m^3 a reduction factor is applied to the appropriate charring rate normally specified for less dense wood. Additionally, increased charring rates are specified for members that will experience the effect of corner rounding.

For members with fire protective gypsum boards, the start of charring is delayed by a calculated time depending on the thickness of the boards. Unless otherwise specified, the time at which the fire protection fails is assumed as the same time at which charring begins. If charring is assumed to begin before fire protection fails, it is calculated at a lower rate than the chosen charring rate until the calculated failure time of the fire protection. This reduced rate is based on thickness of the protection layers. After the fire protection has failed, the charring rate is doubled from the originally chosen value

until the charring depth is equal to either the charring depth of the same member without fire protection, or 25 mm, whichever is less. At this point the charring rate then reverts back to the originally chosen rate.

2.4 CLT Handbook Fire Resistance Calculation Method [15]

FPInnovations has developed a peer-reviewed Handbook covering technical information related to the manufacturing, design and performance of CLT. A section of this handbook provides a calculation method to predict CLT's fire performance, and more specifically, the structural fire-resistance of an assembly exposed to the standard fire. The method is based on the reduced cross-section method and charring calculations from the Eurocode to calculate the moment resistance for floor and wall panels under load.

The method assumes a zero-strength layer of 10.5 mm for floors and 15.9 mm for walls instead of the Eurocode prescribed 7 mm, based on research conducted by Schmid [16]. The moment resistance of the panel is calculated based on the residual cross-section and the assumption that all strength is provided from spanning plies. All cross plies are assumed to provide no structural contribution.

The factored bending moment resistance for floors, as defined by CSA O86 [15], is calculated at each time step using the equation below:

$$M_r = \phi F_b S_{eff} K_{zb} K_L \qquad \text{Eq. 2.1}$$

Where the resistance factor, $\phi = 0.9$, and F_b equals:

$$F_b = f_b(K_D K_H K_{Sb} K_T) \qquad \text{Eq. 2.2}$$

f_b is the specified bending strength and K_{zb}, K_L, K_D, K_H, K_{Sb} and K_T are the size factor in bending, the lateral stability factor, load duration factor, system factor, service condition factor and treatment factor, respectively. All are set to 1 as per definitions given in CSA O86, except for the load duration factor, K_D, which is set 1.15, as specified in the CLT Handbook [15]. The structural model is based on an ultimate limit state approach. In this scheme, the factored bending moment resistance (M_r) from Eq. 2.1, of the remaining panel must be greater than the actual bending moment (M_f) required to support the load, demonstrated in the following equation:

$$M_r \geq M_f = \frac{wL^2}{8} \qquad \text{Eq. 2.3}$$

The time at which this condition is no longer met is considered the fire-resistance of the assembly.

The effective section modulus (S_{eff}) of the panel is calculated based on a neutral axis ($\bar{y}$) and the effective stiffness (EI_{eff}), listed below:

$$\bar{y} = \frac{\sum_i \tilde{y}_i D_i E_i}{\sum_i D_i E_i} \qquad \text{Eq. 2.4}$$

$$EI_{eff} = \sum_i \frac{BD_i^3}{12} E_i + \sum_i BDd_i^2 E_i \qquad \text{Eq. 2.5}$$

$$S_{eff} = \frac{EI_{eff}}{E\left(D_{fire} - \bar{y}\right)} \qquad \text{Eq. 2.6}$$

Where $\tilde{y}_i$ is the distance from the unexposed surface of the panel to the centroid of ply *i*, D_i is the remaining depth of ply *i*, and E_i is the modulus of elasticity of ply *i*. d_i is the

distance from the neutral axis to the centroid of ply *i*, and D_{fire} is the cross-section depth, excluding the zero strength layer and char.

The Handbook also includes guidance for assemblies with gypsum board protection by the addition of 30 minutes to the fire resistance rating for one layer of 15.9 mm type X gypsum and 60 minutes for two layers.

Adhesive failure and subsequent ply delamination can be included for assemblies constructed with thermoplastic adhesives. In this case, it is assumed that once the char layer is within 12 mm of an adhesive bond line, the ply below should be considered to have fallen off.

2.5 Previous CLT Fire Experiments and Computer Analysis Models

2.5.1 FPInnovations [17]

FPInnovations with the help of the National Research Council of Canada (NRCC) conducted a series of full-scale CLT floor and wall tests. Carleton University, in association with NEWBuildS [3], a strategic research Network for Engineered Wood-based Building Systems, has aligned with these research efforts to work toward a goal of developing a design methodology for calculating the fire-resistance of CLT assemblies. A total of eight standard full-scale tests were conducted at the NRCC fire laboratory. The series consisted of three wall and five floor tests. Test panels were constructed with 3, 5 or 7 plies of varying thicknesses while some assemblies were protected using one or two layers of CGC [18] Sheetrock FireCode Core Type X gypsum board.

Panels were instrumented with thermocouples and deflections gauges. Thermocouples were embedded in-between and at mid-depth of each ply, at five different locations in the floor assemblies. During tests with protection, thermocouples were placed at the back surface of each gypsum board. All panels were loaded during each test with a uniformly distributed load according to typical live loads found in the NBCC or a deflection criterion of L/240 [17]. Data was obtained regarding; gypsum performance, fall-off of ply layers, char depth, deflection, structural performance and the overall fire-resistance, as per the CAN/ULC-S101 [5] standard for tests on wall and floor assemblies.

The results of these tests focused primarily on assessing charring rates in CLT panels and future development of a calculation method for the fire resistance of CLT. All information acquired from these tests has been used in conjunction with the research completed in this thesis to continue to achieve this goal. Results are compared in more detail in Section 4.

2.5.2 Frangi [19]

Experiments at Empa, the Swiss Laboratories for Material Testing and Research in Duebendorf, Switzerland, were conducted to investigate the charring and fire behaviour of cross-laminated timber floor panels. The main focus of the research was to determine whether the fire behaviour of CLT is similar to that of homogeneous timber panels and how it compares to the charring calculation method stipulated in EN 1995-1-2 [14]. This involved looking at whether a charred ply layer would remain in place, similar to solid timber, or fall-off. Tests were conducted in a small-scale furnace (1.0 x 0.8 m) on 11

specimens consisting of 2, 3, and 5 layers. Layers were glued together using six different commonly used adhesives; five of which were one-component polyurethane (PU) and one melamine urea formaldehyde (MUF). Layers thicknesses were kept small (10, 20, and 30 mm) as opposed to traditional layer thickness of around 38 mm, in order to reduce the amount of time that char would take to reach a bond line.

The panels were all exposed to the standard ISO 834 [7] fire and temperatures were measured between each layer at one minute intervals. Test results revealed ply fall-off occurred for all panels constructed with PU adhesives when the temperature between layers reached around 300°C. Panels constructed with MUF adhesives did not fall-off. After a ply fell-off, a spike in the charring rate was observed. These increases in charring rate were not constant; the later the ply fell off during the test, the higher the increase in the charring rate. This was due to the increasing fire temperature.

Overall charring rates calculated throughout each test increased as char progressed through all panels constructed with PU adhesives. The opposite was observed in panels constructed with MUF adhesives and demonstrated the lowest overall charring rates at around 0.60 mm/min at the end of these tests. Panels with PU adhesives had higher overall charring rates, and panels with 10 mm plies had the highest overall charring rates at around 1.0 mm/min at the end of the test. This was reasoned to be due to the more frequent layer fall-off.

The char depth calculation used by EN 1995-1-2 [14] for initially protected surfaces was compared to these results and determined to provide a conservative estimate of

charring in CLT. In the Eurocode, after a ply layer falls off, the standard charring rate is doubled (e.g. from 0.65 mm/min to 1.3 mm/min), up to a char depth of 25 mm before it is brought back to the standard rate. Only one test involved a ply thickness greater than 25 mm and the charring rate did reduce slightly in that test, however this reduction in the charring rate could not be completely verified since charring only continued for 5 mm.

2.3.3 Ivalsa tests [26]

Two fire tests were performed at the Ivalsa Trees and Timber Institute in San Michele all'Adige, Italy, to study CLT floor panels exposed to the standard ISO 834 [7] fire. The results of these tests were primarily used to help validate a 2D finite element model implemented in Abaqus [21]. Both test panels consisted of 5-plies with thicknesses of 42, 19, 28, 19, and 42 mm, a span of 5.6 m and a small width of 0.6 m. One of the floors was protected with one layer of 15 mm, type F gypsum, while the other was left unprotected. The floors were instrumented with thermocouples at various depths throughout the panel and the back of the gypsum board. Floors were simply supported over the furnace and a uniformly distributed load of 10 kN/m^2 was applied until structural failure occurred. The unprotected floor test continued for 99 minutes, while the protected floor failed after 110 minutes. The gypsum board on the protected floor failed after 41 minutes. Ply delamination was not discussed in this paper.

The model was built on temperature-dependent relationships for wood properties attained from the European code for fire design of timber structures. After around 80

minutes into the tests, panels deflected into the furnace so much that heat was able to penetrate the sides of the specimens. The model compensates for this by switching from a 2- to 3-dimensional analysis at 80 minutes. To define the elastic-plastic stress strain relationships of wood, the predefined 'concrete damaged plasticity' material model in Abaqus [21] was adopted. Temperature-dependent degradation relationships for strength and stiffness from the Eurocode were also used, shown in Figure 2-5.

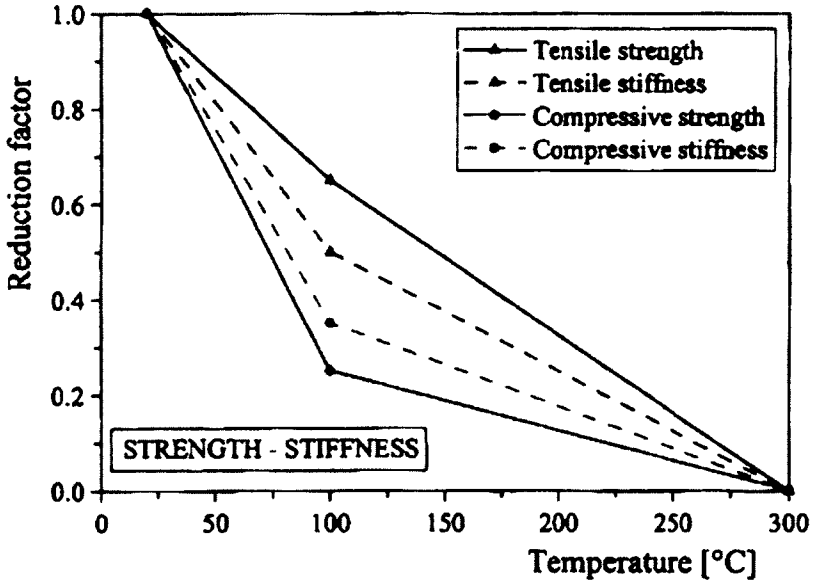

Figure 2-5: Eurocode 5 strength and stiffness relationships for wood in compression and tension

The gypsum was modelled employing thermal properties, but was assumed to add no mechanical resistance to the assembly. Temperature-dependent relationships for gypsum were obtained from a technical guideline from the SP Technical Research Institute of Sweden. A criterion for when gypsum fell-off was not specified in the model. The board was instead stipulated to fall-off after 41 minutes, as observed in the experimental test.

Temperature predictions in the both panels and the gypsum board produced by Abaqus [21], matched experimental results closely. Stresses calculated in both panels demonstrated how tension is redistributed amongst spanning plies as the panel chars.

Fire resistance predicted by the model, determined at structural failure, was very close to experimental times, differing by only one or two minutes.

2.5.4 Schmid [16]

This work focuses on developing a finite element design model using the effective cross-section method to determine the reduction of bending resistance in CLT as a function of time during standard fire exposures. The research also looks to determine the effect that a slower heating rate has on CLT when protected by insulation and/or gypsum plasterboard. The model is formulated based on the result of four fire-tests using beam strips cut from CLT. Adequate side protection was applied in order to maintain one-dimensional heat transfer. Two reference tests at ambient temperature were also performed to act as a benchmark to compare against the moment resistance of the beams tested in fire. All specimens had a span of 2.7 m and width of 150 mm, which is considerably smaller than required for testing of CLT products. Four of the specimens consisted of five layers of equal thickness at 19 mm with a total thickness of 95 mm. The other two specimens had a thickness of 150 mm with irregular layer thicknesses of 42, 19, 28, 19, and 42 mm.

A constant, unspecified load was applied to the beams by a four point loading system and deflection was measured until the load could no longer be maintained. This

occurrence was accompanied by extensive deflections and deemed as the failure time of the beams. Photographs were taken of the residual cross-sections and used to estimate the residual cross-sectional area, second moment of area, and the section modulus. Only spanning plies were considered to contribute to the second moment area calculation.

Thermal properties for wood in the model were based on properties described in the Eurocode [14]. Schmid based the gypsum thermal properties on research from Källsner and König [22] and the thermal analysis was undertaken by the SAFIR 2007 [23] computer software.

Structural analysis in the model was performed using temperature-dependent relationships for strength and stiffness obtained from the Eurocode [14]. These were modified to take into account the effects of moisture movement, moisture content, creep, density and the ductile behaviour of wood at elevated temperatures. Layers oriented perpendicular to the span were considered to contribute zero strength to the assembly. Simulations were carried out for a wide variety of panel thicknesses, ply thicknesses, and total ply layers.

A zero strength layer size was calculated that would produce the same reduction in bending moment as was calculated from model results. The largest value determined from these calculations for 5-ply panels with 20 mm plies was 10.5 mm for a fire-exposed side in tension and 15.9 mm in compression. This is much larger than the

Eurocode prescribed value of 7 mm. From this work it is evident that the Eurocode method would yield non-conservative results.

Simulations of various CLT panel thicknesses that include layers of gypsum protection demonstrate a slower heating rate, stronger panel, and small zero strength layer size, when compared to similar panels, at similar char depths, without gypsum protection. However, these effects were lost and heating quickly increased, creating an even larger zero strength layer once the gypsum protection had fallen-off. Charring rates also increase drastically in the, now, hotter fire.

2.6 Wood Properties

Properties of a variety of species of wood are widely available in the engineering literature. In Canada, the Canadian Standards Association (CSA) [24] offers a large collection of wood mechanical properties for different grades and species of commercial wood products. In the US, the Forestry Products Laboratory [25] offers a very complete listing of both the strength and thermal properties of wood species grown in different regions of the US as well as other countries. A comprehensive literature review was undertaken by Tabaddor [26] and Bénichou [27] regarding the mechanical and thermal properties of wood at elevated temperatures. This review compared the work of many of the major researchers in this field including; Takeda and Mehaffey [28], Lie [29], Janssens [30], Gammon [31], Preusser [32], Schaffer [33], Thomas [34], and Knudson [35], as well as the Eurocode 5 [14] and experiments conducted at the Underwriters Laboratories in the U.S. Tabaddor's work, along with literature covered by Buchanan [8]

on the subject, are the main references for the values incorporated into the numerical model developed in this thesis.

2.6.1 Charring and Charring Rates

As wood is heated it undergoes a thermal degradation process, producing combustible gases and eventually converting the wood to char. The charring rate is the rate at which the boundary between charred and uncharred wood advances and is typically measured in millimeters per minute. This is a significant aspect of the fire resistance of wood, as many of its thermal and mechanical properties are drastically changed when it degrades into char. Bénichou [27] has catalogued a number of different temperatures found in the literature that researchers have stated charring to begin at in wood, ranging from 288°C to 300°C. According to Buchanan [8, p. 277], 288°C is the commonly accepted value in North America, however due to the rapid temperature increase associated with wood charring, the exact value is of little importance. For the purposes of this thesis, a temperature of 300°C has been selected as the point at which char is formed.

2.6.2 Heat-Affected Layer

The thickness of wood beneath the char layer with an elevated temperature above 200°C [8] is called the heat-affected layer. In this layer, thermochemical decomposition occurs in the absence of oxygen known as pyrolysis [11]. The Eurocode 5, Part 1-2 [14], has developed an equation for wood exposed to standard fires that defines the temperature in wood below the char layer which includes a heat affected layer of 40 mm. Janssens and White, as quoted by Buchanan [8, p. 278], show that experimental

data is better fit to a 35 mm heat-affected zone. Wood properties in this layer are drastically affected by the pyrolysis reaction, as described in the following sections.

2.6.3 Mechanical Properties

In order to calculate the structural capacity of CLT as it is exposed to fire, the mechanical properties of wood must be defined as a function of temperature. The main property of interest for the numerical model developed in this thesis is the modulus of elasticity (MOE). Tabaddor [26] shows that as wood temperatures increases and is converted to char, MOE decreases and drops to zero once temperatures reach 300 to 330°C.

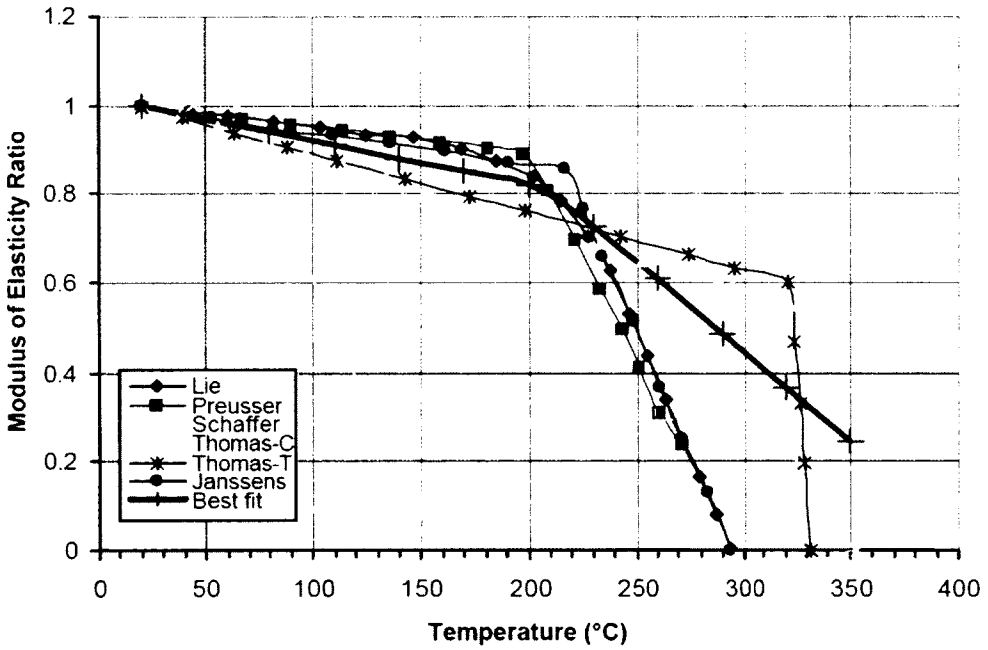

Figure 2-6: Variation of Modulus of Elasticity with temperature for wood (reproduced from [26])

As shown in Figure 2-6, all researchers, except Thomas [34], report one set of values for MOE in tension and compression. Thomas, however, found that the modulus of elasticity in compression loses 70% of its strength in the first 120°C. All research regarding the MOE in tension demonstrates a similar relationship of slow linear decline

up until 200°C. At this point, Preusser [32], Lie [29] and Janssens [30] all observed a rapid linear decline to zero, exhibiting no strength just before 300°C. Schaffer [33] and Thomas [34] observed a continued slow linear decline past 200°C until about 320°C when it drops to zero, which according to Gerhards [27] may be unlikely. Based on these results, Tabaddor [26] developed a best fit curve, shown in Figure 2-6. This curve was slightly modified in this research to drop to zero strength at 300°C and used in the numerical model. The modified model also more closely resembles the curve published by Buchanan [8] and is shown in Figure 2-7.

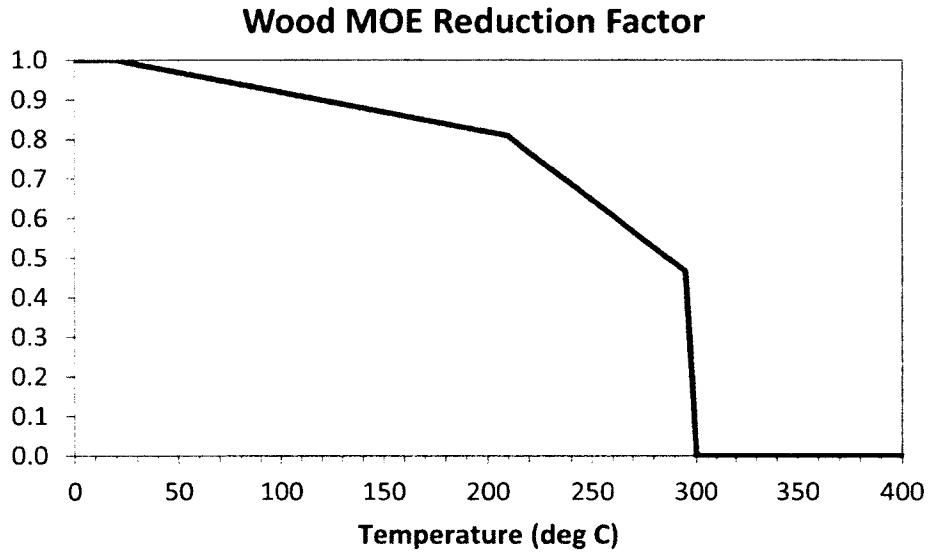

Figure 2-7: MOE reduction factor for wood used in numerical model

Grain orientation is also large aspect of the MOE, demonstrating far stronger properties for bending parallel to the grain than in bending perpendicular to the grain. Forests Products Laboratory [25] lists the MOE perpendicular to the grain as about 4-8% of the MOE parallel to the grain for SPF wood. These factors have also been incorporated into the numerical model to account for a small contribution of the cross plies for the overall effective stiffness calculation.

2.6.4 Thermal Properties

In order to develop a heat transfer model, the thermal properties of wood at elevated temperatures must be defined. The thermal properties of wood are affected by several factors such as temperature, moisture content, density and grain orientation. The thermal properties of interest for this study include; thermal conductivity, specific heat capacity and density. The relationships used for these parameters in the numerical model are summarised in the following sections.

2.6.4.1 Thermal Conductivity

Tabaddor's [26] research shows that the thermal conductivity of wood increases from ambient temperatures up to around 200°C, then decreases linearly until around 375°C, followed again by a continual increase. Thermal conductivity from a series of experiments conducted on several species of wood is summarised by Tabaddor [26] and compared to the conductivity prescribed by Eurocode 5 [14] in Figure 2-8.

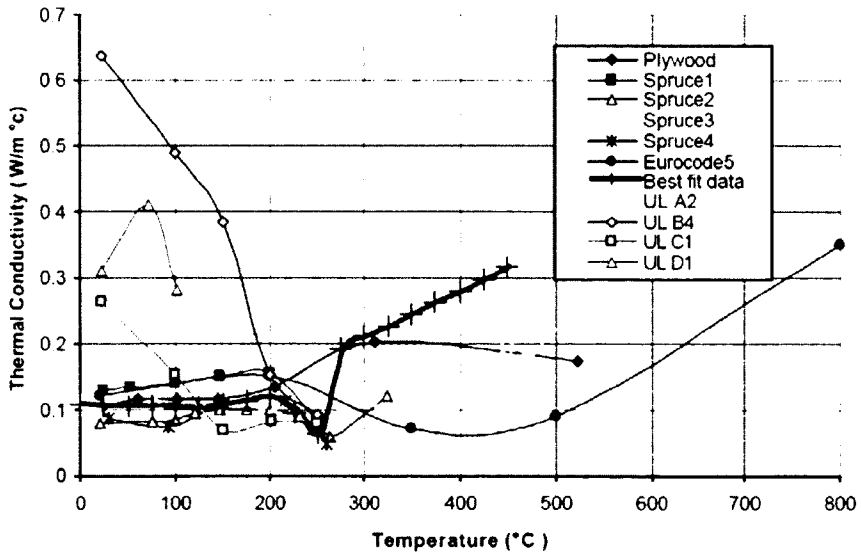

Figure 2-8: Variation of thermal conductivity with temperature for wood (reproduced from [26])

The data from these experiments are scattered due to different species, density, and moisture content studied, as well as the methods of data collection used. The best fit curve in this graph, developed by Tabaddor [26], does not offer an accurate representation of other average thermal conductivity curves developed by other researchers, as shown by Bénichou [27] in Figure 2-9.

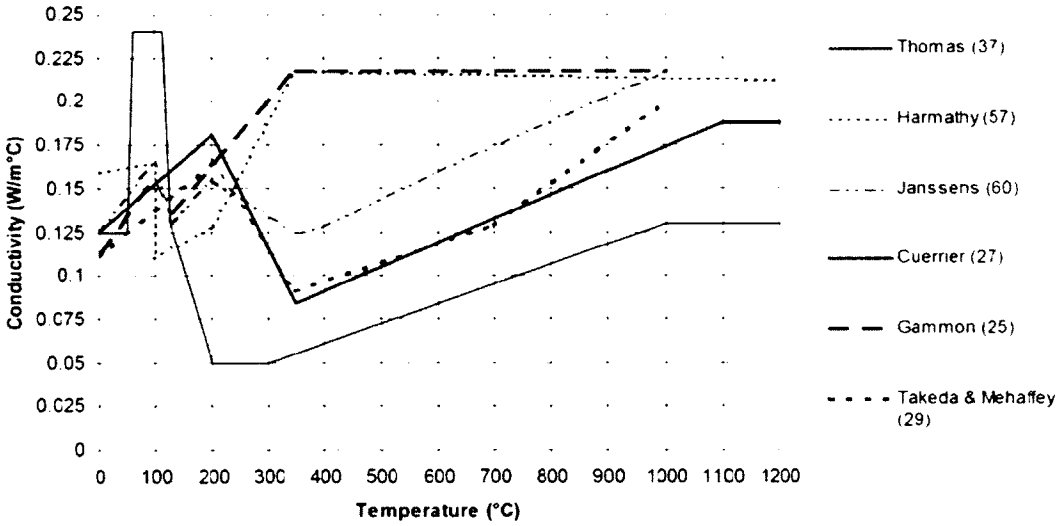

Figure 2-9: Summary research on thermal conductivity of wood (reproduced from [27])

These values still demonstrate some degree of variance; however, curves produced by Takeda and Mehaffey [28], Thomas [34], Cuerrier [36], and Janssens [37], all follow similar trends. Buchanan [8, p. 279] delineates a curve shown in Figure 2-10 that exhibits an equivalent trend and offers a decent representation of the average conductivity curves found in the literature. Importantly, the data from almost all of the previous research is very similar over the first 200°C, which represents the most important aspect of the simulation. Beyond 200°C, the wood loses most of its strength and is converted to char at 300°C at which point it contributes no strength to the panel.

The data represented in the graph in Figure 2-10 has been incorporated into the numerical model in this thesis.

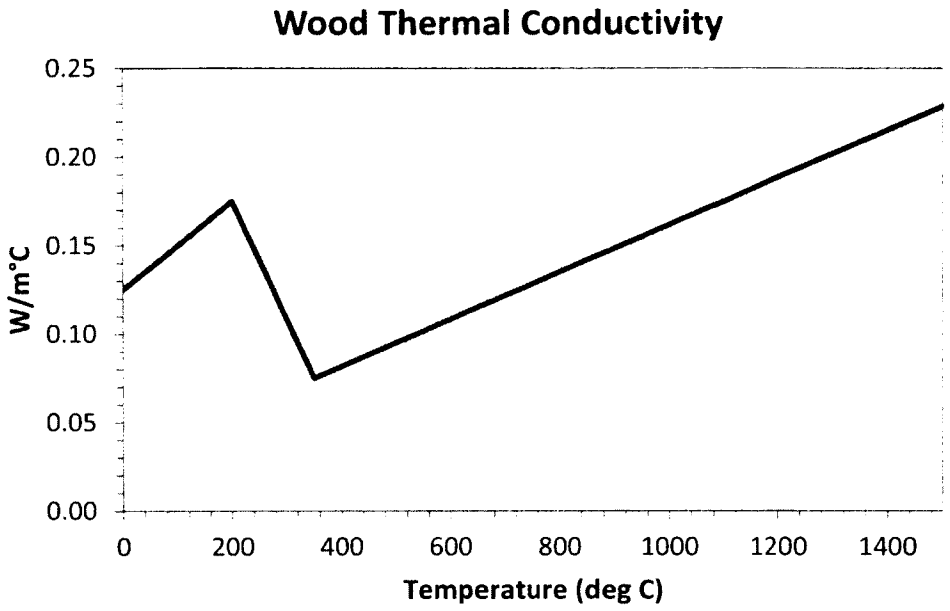

Figure 2-10: Thermal conductivity of wood with temperature used in numerical model

2.6.4.2 Specific Heat Capacity

Research on the specific heat capacity (SHC) of wood has yielded some disagreement. As wood heats up and causes moisture to evaporate, a tremendous increase in SHC is produced at a temperature range between 100°C and 200°C. There is little consistency in the reported findings due to differences in species, moisture content and the rate at which the wood is heated during experiments. Tabaddor [26] summarised the work of Janssens [30], Gammon [31], Lie [29], and experiments conducted at Underwriters Laboratories [26] and compared it with the relationship used by the Eurocode 5 [14] in Figure 2-11.

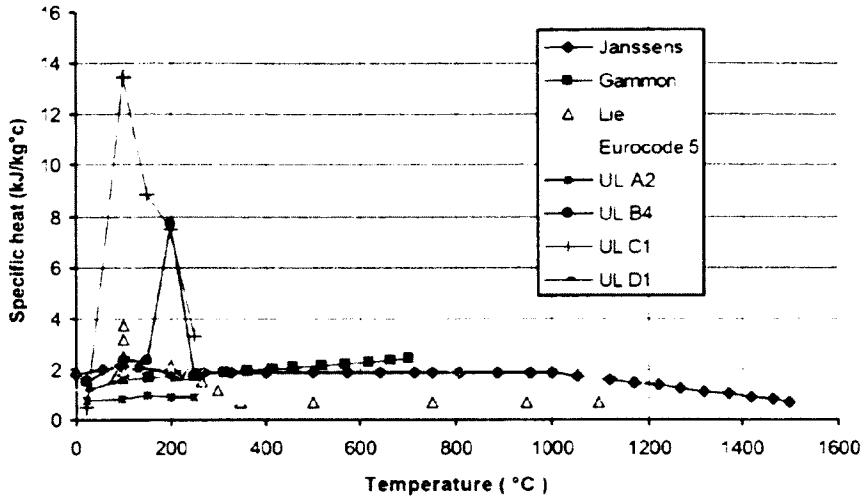

Figure 2-11: Variation of specific heat capacity with temperature [26]

Peak values during evaporation vary greatly from around 8 to 14 kJ/kg°C, while some tests do not register an increase at all; however, the majority of peaks occur at around 100°C. Tabaddor proposes a set of data that best fits the variation observed above, which also agrees very well with a graph proposed by König and Walleij cited by Buchanan [8, p. 279]. The values created by Tabaddor [26] are listed in Table 2-1 and are very similar to the values used in the numerical model developed in this thesis, illustrated in Figure 2-12.

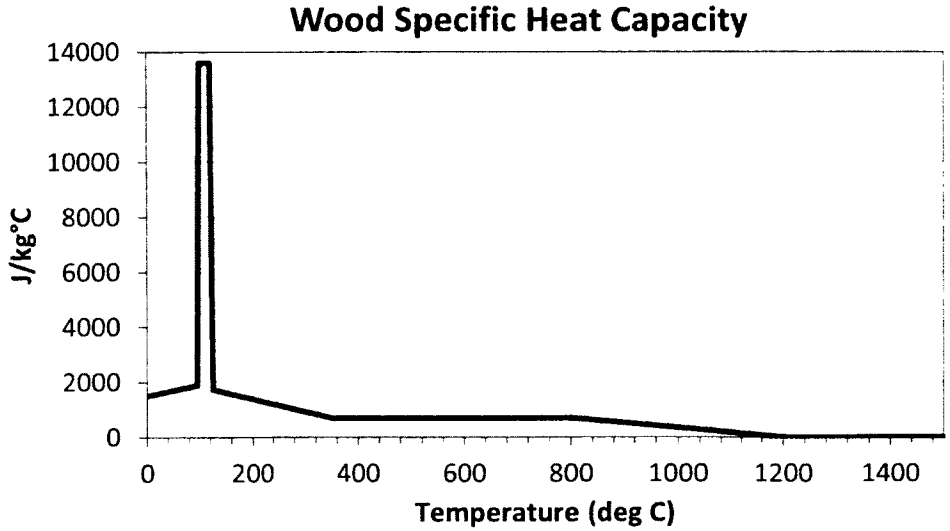

Figure 2-12: Specific heat capacity of wood with temperature, used in the numeric model

Table 2-6: Specific heat of wood at various temperatures [26]

Temperature (°C)	Specific heat (kJ/kg°C)
20 to 90	1.53
90	1.77
100	13.60
120	2.12
200	2.00
250	1.62
300	0.71

2.6.1.3 Density

Wood density can range from 300 to 700 kg/m^3, however as illustrated by Tabaddor [26] in Figure 2-13, values for the density ratio of wood at elevated temperatures from Takeda and Mehaffey [28], Lie [29], Janssens [30], the Eurocode 5 [14] and experimental data from UL [26] are all still very similar to each other. The density ratio drops slightly to a value between 0.9 and 0.95 at 200°C, and then declines sharply to about 0.3 at approximately 350°C. After this point, wood density slowly decreases to zero at temperatures above 1200°C.

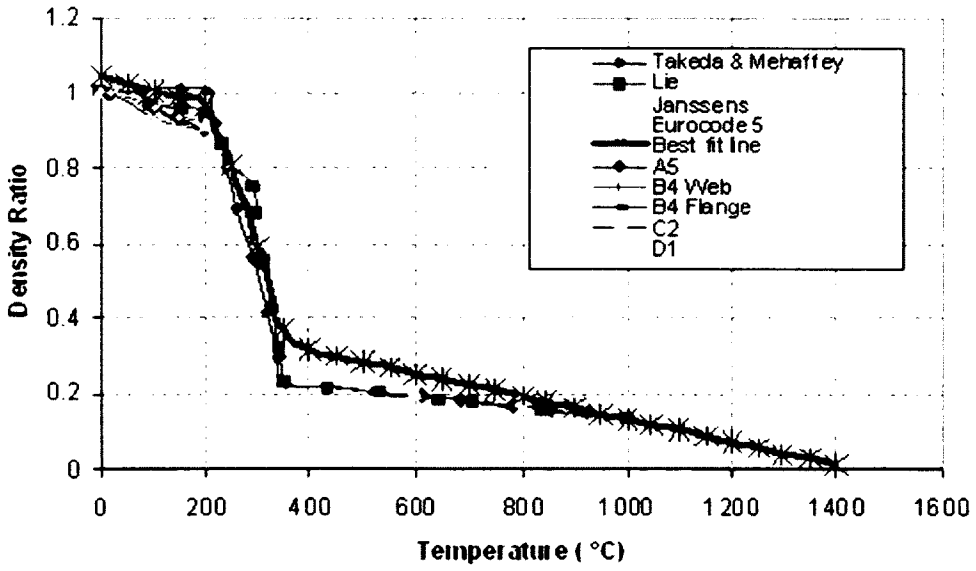

Figure 2-13: Variation of density ratio with temperature for wood

The best fit curve generated by Tabaddor [26], has been slightly modified and adopted for usage in the numerical model presented in this thesis. The modification used is graphed in Figure 2-14, and is represented by the following equations:

$$\text{Density Ratio} = \begin{cases} 1 & T \le 115°C \\ 1.046 - 0.0004 \cdot T & 115°C < T \le 240°C \\ 1.910 - 0.004 \cdot T & 240°C < T \le 350°C \\ 0.435 - 0.0003 \cdot T & 350°C < T \end{cases}$$

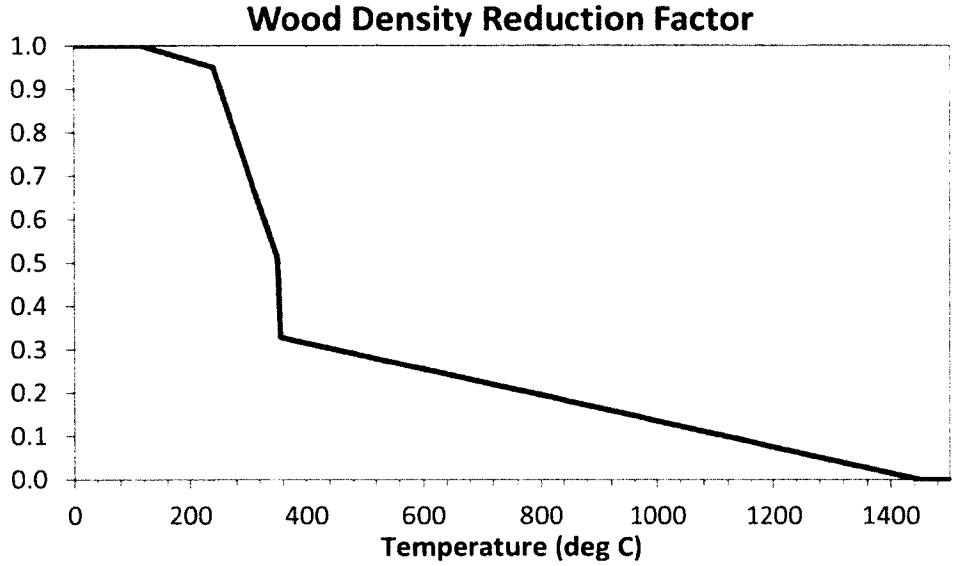

Figure 2-14: Density ratio for wood used in numerical model

2.7 Thermal Properties of Gypsum

Gypsum Board is a common building material typically used in wall and ceiling assemblies as an alternative to plaster due to its relative ease and short time to install. It is made by pressing gypsum, a soft mineral, between two thick sheets of paper. Gypsum itself is comprised of a calcium sulfate molecule, bonded to two water molecules. The bonded water molecules, combined with the low thermal conductivity of gypsum, give the boards much of their fire resistant properties [38]. The basis of this arises from the evaporation of the bound water in the gypsum board when heated, called calcination,

which absorbs a considerable amount of heat, thereby delaying temperature rise through the system [39]. Fire-rated gypsum boards, commonly labeled as Type X or C in North America and Type F in Europe, have glass fibers or vermiculite added to them in order to improve the mechanical strength and reduce shrinkage as calcination occurs. As a result, the boards remain in place longer during a fire and thus offer increased fire resistance [40].

The changes in thermal conductivity, specific heat capacity, and density with respect to temperature are of most interest in the development of the numerical model described in this thesis and are discussed in more detail in the following sections.

2.7.1 Thermal Conductivity

The results of the research by Park [41] and Thomas [42] to calculate how thermal conductivity is affected by temperature are compared in Figure 2-15 and Figure 2-16. Rahmanian [39] developed a model based on experimentation nearly identical to results from Mehaffey's [41] experiments for Type X gypsum, despite having being calculated in different ways. Calcination occurs at 100°C, and is signified by a drop in conductivity. After this drop, very little change in conductivity occurs until temperatures reach around 400°C to 500°C, when the conductivity begins to increase again. Models used by Thomas [42] along with research from Mehaffey [41], show a rapid increase once temperatures exceed 800°C.

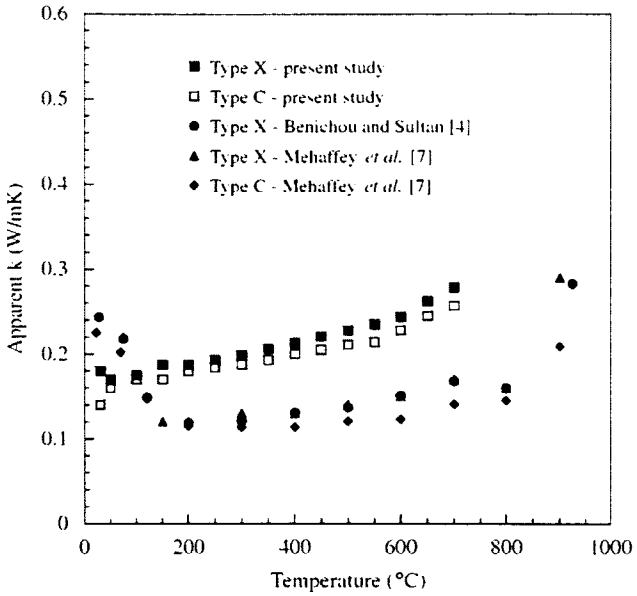

Figure 2-15: Variation of thermal conductivity in gypsum reproduced from [43]

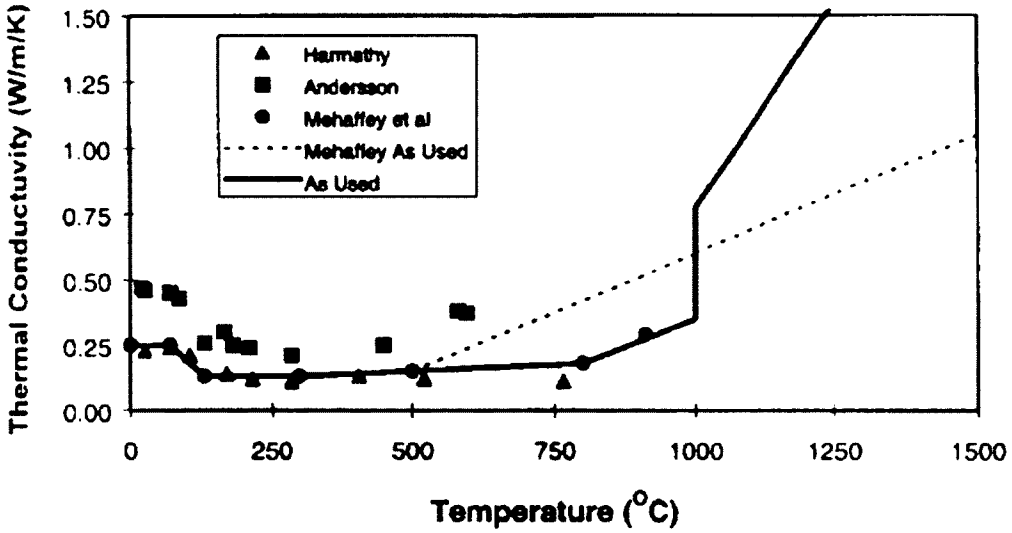

Figure 2-16: Variation of thermal conductivity in gypsum (reproduced from [42])

A model based on tests conducted by Bénichou and Sultan [43] on Canadian Type X gypsum boards, cited by Buchanan [8]; match most closely with the scattered values found in the published literature. Due to its basis on Canadian Type X gypsum and relatively average representation, Buchanan's model was used in the numerical model created in this thesis and is shown in Figure 2-17.

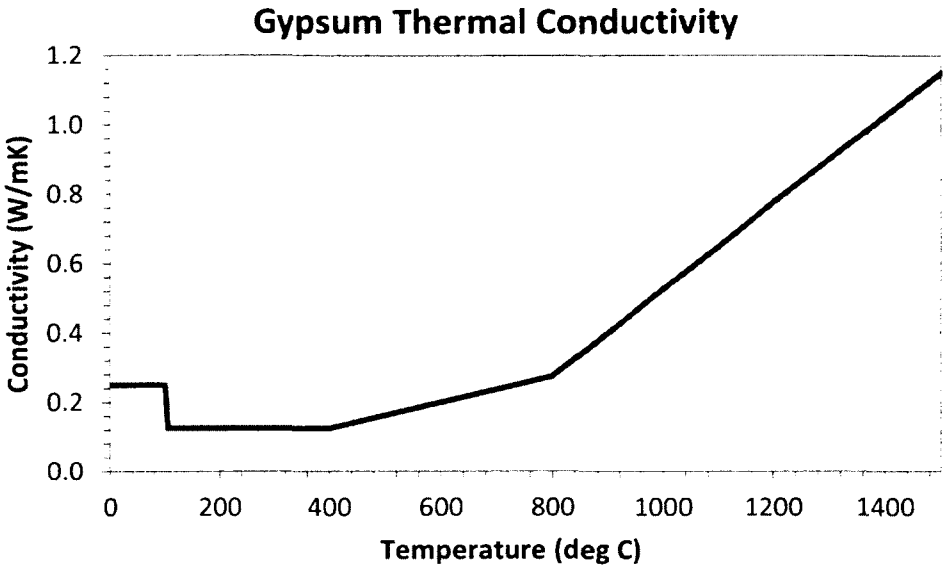

Figure 2-17: Thermal conductivity of gypsum board type X used in numerical model

Park [41] conducted experiments on the conductivity of gypsum boards during a second heating cycle, which resulted in a different set of data from those expected during the first heating cycle. Experiments revealed a lower initial conductivity and do not possess the same drop observed at 100°C since all bound water in the board has been evaporated. This effect was not included into the numerical model, as it was assumed that all gypsum boards simulated have not undergone any initial fire exposure.

2.7.2 Specific Heat Capacity

Research shows that the specific heat capacity (SHC) of gypsum is around 1 kJ/kg·K for nearly all temperatures. However, a spike of short duration, measured from 8 to over 50 kJ/kg·K, is observed when temperatures are around 100°C. This is illustrated by various researchers and reported by Thomas [42] in Figure 2-18. The spike in SHC can be attributed to heat absorbed during the calcination reaction and evaporation of bound water molecules in the gypsum. A second dehydration reaction occurs when

temperatures are around 200°C, and is identified by a spike in SHC up to 20 kJ/kg·K. A similar reaction occurs at temperatures between 600°C and 700°C, yet only increases to a value of around 3 kJ/kg·K. These secondary and tertiary reactions are consistent among research that exhibits them, however, they are not observed in all experiments and largely dependent on the gypsum board manufacturer.

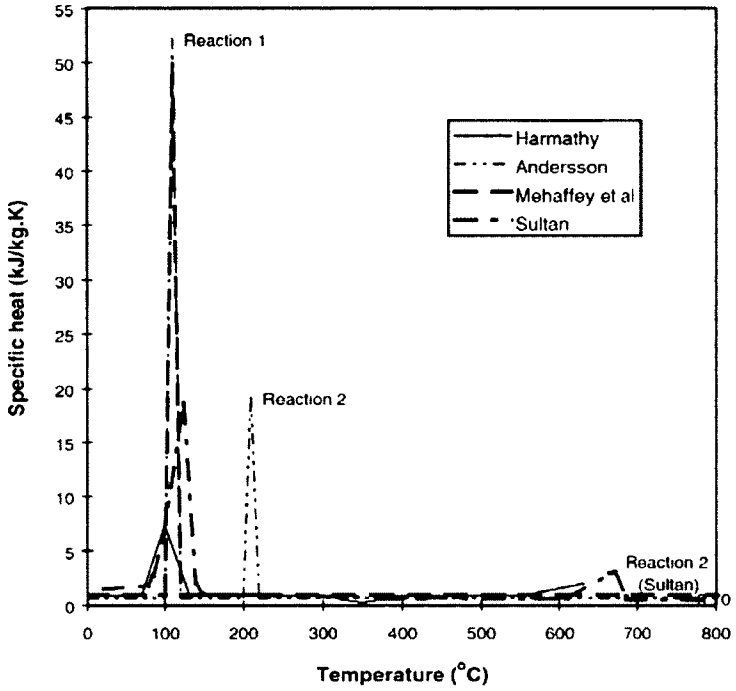

Figure 2-19: Variation of Specific heat capacity of gypsum boards (reproduced from [42])

Experimentation completed by Park [41] shows very similar trends (Figure 2-19), with the first dehydration reaction at 150°C peaking at around 20 kJ/kg·K. This peak corresponds well with results from Sultan [42]. A secondary reaction at 200°C was also observed reaching 10 kJ/kg·K, which is about half of what Andersson [42] reported.

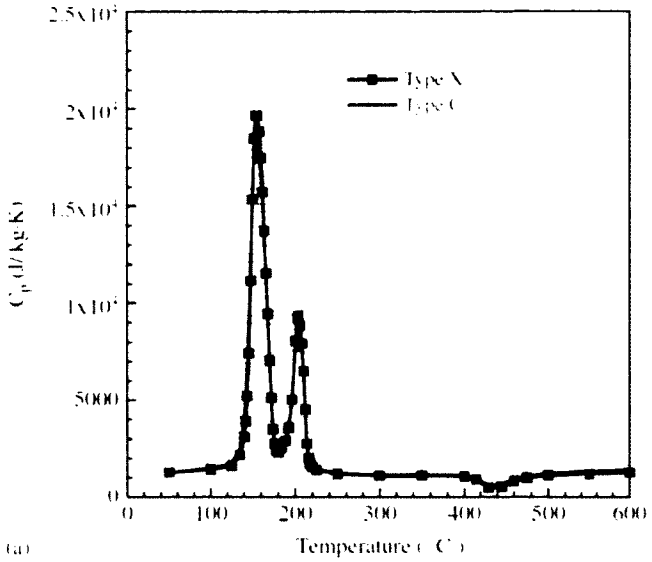

(a)

Figure 2-19: Specific heat capacity of gypsum board reproduced from [43]

Due to the large amount of variance for peak SHC values reported during dehydration reactions, a model based on tests performed by Bénichou and Sultan [43] and cited by Buchanan [8], on Canadian Type X gypsum boards was adopted to best represent the gypsum being simulated in the numerical model developed in this thesis. This model also offers a good representation of the values in the published literature and is shown in Figure 2-20.

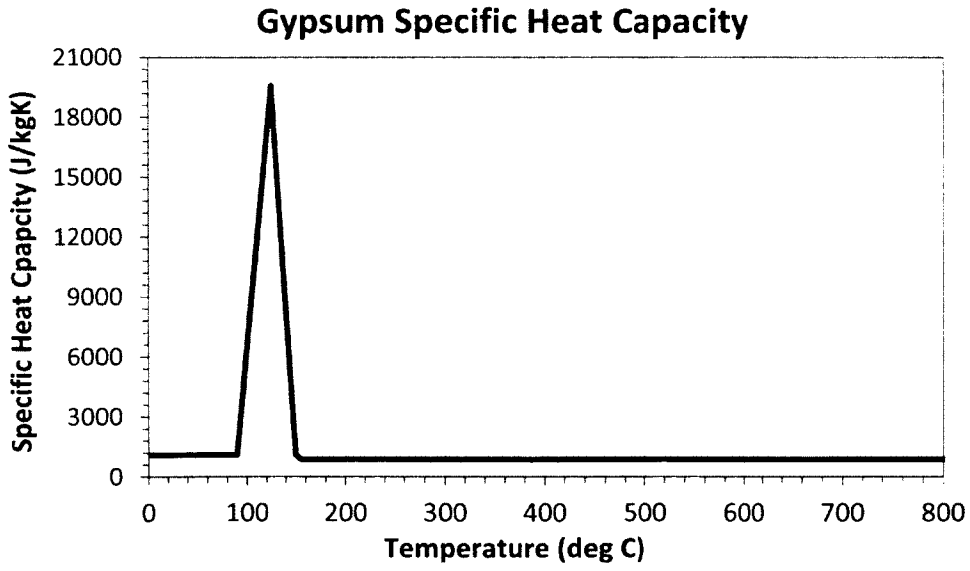

Figure 2-20: Specific heat capacity of gypsum at elevated temperatures used in the numerical model

2.7.3 Mass Loss

Mass loss of gypsum when exposed to elevated temperatures observed by several researchers follows very similar trends. Two examples of such research conducted by Park [41] and Cramer [40], display nearly identical results, shown in Figure 2-21 and Figure 2-22. A sharp decline in mass occurs after heating beyond 100°C due to a loss of water during the dehydration reaction. The mass loss then slows until 400°C at which point it begins to level-off to about 75% of the original mass at 700°C.

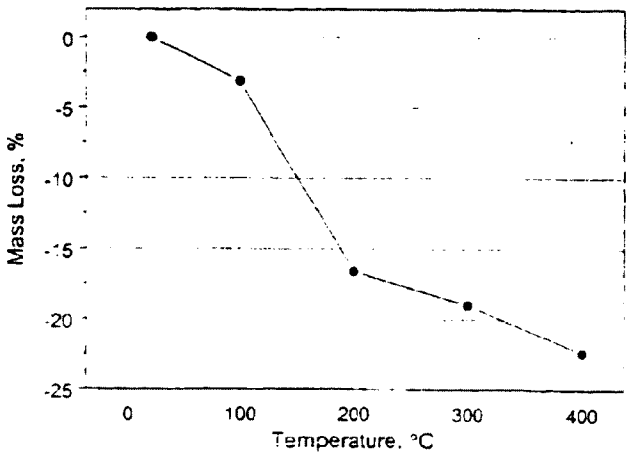

Figure 2-21: Percentage of mass loss in gypsum (reproduced from [40])

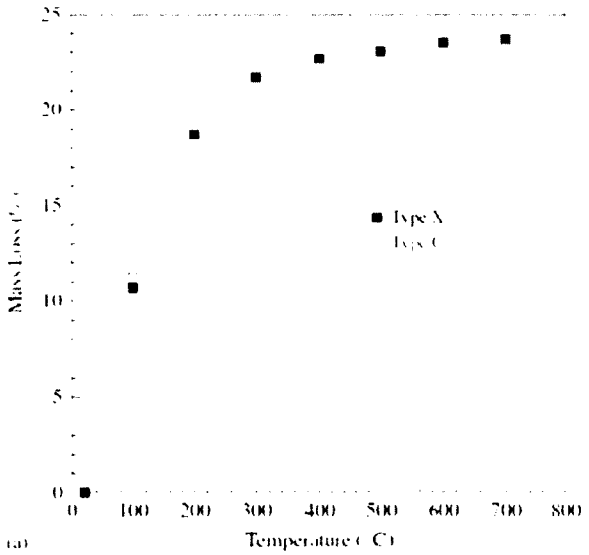

Figure 2-22: Percentage of mass loss in gypsum (reproduced from [41])

The reduction in the mass of gypsum from Park [41] was delineated and incorporated into the numerical model developed in this thesis, as shown in Figure 2-23 below.

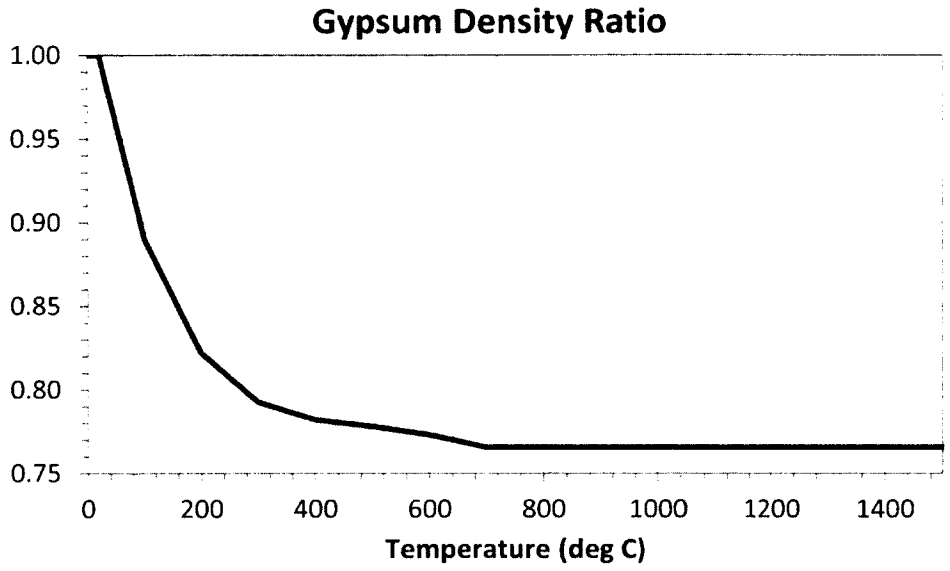

Figure 2-23: Gypsum density ratio at elevated temperatures used in numerical model

2.8 Gypsum Fall-Off Criteria

Gypsum boards fastened to assemblies exposed to a fire eventually fall-off after a certain amount of time. This is typically caused by linear contraction and cracks forming in boards as they thermally degrade. Park [41] observed cracks forming in Type X gypsum when the average temperature of the board was around 600°C, which correlates well with contraction data from the same test series. Contraction and cracking is a precursor to gypsum fall-off, since the board pulls on the screws, cracks and subsequently falls off its mounting. Sultan [38] looked at four different criteria to determine the best metric for assessing when gypsum fall-off would occur; the average of the time when the first and last piece fell-off, the average temperature of the board at fall-off, the interpolated temperature at the average fall-off time, and the time when a sudden temperature rise in the board was observed. From the results obtained with

each approach, the time when a sudden rise in temperature occurred was found to be the most accurate representative method. This method has been adopted in this thesis for determining when gypsum fell-off in experiments.

A study done by König and Walleij, quoted by Buchanan [8], states that the critical falling-off temperature for gypsum boards used as ceiling linings is 600°C. Buchanan also states that gypsum will fall off at about the same time that charring of the wood beneath it begins. Results from eighty full-scale standard fire tests on lightweight frame floor assemblies, protected with either one or two layers of type X gypsum board performed by Sultan [38], yield fall-off temperatures of around 600°C. However, closer screw spacing and the addition of insulation against the gypsum board can increase the fall-off temperature and thus offer higher levels of fire protection.

2.9 Gypsum Finish Rating

The Gypsum Association [44] defines the finish rating of gypsum boards similarly to the method used in ASTM E119 [6] and CAN/ULC-S101 [5] to establish insulation failure during standard fire-resistance tests. The finish rating is the shorter of the time taken for an average rise in temperature of 140°C, or a maximum rise of 180°C at any single point to occur, as measured at the back (unexposed) surface of the gypsum board.

3 Experimental Program

This chapter provides an overview of the background, process of design and procedural execution of the test series conducted in this report.

3.1 Introduction

Eight medium-scale CLT tests were conducted to determine the overall fire resistance of CLT floor panels exposed to both standard and non-standard fires. Four of these tests were designed to imitate four similar full-scale tests conducted by FPInnovations and NRC Canada [17], as listed in Table 3-1 and Table 3-2. These tests were intended to assess the accuracy of utilising medium-size test data in evaluating the fire performance of full-scale floors. The 7-ply full-scale floor test was not reproduced on the medium-scale furnace, due to the large loading and structural requirements that would have been necessary in the furnace. An unprotected 3-ply panel was investigated in its place.

Table 3-1: Summary of medium-scale tests completed

# of Plies	Type X Gypsum Protection	Fire
3	**Unprotected**	**CAN/ULC**
***3**	**1x 5/8"**	**CAN/ULC**
***3**	**2x 1/2"**	**CAN/ULC**
3	2x 1/2"	Non-Std
***5**	**Unprotected**	**CAN/ULC**
5	Unprotected	Non-Std
***5**	**1x 5/8"**	**CAN/ULC**
5	1x 5/8"	Non-Std

**Similar test performed by FPInnovations at the full scale*

Table 3-2: Summary of full-scale tests completed by FPInnovations

# of Plies	Type X Gypsum Protection	Fire
3	**1x 5/8"**	**CAN/ULC**
3	**2x 1/2"**	**CAN/ULC**
5	**Unprotected**	**CAN/ULC**
5	**1x 5/8"**	**CAN/ULC**
7	**Unprotected**	**CAN/ULC**

Three of these assemblies were exposed to a non-standard design fire. The details of the non-standard fire are discussed further in Section 3.5.2.

Along with the overall fire resistance of the CLT assemblies, tests were also conducted to evaluate a number of parameters such as the charring rate, temperature profile, deflection, and adhesive performance. Five of the tests included gypsum board protection to assess and compare the performance of gypsum on CLT to its performance in traditional wood constructions, such as light frame assemblies.

The test data acquired contributed to the development of a numerical model, described in Section 5. The program is intended to simulate and predict the performance of future CLT tests, as well as provide insight for designers and code consultants when calculating CLT fire design related alternative solutions.

3.2 Medium-Scale Furnace

The major drawbacks associated with full-scale fire tests are the high costs of purchasing materials and operating test facilities. As a result, full-scale test series are usually limited to a small number of tests. In order to increase the amount of experiments conducted for this project, a medium-scale furnace was constructed at Carleton University's fire lab as shown in Figure 3-1.

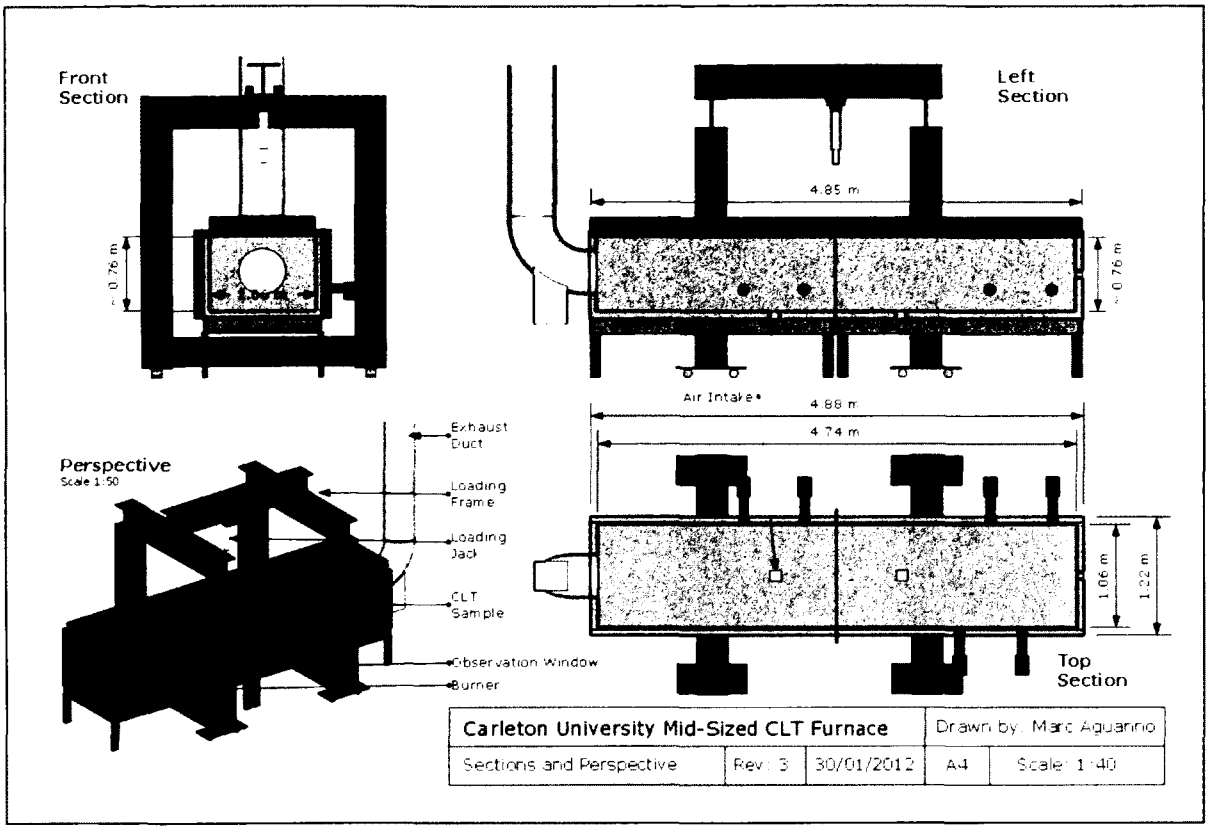

Figure 3-1: Sections and perspective of Carleton University medium-sized furnace

The furnace was designed to have the same spanning length as the full-size furnace at the National Research Council of Canada Fire Lab [9] used for FPInnovations' tests [17], shown in Figure 3-3. Panels were tested in one-way bending along the spanning length. The unsupported length of a panel in both furnaces was 4.74 m. The width of the furnace was approximately one-quarter of the width of the full-scale furnace, at a little over one meter. The medium-scale furnace (Figure 3-2) was constructed from 3/8" (9.5 mm) steel plates, lined with a layer of 1/2" (12.7 mm) Fiberfrax board, standard ceramic fire bricks and finally covered with a layer of 1/2" (12.7mm) Fiberfrax blanket.

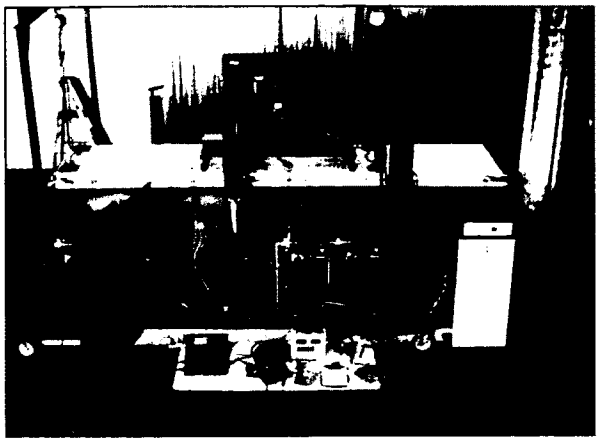

Figure 3-2: Medium-scale floor tests furnace at Carleton University fire lab

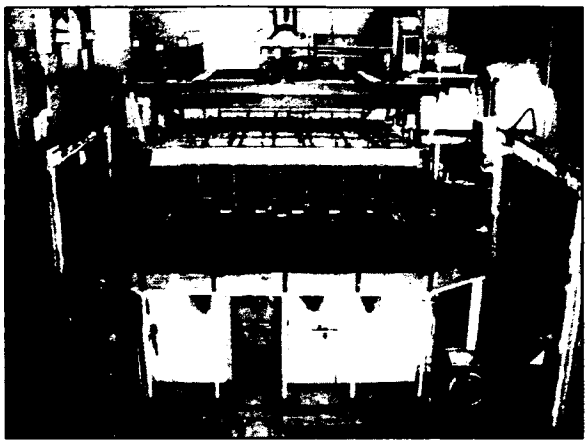

Figure 3-3: Full-scale floor test furnace at NRC Canada fire lab [9]

A 36" (914.4 mm) diameter exhaust duct was attached to the end of the furnace and connected to the laboratory exhaust system to remove products of combustion from the burners and assemblies being tested. Air was supplied by each burner's premixing system and two small air intake holes on the floor of the furnace. Air was drawn through these holes due to a pressure reduction in the furnace caused by the exhaust system. Pressure was monitored in the furnace using a simple manometer and the exhaust fans were adjusted to ensure that pressure in the furnace was always at least 20 Pa below the ambient pressure in the lab.

Seven thermocouples were installed along the length of the furnace in accordance with the CAN/ULC-S101 standard [5] as shown in Figure 3-4. Two plate thermometers were installed, one at the center of the furnace and another three-quarters of the length of the furnace from the front. Six commercial Carlin [45] premixed gas burners were installed along the sides of the furnace and supplied by the laboratory propane gas line as shown in Figure 3-5.

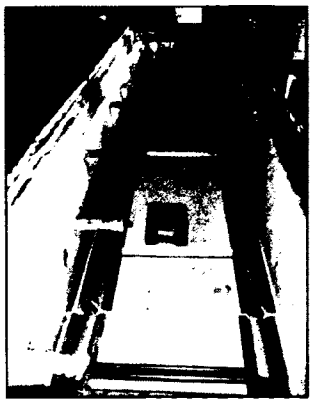

Figure 3-4: Inside the medium-scale furnace showing thermocouples and insulation

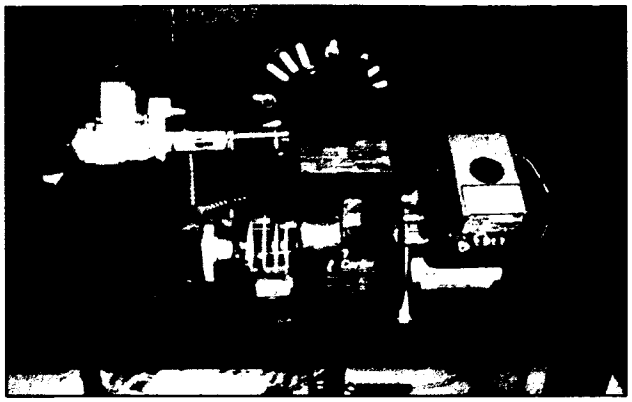

Figure 3-5: One of the Carlin burners used in the medium-scale furnace

In full-scale testing, a uniformly distributed load was applied by the NRC loading system shown in Figure 3-6. This was replaced by a four-point loading system shown in Figure 3-7 and Figure 3-8 for the medium-scale tests due to budget and space constraints.

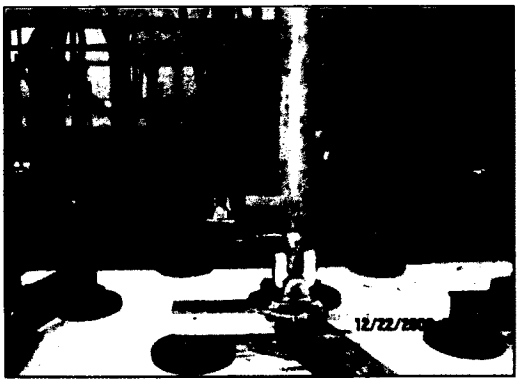

Figure 3-6: NRC uniformly distributed loading jack system in full-scale furnace [9]

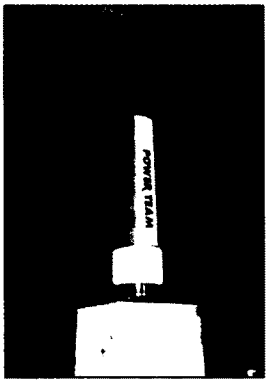

Figure 3-7: Hydraulic jack used to apply 4-point load in medium-scale furnace

In the medium-scale furnace, the load was applied during the test by a hydraulic jack fastened to the loading frame as shown in Figure 3-7. A loading beam, fitted with rollers set apart a distance of one-third of the length of the panel, is used to apply the load from the jack to two points on the panel (Figure 3-9). The assembly rests on supports at either end to provide simply-supported end conditions for the additional two points to resist the load as shown in Figure 3-8. The floor rested on wooden supports, each 70mm

wide, across the full width of the floor. This reduced the effective span of the panels from 4.87 m to 4.73 m.

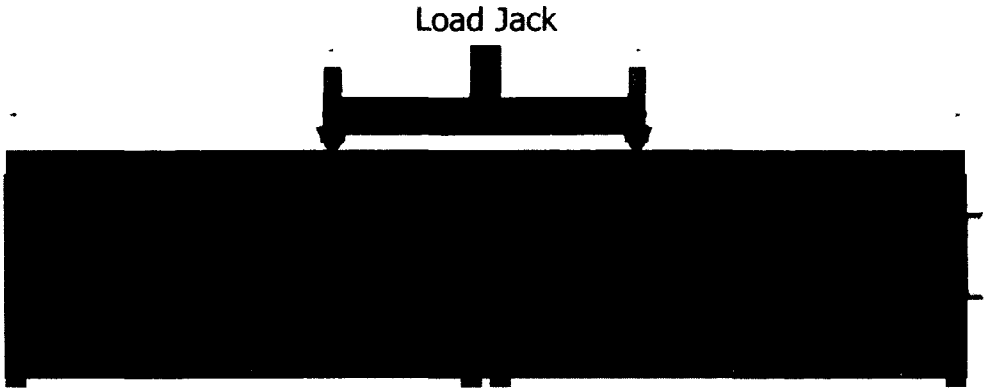

Figure 3-8: 4-point load applied to CLT sample through loading beam by hydraulic jack

Figure 3-9: Loading beam placed on CLT sample before hoisting onto furnace

Figure 3-10: Overhead picture of furnace showing 4-point loading system in place

3.3 Medium-Scale Floor Test Panels

The test panels consisted of eight CLT floors manufactured by Nordic Engineered Wood [46]. Four of which were 3-ply panels and four 5-ply panels (Figure 3-11), as summarised in Table 3-1. Panels were manufactured to the dimensions shown in Figure 3-13.

Figure 3-11: 5-Ply CLT floor from Nordic Wood

Figure 3-12: 3-Ply CLT floor with 2 Layers of [illegible] gypsum protection

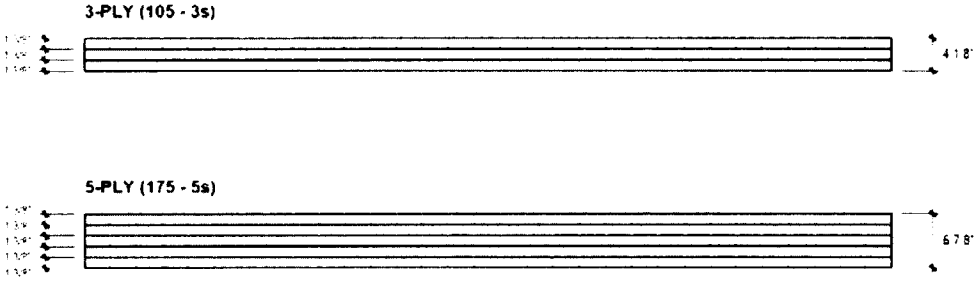

Figure 3-13: Nordic CLT panels used for testing [46]

All panels were 4.87 x 1.02 m wide, with 35 mm thick ply layers. Spanning layers were constructed with SPF 1950F_b MSR nominal 2 x 4"s (38 x 89 mm) and cross layers with SPF No.3/Stud nominal 2 x 4"s (38 x 89 mm) [47]. Layers were glued together using a one-part, moisture reactive polyurethane adhesive (PUR).

Two tests included two layers of 1/2" (12.7 mm) gypsum board and three others had one layer of 5/8" (15.9 mm) gypsum protection. All gypsum boards were SHEETROCK® FIRECODE® Type X and were manufactured by CGC Inc. [18]. Gypsum boards were fastened to the underside of test specimens using 1-5/8" (41.3 mm) drywall screws with a 300 mm screw spacing. Panels were cut and installed in the configurations shown in Figure 3-14 and Figure 3-15.

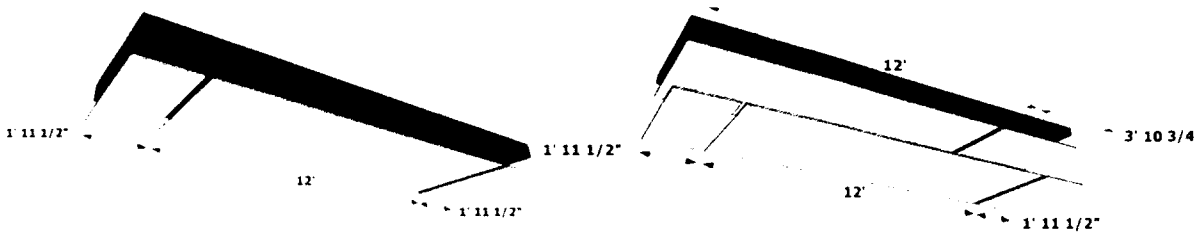

Figure 3-15: Application of one layer of gypsum protection to test specimens

Figure 3-15B: Application of two layers of gypsum protection to test specimens

Temperatures in the panels were monitored by shielded thermocouples embedded at various depths. These were installed at three locations along the length of each panel labeled; "Front", "Center", and "Exhaust", in relation to the furnace, as shown in Figure 3-16. From these, a temperature profile measured throughout the panel depth could be delineated as it was heated.

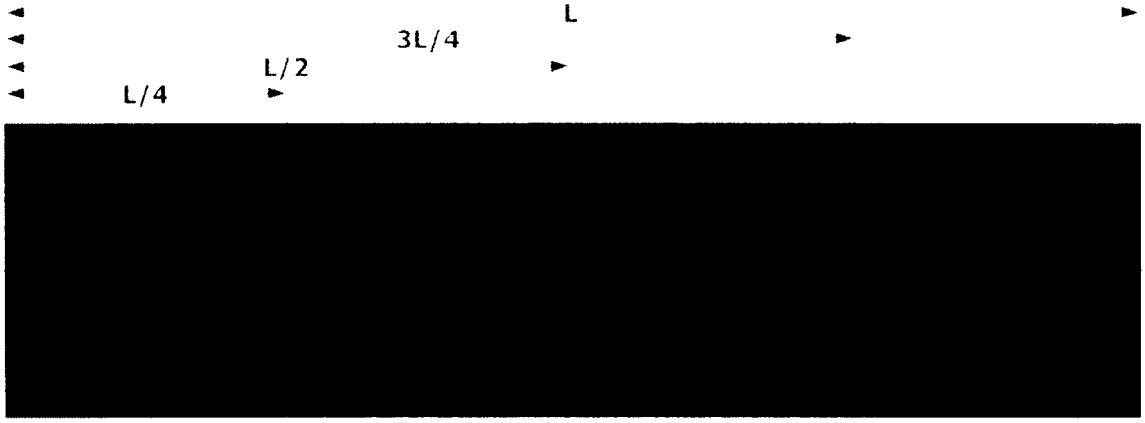

Figure 3-16: Placement of embedded thermocouples in test assemblies

At each location, holes were drilled into the panel for thermocouples to be set in (Figure 3-17), at 17.5 mm depth intervals from the exposed surface of the panel. This created a measuring point at the mid-ply depth and the adhesive interface between each ply layer, as shown in Figure 3-18. When gypsum protection was present, thermocouples were placed at the back of each board. Thermocouples were not embedded in any plies

beyond the third layer, since temperatures this far from the exposed surface did not increase more than a few degrees and were deemed unnecessary to record.

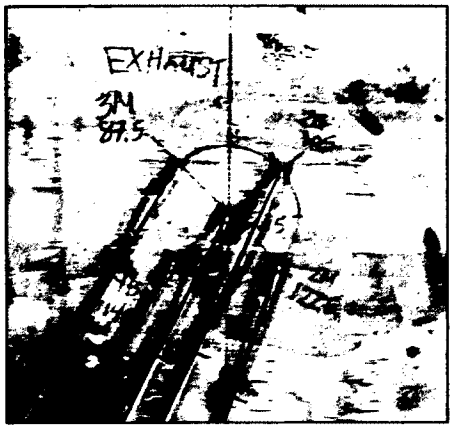

Figure 3-17: Shielded thermocouples entering surface of 5-Ply layup without gypsum

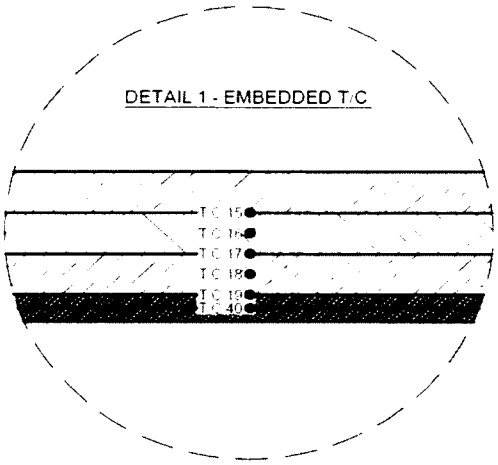

Figure 3-18: Section of 3-ply layup with 2 layers of gypsum, showing measurement points of shielded thermocouples [27]

In the three tests performed using non-standard fire exposures, thermocouples were placed at 8.75 mm depth intervals (Figure 3-19) due to concerns that the increased heating rate from the more intense and faster growing non-standard fire would not be captured with enough detail using 17.5 mm depth intervals.

Figure 3-19: Shielded thermocouples entering surface of 3-ply layup at 8.75mm intervals with 2 layers of gypsum

Deflection from the load was measured at two locations on the panel; the center and three-quarters of the length of the panel from the front of the furnace. Measurements were taken using a linear variable differential transformer (LVDT), shown in Figure 3-20.

Figure 3-20: LVDT setup above the 3-ply panel to measure center deflection

All temperature, load, and deflection data were monitored in real time at one second intervals and recorded using a program specifically developed for these experiments with the National Instruments software, LabView. A video camera mounted at the front of the furnace recorded each test through a small observation window, shown in Figure 3-1, and both the program and video camera output were displayed on screens beside the control desk, as shown in Figure 3-21.

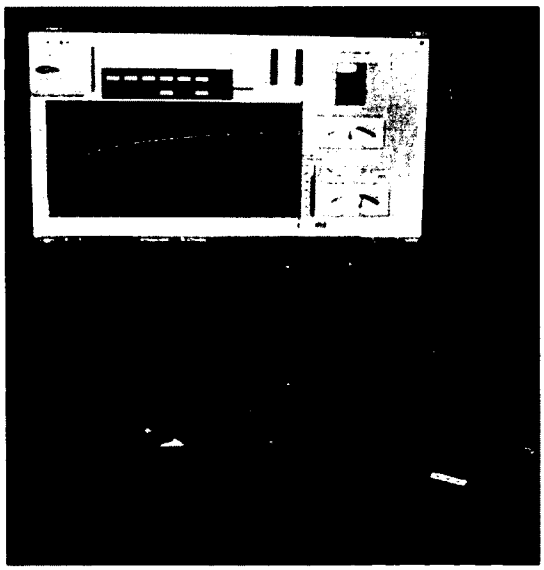

Figure 3-21: LabView program displaying temperature, load, and deflection data (top screen) and video camera output (bottom screen) next to the control desk

3.4 Loading Criteria

According to CAN/ULC-S101 requirements for tests of roof and floor assemblies, test samples must be loaded with a superimposed load throughout fire endurance tests [5]. The superimposed load shall represent either a *full specified load condition* or a *restricted load use condition*. A full specified load condition, as defined by CAN/ULC-S101, is "the specified gravity loads that produce a factored load effect as close as practicable to the factored resistance of the test specimen. The factored load effect and the factored resistance of the test specimen shall be determined in accordance with the appropriate limit states design standard published by the Canadian Standards Association" [5, p. 16].

Following the Canadian Standard for Engineering Design in Wood (CSA O86) [24], the factored bending moment resistance, M_r, (Eq. 3.1) and factored shear resistance, V_r, (Eq. 3.2) of the panel can be calculated using the following formulas:

$$M_r = \emptyset F_b S K_{zb} K_L \qquad \text{Eq. 3.1}$$

$$V_r = \emptyset F_v \frac{2A_n}{3} K_{zv} \qquad \text{Eq. 3.2}$$

Where the resistance factor, $\phi = 0.9$ and

$$F_b = f_b(K_D K_H K_{Sb} K_T) \qquad \text{Eq. 3.3}$$

$$F_v = f_v(K_D K_H K_{Sv} K_T) \qquad \text{Eq. 3.4}$$

Where f_b and f_v are the specified bending and shear strength, respectively. A_n, K_z, K_L, K_D, K_H, K_S *and* K_T are the net cross-sectional area, size factor in bending, the lateral stability factor, load duration factor, system factor, service condition factor and treatment factor.

Applying various loads, and checking the required bending and shear strength against the factored resistance (Eq. 3.5 and Eq. 3.6), it is clear in all reasonable cases of CLT floor assemblies with a 4.74 m span, that structural failure due to fire exposure will occur in bending far before shear failure occurs. Thus the governing factor when determining the fire resistance of a CLT panel is the bending moment resistance.

$$M_f = \frac{wL^2}{8} \leq M_r \qquad (governs) \qquad \text{Eq. 3.5}$$

$$V_f = \frac{wL}{2} \leq V_r \qquad \text{Eq. 3.6}$$

Where w is the combined live and dead load and L is the span of the panel.

The superimposed live (w_L) and dead (w_D) loads that represent the full specified load condition are found to produce a factored moment (M_f) as close as practicable to the factored resistance (M_r) of the test specimen. This process is shown in Eq. 3.7 and Eq. 3.8.

$$\frac{\alpha(w_L + w_D)L^2}{8} \leq M_r \qquad \text{Eq. 3.7}$$

$$w_L = \frac{8M_r}{\alpha L^2} - w_D \qquad \text{Eq. 3.8}$$

Based on the method used by FPInnovations and the statement that existing CLT constructions tend to have a dead-to-live load ratio close to unity [17], a value for alpha (α) of 1.375 is adopted, as specified in CAN/ULC-S101 [5, p. 55].

Panels in the medium-scale experiment from Nordic Engineered Wood had a specified bending strength of 28.2 MPa in the spanning plies [47], which results in considerably large moments of resistance. The full specified loads required to produce these

moments for both the 3- and 5-ply panels were found to be very high when compared to typical residential and office loads found in the Ontario Building Code. Loads from the Specified Uniformly Distributed Live Loads on an Area of Floor or Roof [48, p. 427] are compared in Table 3-3.

Table 3-3: Full specified live loads for 3- & 5-ply panels with typical office and residential live loads

	Full Specified Live Load (w_L)	Office Areas – Basement & 1st storey	Office Areas – Floors above 1st storey	Residential Areas
3-Ply Panel	11.1 kPa	4.9 kPa	2.4 kPa	1.9 kPa
5-Ply Panel	25.9 kPa			

Imposing the required full specified loads on a 3-ply panel would produce large initial deflections of around 70 mm during preloading and may have damaged any gypsum boards attached before the test even began. Further, as the panel weakens in the fire and the deflections increase, the gypsum board may crack and fall off prematurely. There was also concern that the panel may deflect enough into the furnace to damage the thermocouples during the test.

The required full specified loads for 5-ply panels were large enough to jeopardize the strength capacity of the furnace structure and loading equipment. Loading the equipment this heavily also endangered the safety of the researchers conducting the experiments.

The full specified load condition required loads two to 13 times higher than would normally be seen in a typical building of this construction. For these reasons the full specified loads calculated were not used in the experiment and a *restricted load use condition* was used instead.

The CAN/ULC-S101 does not state any particular method for following the restricted load use condition, and only insists that; "When a test is conducted with a load condition that is less than the full specified load condition, the restricted load use condition shall be identified and reported" [5, p. 16]. CSA-O86 [24] provides deflection guidelines for the serviceability limit state of structural members under load combinations, stating that deflection shall not exceed L/180 of the span. The Wood Design Manual [49] also provides a maximum suggested deflection criteria of L/360 for floors and L/240 for roofs. Since one of the objectives of this test series was to replicate the full-scale tests conducted by FPInnovations at the medium-scale, the loading criteria used by FPInnovations of L/240 was chosen as the restricted load condition for all eight medium-scale CLT tests performed. The total load that produced a maximum center deflection of L/240 in a 4-point loading system was calculated using Eq. 3.9 and Eq. 3.10.

$$\Delta = \frac{5w_D L^4}{384EI_{eff}} + \frac{aP(3L^2 - 4a^2)}{24EI_{eff}} \qquad \text{Eq. 3.9}$$

Where w_D is the dead load, L is the span, EI_{eff} is the effective stiffness, P the applied load, and a, is the distance from the outer edge of the panel to the point of load, illustrated in Figure 3-22. The first term in Eq. 3.9 calculates the deflection from the weight of the dead load. The second term calculates the deflection from the applied load from the 4-point system.

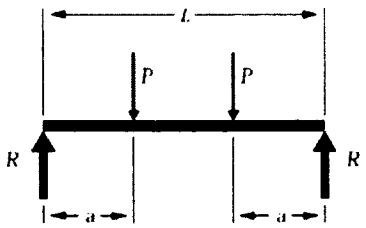

Figure 3-22: 4-point load

Rearranging Eq. 3.9 for the applied load, *P* yields:

$$P = \frac{24EI_{eff}\left(\frac{L}{240} - \frac{5w_D L^4}{384EI_{eff}}\right)}{a(3L^2 - 4a^2)} \qquad \text{Eq. 3.10}$$

Table 3-4 outlines the loads calculated using Eq. 3.10 that were applied to both 3- and 5-ply panels in order to produce the initial deflection criteria of L/240, or 19.7 mm for the 4.73 m spanning panels. These results have taken into account the dead load of the panel, gypsum, and the 112 kg loading beam resting on top of the panel.

Table 3-4: Loading requirements for restricted load condition of L/240 deflection

Plies	Gypsum	Gypsum Thickness	M_r	Self-Weight w_d	Required applied load per point (P)	Required Applied Load from Jack	Load Ratio
[#]	[#]	[mm]	[kNm]	[kPa]	[kN]	[kN]	[%]
3	0	0	44.95	0.577	4.70	8.31	28%
3	1	15.9	44.95	0.688	4.51	7.93	28%
3	2	12.7	44.95	0.755	4.40	7.70	28%
5	0	0	103.32	0.962	20.24	39.38	47%
5	1	15.9	103.32	1.073	20.00	38.90	47%

The load ratio in Table 3-4 is determined by dividing the factored moment (M_f) produced from restricted load condition, by the factored moment produced by the full specified load condition. The load ratio represents the percentage of the full specified load that is imposed by the restricted loading condition and is displayed simply for interest's sake.

In order to compare the load imposed by the restricted load condition with typical office and residential live loads, a uniformly distributed load that produces an L/240 deflection

is calculated for a 3- and 5-ply panel without any gypsum boards using Eq. 3.11. These are listed in Table 3-5.

$$w_L = \frac{384EI_{eff}\left(\frac{L}{240}\right)}{5L^4} - w_D \qquad \text{Eq. 3.11}$$

Table 3-5: L/240 limit loads for 3- and 5-ply panels compared to typical office and residential floor loads

	Restricted Load Condition (w_L)	Office Areas – Basement & 1st storey	Office Areas – Floors above 1st storey	Residential Areas
3-Ply Panel	2.9 kPa	4.9 kPa	2.4 kPa	1.9 kPa
5-Ply Panel	11.9 kPa			

The load calculated for a 3-ply panel is slightly higher than typical office loads above the first storey and residential loads, but lower than office loads in the basement and first storey. The load calculated for a 5-ply panel is still much higher than typical office and residential loads. However, it should be noted that the loads imposed on a floor panel to produce an L/240 deflection are a function of its span, such that, as the span of a floor is reduced, the load required to produce the same deflection is increased. In practice, the span of a CLT floor panel is limited by a deflection or vibrational criteria. As recommended by Nordic Wood [46], a simply supported 3-ply panel, similar to those used in the experiments in this thesis, can span up to 4.8 m under an L/360 deflection criteria based on a typical office load. In the same way, the 5-ply panels used can span up 7.4 m. The objective of these experiments was to reproduce the maximum stress the panels would experience in these particular instances. Therefore, since the 3-ply panel had a span nearly identical to the maximum recommended span, only a slightly higher load was imposed, due to the more severe L/240 criteria, rather than L/360. The 5-ply panel, with a much shorter span than the maximum recommended span, used a much

higher load in order to produce the same stresses as a longer spanning floor. Again, a more severe load was imposed using the L/240 restricted load condition rather than the L/360.

3.5 Standard and Non-Standard Fire Exposures

Five of the eight tests listed in Table 3-1, were exposed to the CAN/ULC-S101 [5] standard fire exposure displayed in Figure 3-23.

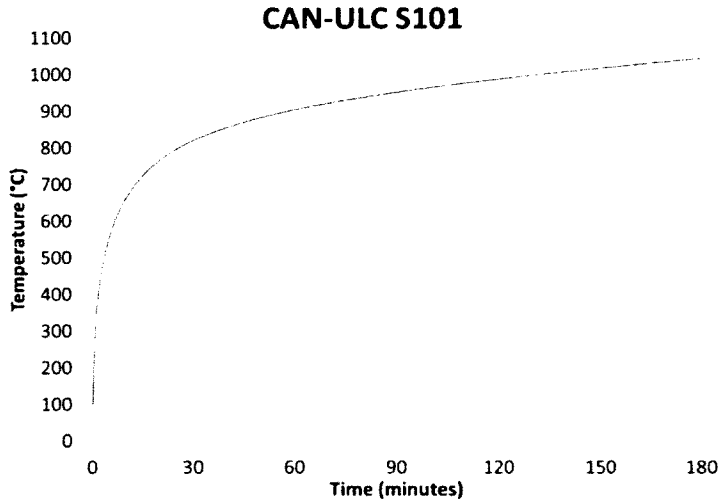

Figure 3-23: CAN/ULC-S101 standard fire exposure

The other three tests were exposed to a non-standard fire. This fire was designed to conservatively replicate a fire that would occur in a room constructed of CLT with a typical residential bedroom fire load. Two furnished CLT room tests were conducted by McGregor [50] in a 4.5 x 3.5 x 2.5 m high room with a 1.07 x 2 m high door as shown in Figure 3-24 and Figure 3-25. The walls and a ceiling in both rooms were built with 3-ply CLT panels. The floor was laid with cement board and covered with hardwood. One of the rooms was lined with two layers of 1/2" (12.7 mm) Type C gypsum protection, while the other room had exposed CLT for the walls and ceiling. Both rooms had nearly

identical fuel loads of around 560 MJ/m^2 involving a bed, two night tables, two dressers and various linens and books.

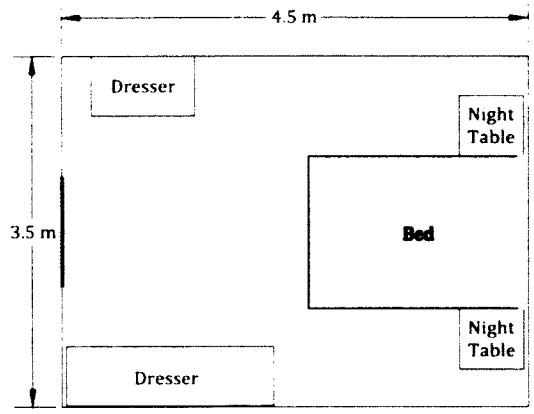

Figure 3-24: CLT room testing layout and dimensions

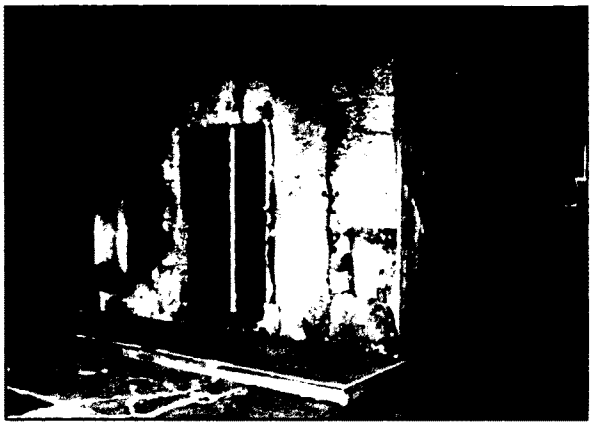

Figure 3-25: Furnished and unlined CLT test room

Temperature data from plate thermometers in the rooms were used to design the non-standard fire used in this test series. Plate thermometer data was utilised over shielded thermocouple data due to its faster response time to the actual temperatures during the rapid heating phase at the beginning of a fire [51]. Further to this, any fire curve developed from plate thermometers would, in return, be required to be controlled by plate thermometers to ensure a similar accuracy [52].

Fire temperatures observed in both room tests followed very similar curves for the first 17 minutes, shown in Figure 3-26. Growth phases during both gypsum lined and unlined room fires were very similar, rising to just over 700°C in about two and a half minutes. Both fires continued to get hotter over the next three minutes, yet at a slower rate, to a temperature of around 950°C. From here both fires seem to enter a relatively steady burning period for 11.5 minutes, during which, both fires experienced a small drop in temperature before rising to a maximum temperature of roughly 1100°C at the end of the steady burning phase. At this point the gypsum lined room entered a decay phase

and temperatures dropped to 400°C over the next 30 minutes when the test was ended. In the unprotected room, the CLT ceiling and walls became involved in the fire which resulted in the temperature increasing to 1200°C and continuing to burn for 40 minutes. The test was ended at this point, as it was clear that the room was not going to self-extinguish.

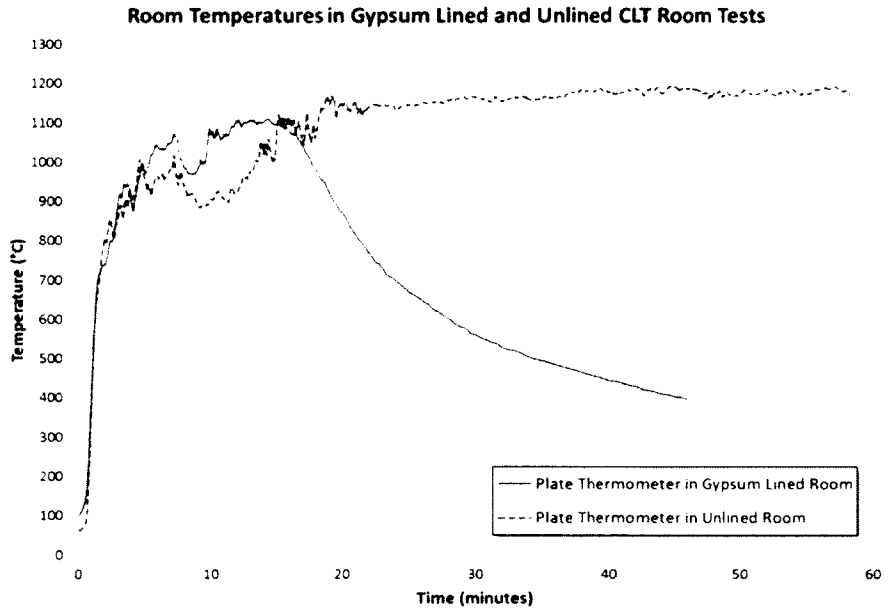

Figure 3-26: Fire temperatures observed in both protected and unprotected CLT room tests

Based on these room tests, two options must be considered in the design of the non-standard fire; a decay phase or continued steady burning. Maintaining a high temperature, as seen in the unlined room test, is not representative of a fire that would occur in a gypsum lined room constructed of CLT. Since CLT construction typically involves gypsum protection, a decay phase was preferred, however the decay phase observed in the protected room test was considered too rapid to represent a severe enough fire to cause structural failure during the tests. Consequently, a much slower decay phase was adopted. The temperature was decreased from 1100°C to 300°C over a

period of two hours. The temperature was kept above 300°C for this length of time to ensure that it was possible for charring to continue in the wood long enough to cause structural failure to occur.

Based on the aforementioned observations, a design fire was developed to simulate real CLT room tests, as well as to continue long enough to cause structural failure. This involves the following stages:

- Fast growth rate to reach 700°C in about two and a half minutes.
- Steady burning at 1100°C for at least 11.5 minutes.
- Temperatures above 300°C for at least two hours.

3.3.1 Preliminary Non-Standard Fire-Temperature Curve Furnace Tests

In order to determine whether the furnace would be able to follow such a steep growth curve, preliminary temperature tests were run using three CLT floor panels left over from previous testing done at the National Research Council of Canada's Fire Lab. For each test, all six burners in the furnace were turned on and left to run at full capacity while temperatures were recorded by the two plate thermometers. The results of the three tests are presented in Figure 3-27.

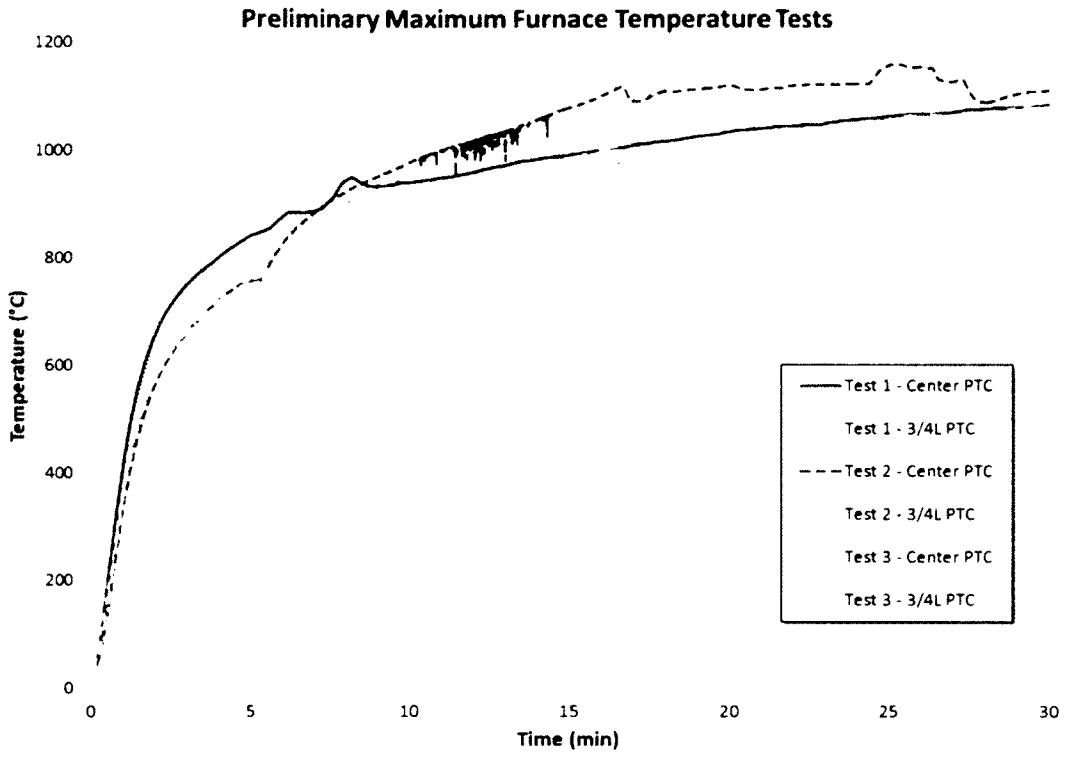

Figure 3-27: Furnace temperatures from preliminary tests to determine maximum fire growth

From these preliminary tests it was determined that a steep growth rate could be achieved in the furnace for a little over two minutes, up to a temperature of around 630°C. After this the heat lost to the surroundings and mostly through the exhaust, caused a visible reduction in the rate of temperature increase. From this point, the burners were able to continually raise the internal temperature, but on average took over 20 minutes to reach 1100°C. Based on these observations, running all six burners at once would not be sufficient to identically match the fire growth witnessed in the room tests. However, a close alternative can be achieved and the average temperatures found during the preliminary tests is compared to the room test curves in Figure 3-28.

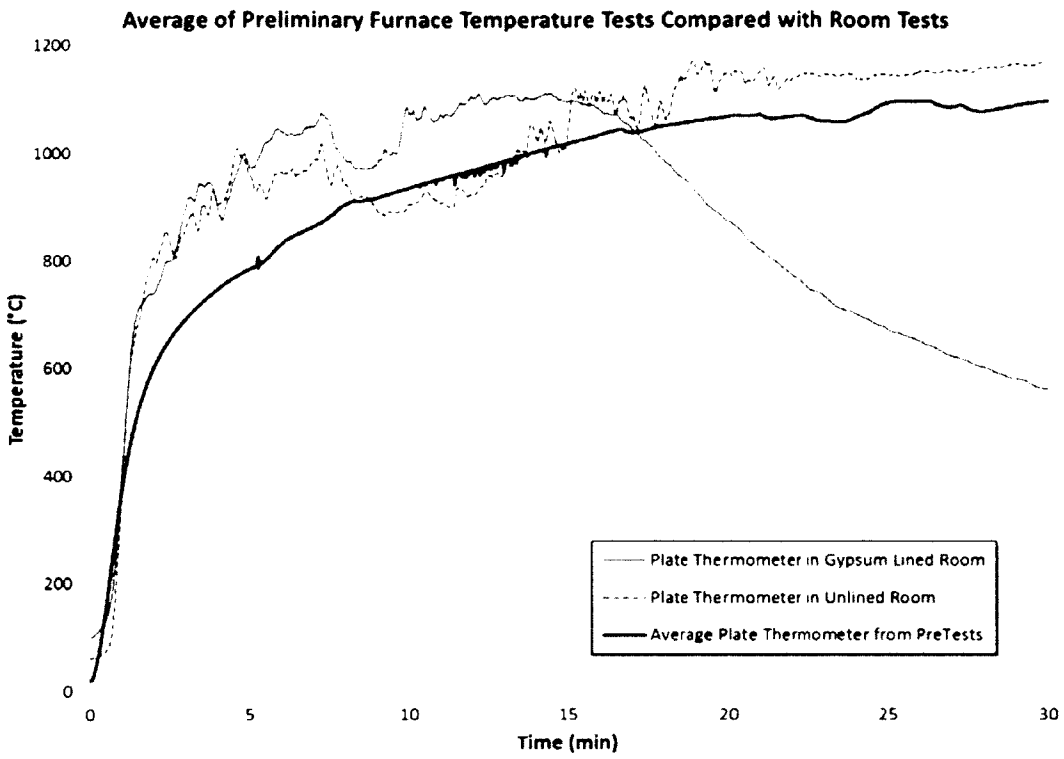

Figure 3-28: Average plate thermometer temperature from three preliminary tests compared with two CLT room tests

While this is not the ideal growth rate for simulating the room fire tests, this was the best fire curve possible with the medium-scale furnace. The non-standard fire was developed based on this curve.

3.5.2 Non-Standard Time-Temperature Curve

The curve was fitted to the preliminary test data for the first 24 minutes, up to a temperature of 1100°C. Steady burning was then simulated by holding the temperature at 1100°C for 12 minutes, as observed in both room tests. A decay phase was then formulated to drop from 1100°C to 300°C over a period of nearly two hours. The curve produced can be seen in Figure 3-29.

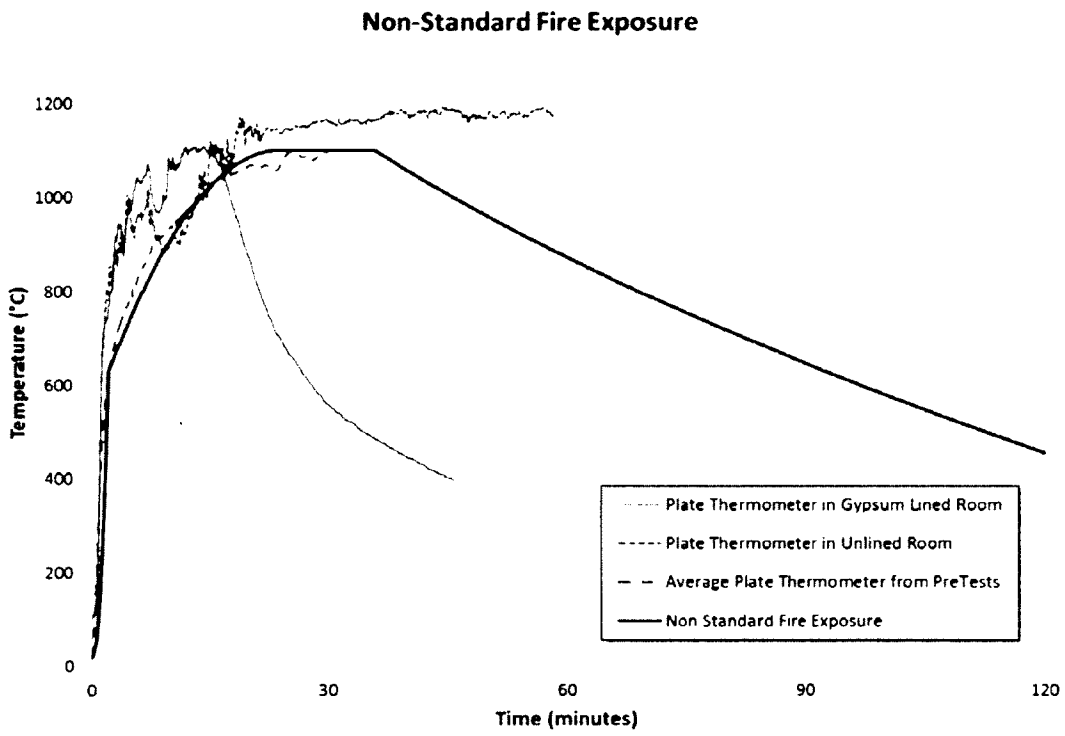

Figure 3-29: Non-standard design fire developed for CLT floor tests

The curve is defined by the following equations:

$$T = 126.446t^2 + 18 \qquad for\ 0 \leq t < 2.2 \qquad \text{Eq. 3.12}$$

$$T = 1100 - \left(\frac{t - 24}{1.005559}\right)^2 \qquad for\ 2.2 \leq t < 24 \qquad \text{Eq. 3.13}$$

$$T = 1100 \qquad for\ 24 \leq t < 36 \qquad \text{Eq. 3.14}$$

$$T = 1881.12 - 130.186\sqrt{t} \qquad for\ 36 \leq t \leq 200 \qquad \text{Eq. 3.15}$$

3.6 Test Procedure

All eight tests were conducted in a similar manner. Once the panels were instrumented and, if necessary, gypsum board(s) fixed, the assemblies were hoisted onto the furnace. The edges around the furnace and specimen were packed with Fiberfrax blankets to prevent flames from impinging on the sides of the specimen during the test. The preload was then incrementally applied, as per CAN/ULC-S101 [5] loading requirements, and left

to settle for at least 30 minutes before the start of the test. Once all equipment and data recording was checked, the burners were ignited (Figure 3-30) and the temperature in the furnace was controlled by switching them on and off in order to follow the desired fire time-temperature curve, shown in Figure 3-31 and Figure 3-32.

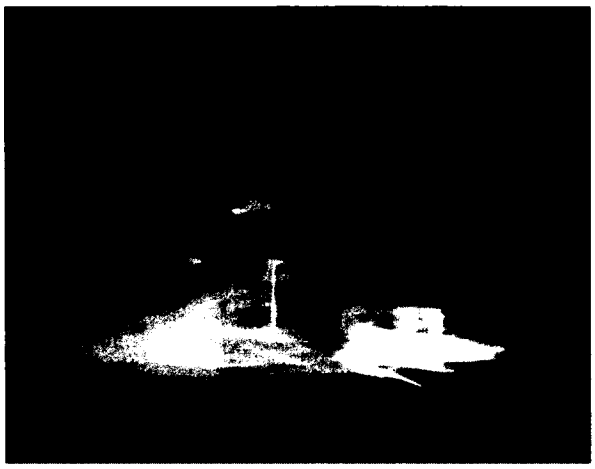

Figure 3-30: Image of the inside of the furnace with thermocouples visible during the first few minutes of a 3-ply test with 2 layers of gypsum

The average temperature inside the furnace was calculated at one second intervals from the five centermost thermocouples of the six installed and graphed on a monitor in real-time in order to ensure the curve was followed correctly. Requirements for standard testing set out in CAN/ULC S101 [5]; the accuracy of the furnace temperature must be controlled such that the area under the averaged time-temperature curve must be within ±7.5% of the corresponding area under the standard time-temperature curve for tests over 1 hour and not more than 2 hour, and ±5% for tests exceeding 2 hours. Plate thermometers were used to measure temperatures during the first 10 minutes of all non-standard fire-resistance tests since the temperature initially increases much more rapidly than the standard fire curve. During the first few minutes of exposure, shielded thermocouples report lower temperatures than plate thermometers, as

reported by Sultan [51]. This is also evidenced during testing and illustrated in Figure 3-32.

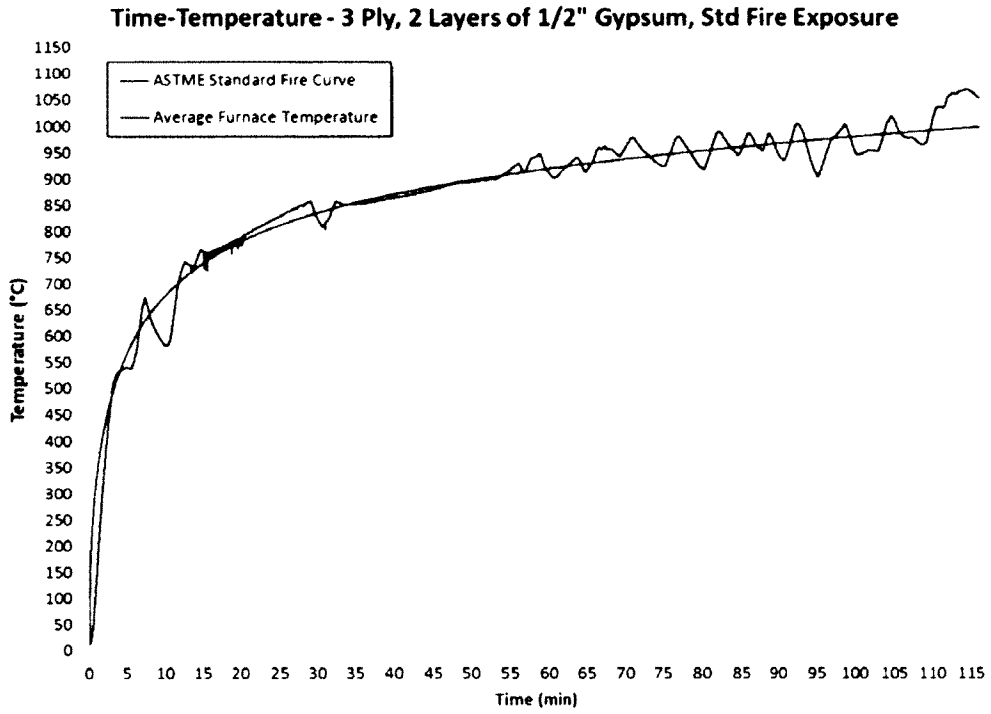

Figure 3-31: Standard time-temperature fire curve and average furnace temperature for a 3-ply test

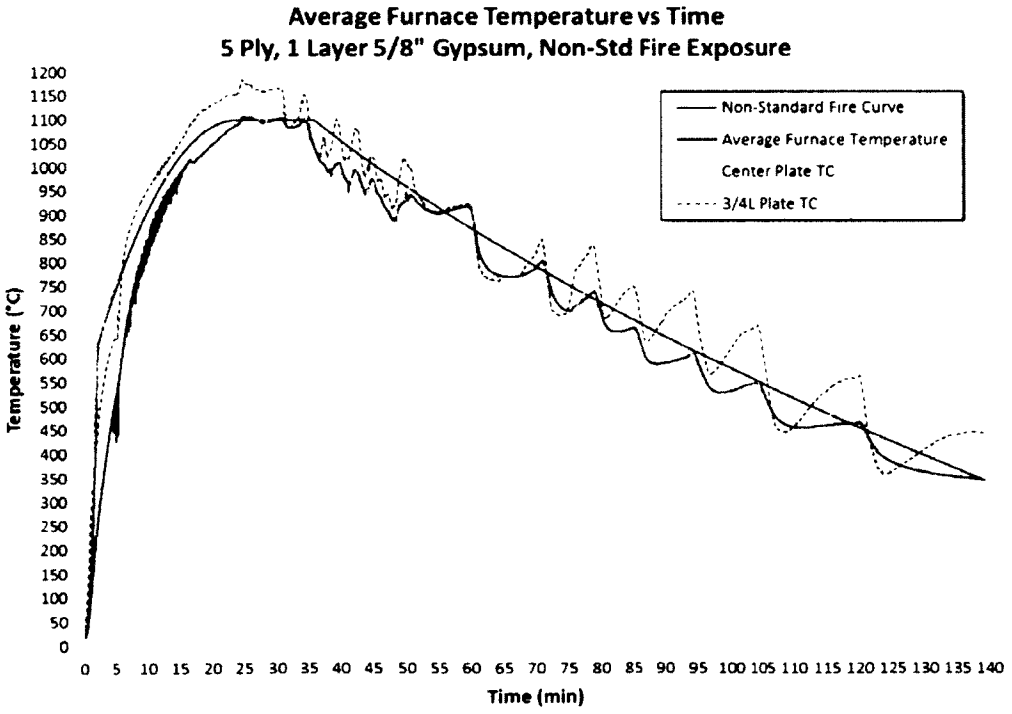

Figure 3-32: Non-standard time-temperature fire curve and average furnace temperature for 5-ply test

During the decay phase of the non-standard fire, water was intermittently sprayed onto the bottom of the furnace in order to reduce and control the temperature.

Deflection and load data were recorded and monitored in a similar fashion to temperature. A relatively constant load was maintained by manually pumping a hydraulic jack throughout the entire test as demonstrated in Figure 3-33.

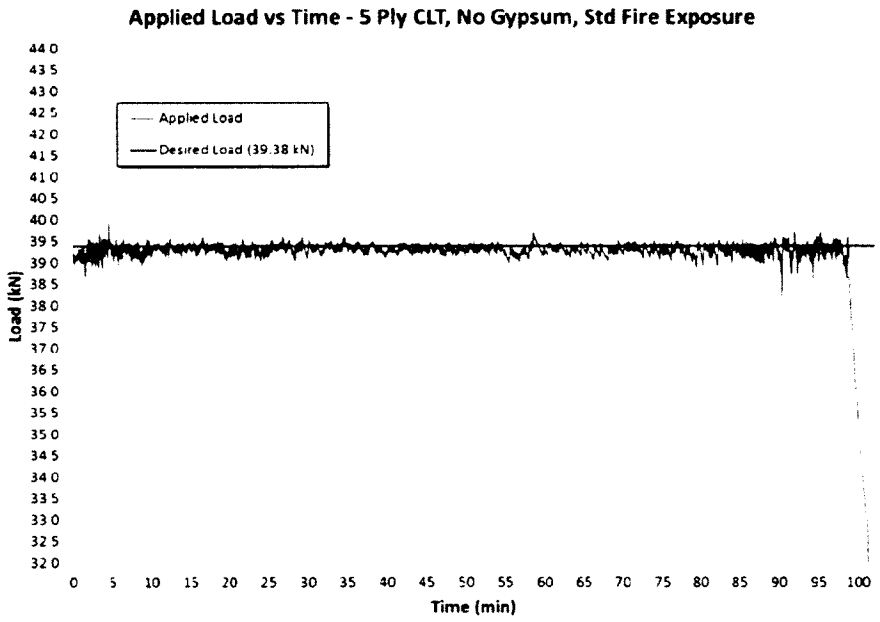

Figure 3-33: Graph of load applied to 5-ply panel

Tests were continued as long as possible, however, no test was ever taken to structural failure due to safety concerns for the furnace, equipment, and researchers if the panel were to collapse. Tests were ended if deflections in the panel increased to a point where it threatened to damage the thermocouples inside the furnace, such as in Figure 3-34. If a rapid increase in deflection was observed combined with the sound of the panel cracking, the test was ended since it was likely that structural failure was imminent.

Figure 3-34: 3-ply panel without gypsum protection, moments before load was removed due to excessive deflection with estimated total center deflection denoted

Once a test was considered ended, the load was removed, but burners were kept running to continue following the time-temperature curve. This was done to allow further collection of temperature data and gain additional insight into charring trends and ply layer fall-off behaviour.

After enough data was deemed collected, burners were turned off and panels were extinguished and removed from the furnace (Figure 3-35). The furnace was cleared of all debris from falling gypsum board and charred wood and any damaged equipment was repaired and tested before the next experiment.

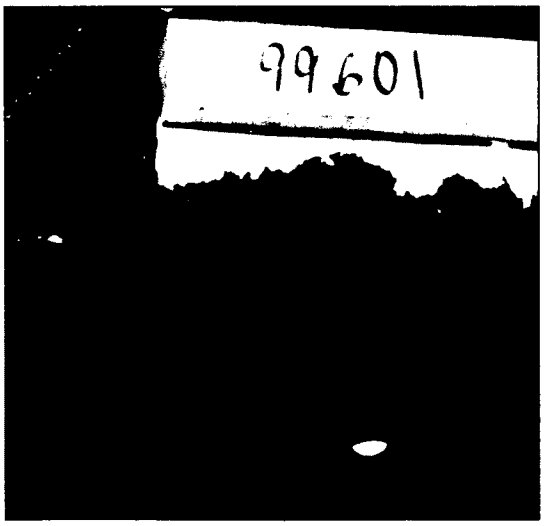

Figure 3-35: 3-ply panel with 2 layers of gypsum lifted off of furnace after test and extinguishment

4 Medium-Scale Test Results and Discussion

The results of the 3-ply and 5-ply tests conducted with the medium-scale furnace are listed in Table 4-1 and Table 4-2:

Table 4-1: Results from medium-scale 3-ply tests

# of Plies	Type X Gypsum Protection	Fire	Load Criteria	Applied Load* (kPa)	Load Ratio	Test Ended
3	Unprotected	CAN/ULC	L/240	2.86	29%	46min
3	1x 5/8"	CAN/ULC	L/240	2.75	29%	74min
3	2x 1/2"	CAN/ULC	L/240	2.68	29%	92min
3	2x 1/2"	Non-Std	L/240	2.68	29%	93min

Table 4-2: Results from medium-scale 5-ply tests

# of Plies	Type X Gypsum Protection	Fire	Load Criteria	Applied Load* (kPa)	Load Ratio	Test Ended
5	Unprotected	CAN/ULC	L/240	11.7	47%	99min
5	Unprotected	Non-Std	L/240	11.9	48%	101min
5	1x 5/8"	CAN/ULC	L/240	11.8	47%	115min
5	1x 5/8"	Non-Std	L/240	11.8	47%	122min

** 4-point loading for L/240 deflection actually applied in tests; Equivalent uniformly distributed load listed for comparison purposes*

4.1 Gypsum Boards

Gypsum boards fixed to assemblies were monitored throughout tests via video camera, as shown in Figure 4-1. Observations made are compared to temperature data from the back surface of each board at three different locations to determine failure times.

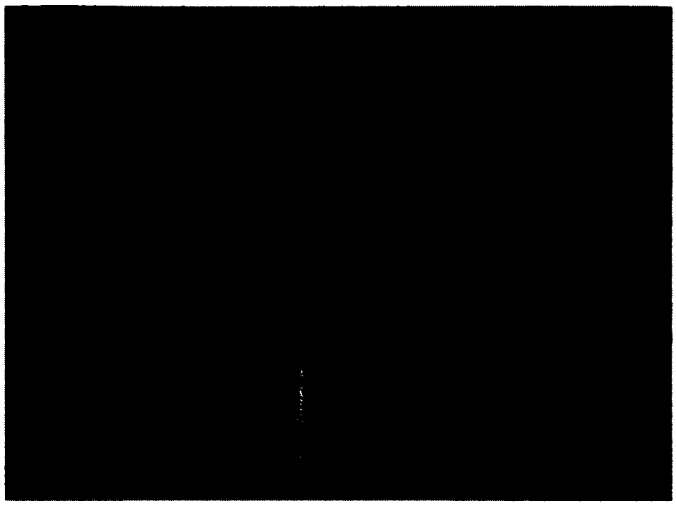

Figure 4-1: Video snapshot of 3-ply panel with 2 layers of ½" (12.7 mm) gypsum as first layer begins to fall after around 52 min

A sudden rise in temperature on the unexposed side of each board was adopted as criteria for determining when gypsum boards had fallen off, as discussed by Sultan [38]. This trend is easily detectable as the thermocouples become exposed to the fire, as shown in Figure 4-2.

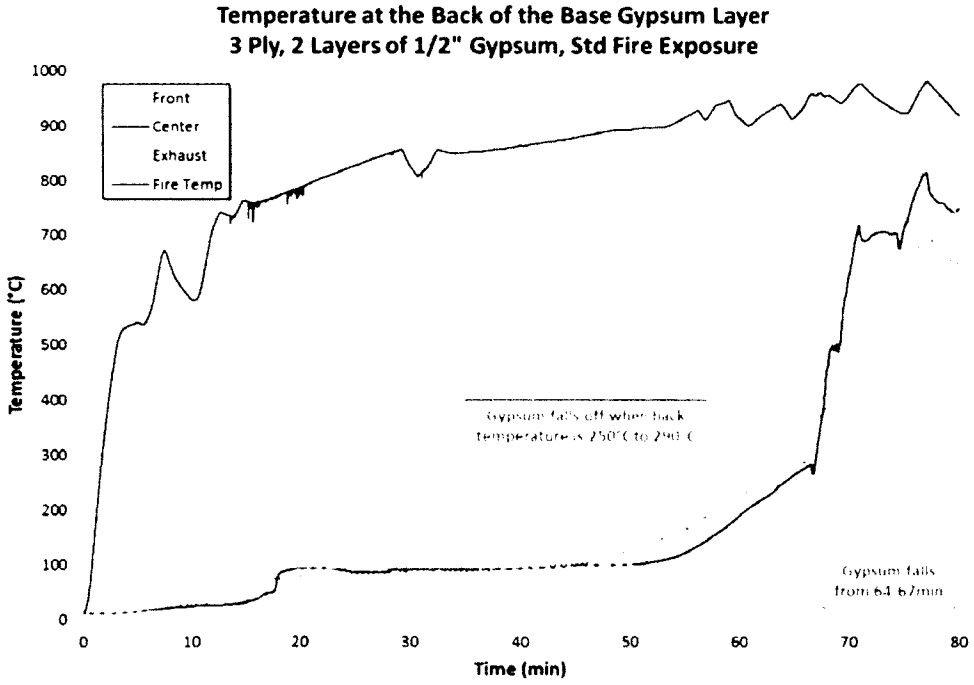

Figure 4-2: Temperature at the back of the base gypsum layer of a 3-ply with 2 layers of ½" gypsum

Gypsum boards never fell off the specimen all at once and would fall off in pieces over a period of a few minutes, similar to fire-resistance tests with gypsum protection, as documented in the literature. Times associated with each spike in temperature are recorded and summarised in Table 4-3.

Table 4-3: Gypsum failure times and temperatures

# of Plies	Type X Gypsum Protection		Fire	Face Gypsum Board			Base Gypsum Board		
				Failure Time (min)	Failure Temp (°C)	Finish Rating (min)	Failure Time (min)	Failure Temp (°C)	Finish Rating (min)
3	1x	5/8"	CAN/ULC	-	-	-	44-50	340-390	24
3	2x	1/2"	CAN/ULC	48-53	190-334	28	64-67	250-290	55
3	2x	1/2"	Non-Std	21-37	170-220	21	78-87	410-480	42
5	1x	5/8"	CAN/ULC	-	-	-	36-39	273-330	23
5	1x	5/8"	Non-Std	-	-	-	16-31	145-300	17

The Gypsum Association [44] defines the finish rating of gypsum boards similarly to the method used in ASTM E119 [6] to establish insulation failure during standard fire-resistance tests. The finish rating is the shorter of the time taken for an average rise in temperature of 140°C, or a maximum rise of 180°C at a single point to occur, as measured at the back (unexposed) surface of the gypsum board.

4.1.1 Comparison of Medium- and Full-Scale Gypsum Board Performance

All gypsum boards used in both the medium and full-scale testing were Type X Firecode boards manufactured by CGC Inc. [18]. The boards used in the medium-scale tests were from the same manufacturer, but from a different batch than the boards used in the full-scale tests, i.e. manufactured at different times.

Gypsum boards in the medium-scale tests typically fell off around 5-10 minutes earlier than was observed in full-scale testing. Fall-off temperatures observed in the medium-scale standard fire tests were much lower than full-scale temperatures, ranging from 190°C to 390°C with an average fall-off temperature of 300°C. Full-scale test temperatures ranged from 350°C to 700°C with an average temperature of 630°C.

When comparing gypsum board finish ratings, medium-scale boards tended to exhibit longer finish ratings than full-scale boards, as listed in Table 4-4. Indicating that gypsum in the medium-scale furnace heated more slowly during the initial stages of the fire, yet still experienced sooner fall-off at lower temperatures. The exception is the 5/8" (15.9 mm) board in the 5-ply medium-scale test that lasted 11 minutes longer than the full-scale test, although both of these boards were deemed to have fallen sooner than was expected.

Table 4-4: Comparison of medium- and full-scale gypsum average failure times and finish ratings

# of Plies	Type X Gypsum	Face Gypsum Board				Base Gypsum Board			
		Medium-Scale		Full-Scale		Medium-Scale		Full-Scale	
		t_f (min)	FRa (min)	t_f (min)	FRa (min)	t_f (min)	FRa (min)	t_f (min)	FRa (min)
5	1x 5/8"	-	-	-	-	37	23	26	22
3	1x 5/8"	-	-	-	-	47	24	52	21
3	2x 1/2"	51	28	65	15	66	55	77	46

t_f: *Average failure time*, **FRa**: *Finish Rating*

In both 5-ply tests, the 5/8" (15.9 mm) board was expected to remain in place as long as the 5/8" (15.9 mm) panel in the 3-ply tests, at around 50 minutes. In the medium-scale test, it was believed that the gypsum fell off prematurely due to insufficient insulation protection around the edges of the furnace. In all medium-scale tests, Fiberfrax

insulation packed around the edges of the specimen in the furnace prevented heat from penetrating the sides of the wood or beneath the gypsum. However, as illustrated in Figure 4-3 to Figure 4-6, this was likely to have occurred. Heat penetrating the edge of the assembly caused the wood to catch fire, shown in Figure 4-3. After 20 minutes, intensified heating between the board and panel caused the gypsum here to weaken faster than other sections of the board. The degraded section of gypsum at that edge came free of its fastenings and fell-off prematurely. This began a chain of events that caused the entire board to fall-off; adjacent gypsum, which still maintained some strength, was pulled down with the weakened piece, further exposing more wood, which was then ignited causing more gypsum fall-off. After the test, it was apparent from the excessive charring at that location (Figure 4-6), that that section of the panel was insufficiently protected with Fiberfrax blankets.

Observations made during the similar full-scale test indicate the gypsum failed from the corner first, yet no further specifics were listed, other than that it was expected to remain in place much longer [17]. Interestingly though, the finish ratings of both these boards are consistent with both 3-ply medium- and full-scale 5/8" (15.9 mm) gypsum board tests. This would indicate that the gypsum was not damaged or faulty and performed as expected for the first 20 minutes of fire exposure.

Figure 4-3: Video snapshot of 5-ply panel with 1 layer of gypsum showing initial flaming beneath gypsum at right edge after 11 min.

Figure 4-4: Video snapshot of 5-ply panel with 1 layer of gypsum showing significant flaming beneath gypsum at right edge after 23 min.

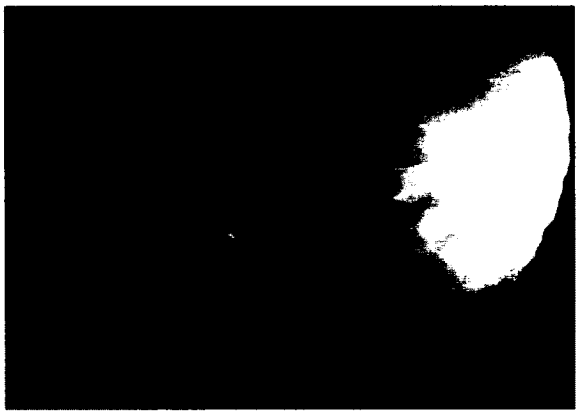

Figure 4-5: Video snapshot of 5-ply panel with 1 layer of gypsum showing intense flaming beneath gypsum at right edge after 35 min. just before panel fell

Figure 4-6: 5-Ply Panel after test revealing significant charring at right edge of panel

A plateau observed in all gypsum time-temperature graphs at 100°C, shown in Figure 4-8 to Figure 4-18, indicates that heat flux into the board was absorbed by the liberation and evaporation of bound water molecules [41]. During similar medium- and full-scale tests, this plateau appears to begin and end at consistent times. However, after all water has evaporated from the boards, it is clear that different heating rates in the boards occur depending on the furnace, the slower of which being in the medium-scale

furnace. This could be the result of numerous different factors; the size of the combustion chamber in the furnaces, the rate of hot gases being exhausted, the proximity of the burners to the specimen, the perimeter to surface area ratio of the gypsum boards, or the batch of gypsum boards themselves. Without a much larger test series, it is difficult to determine which one, or combination of these factors, played a significant role in the discrepancy in gypsum board performance.

Overall, gypsum boards performance was consistent until the dehydration reaction in the gypsum board was complete. After this point gypsum performance did not show completely consistent results between medium-scale and full-scale testing. Gypsum boards in medium-scale tests exhibited a trend of longer finish ratings and shorter failure times than those found in full-scale tests. These trends are illustrated in Figure 4-8 to Figure 4-15. Although temperatures in both furnaces were maintained to a similar standard, it is believed that the main cause of the shorter failure times was attributed to the larger perimeter to surface area ratio of specimens in medium-scale tests then in the full-scale tests. Insulation protection around the edges of the panels does not offer total protection from heat penetration on the sides of the panel and flaming was observed to occur on the sides of all medium-scale test panels before tests were deemed finished. This was confirmed by the presence of char that had formed on the sides of all test panels after they were removed from the furnace. Due to the higher perimeter per square meter of surface area in the medium-scale tests, panels were more vulnerable to heat entering the sides of the panel, causing the wood above the

gypsum boards to be heated at a faster rate than if only the bottom surface was exposed. This was likely the cause of the earlier gypsum failure.

The following graphs illustrate the temperature at the back of gypsum boards in both medium- and full-scale tests throughout fire exposures. In full-scale tests, Q1 – Q4 indicate the location of thermocouples on the panels, as illustrated in Figure 4-7.

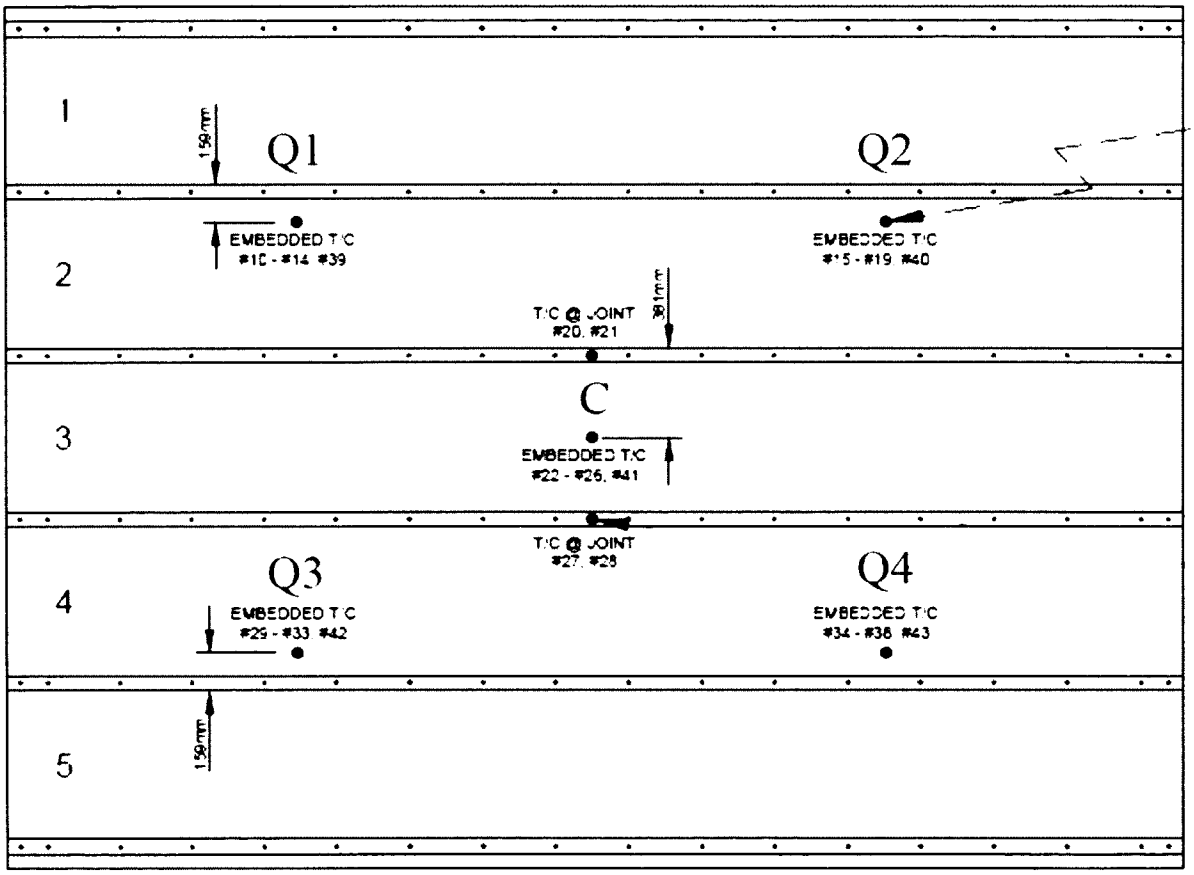

Figure 4-7: Location of thermocouples on full-sale test panels (reproduced from [17])

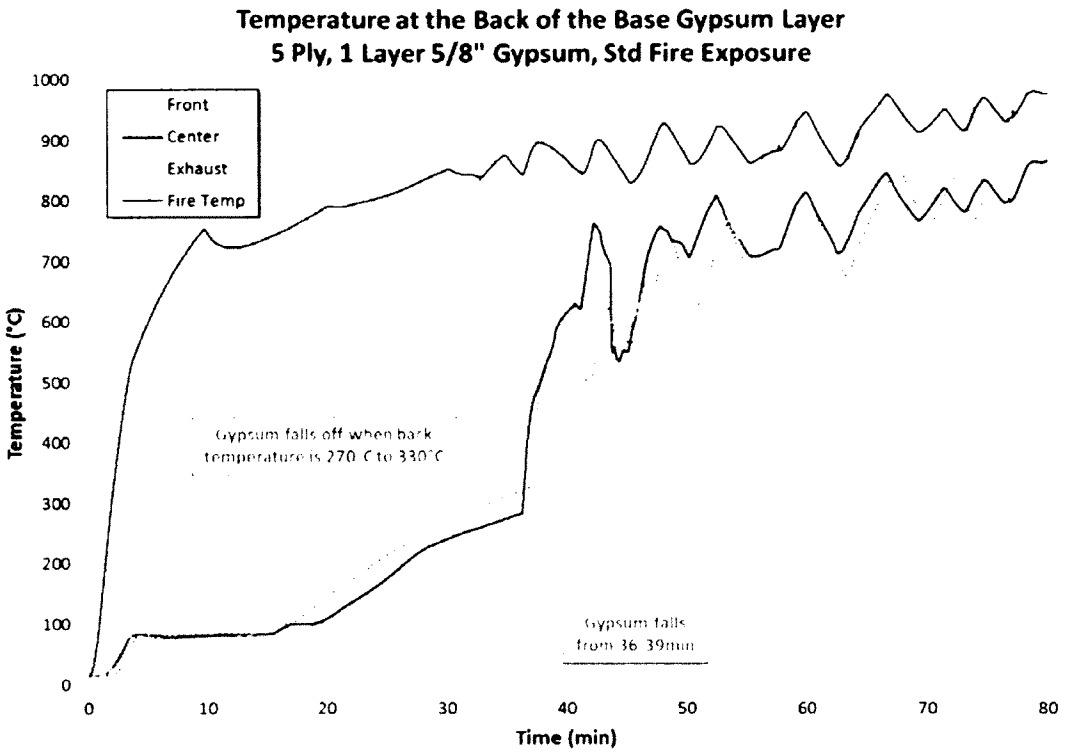

Figure 4-8: Temperatures behind gypsum for medium-scale 5-ply floor with 1 layer of 5/8" (15.9 mm) gypsum

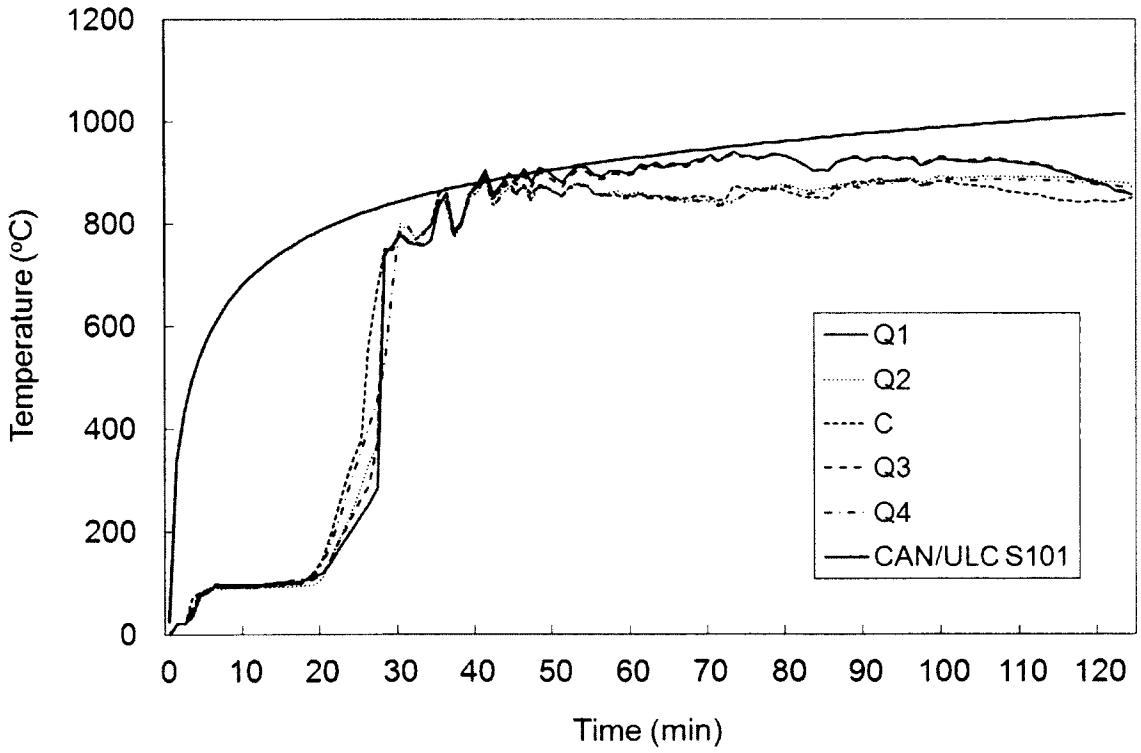

Figure 4-9: Temperatures behind gypsum for full-scale 5-ply floor with 1 layer of 5/8" (15.9 mm) gypsum

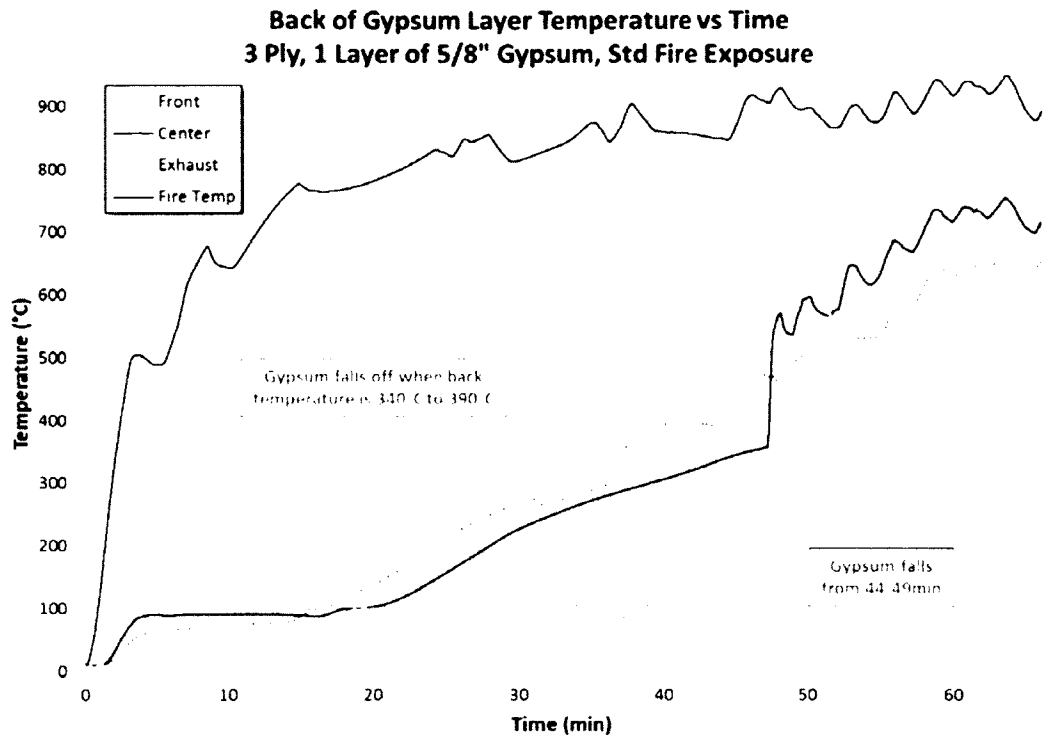

Figure 4-10: Temperatures behind gypsum layer for medium-scale 3-ply floor with 1 layer of 5/8" (15.9 mm) gypsum

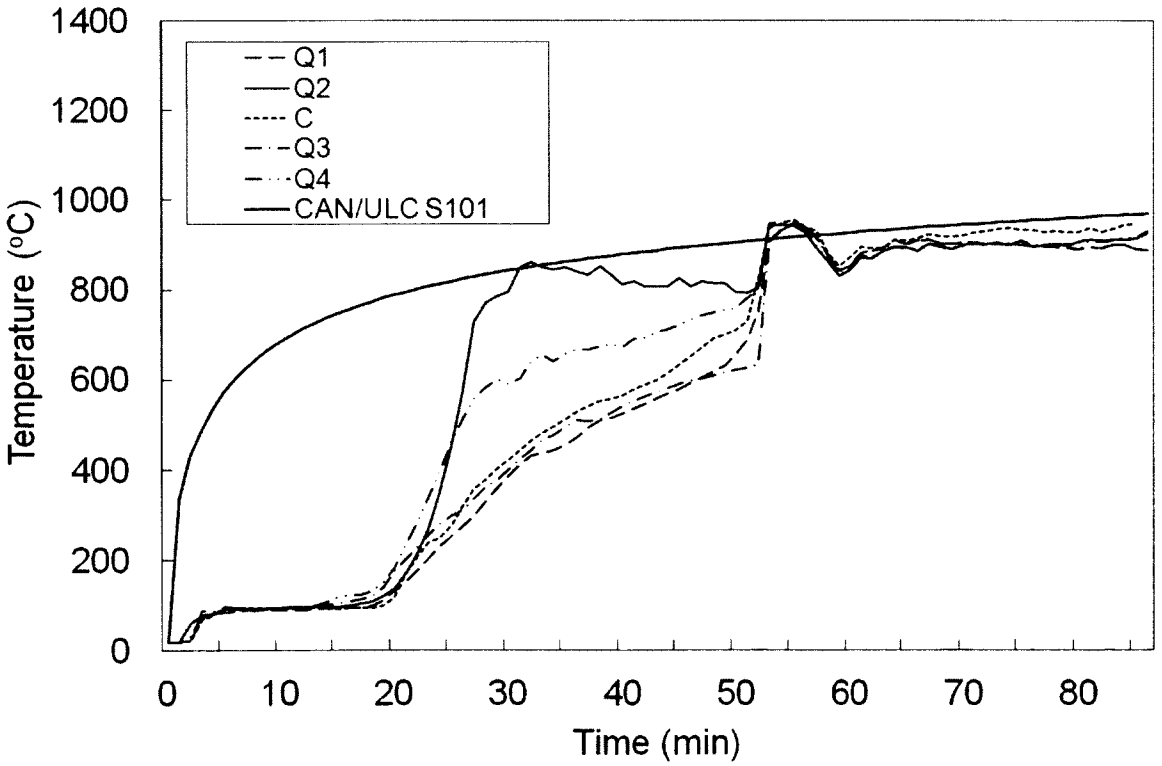

Figure 4-11: Temperatures behind gypsum for full-scale 3-ply floor with 1 layer of 5/8" (15.9 mm) gypsum

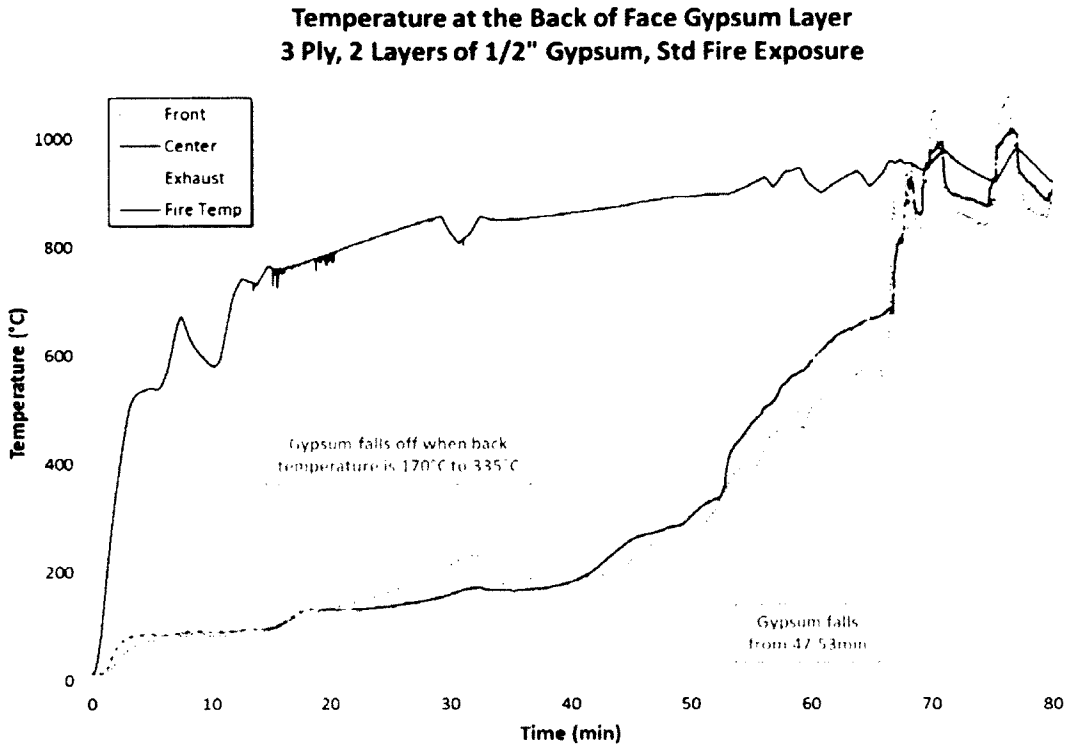

Figure 4-12: Temperatures between gypsum layers for full-scale 3-ply floor with 2 layers of ½" (12.7 mm) gypsum

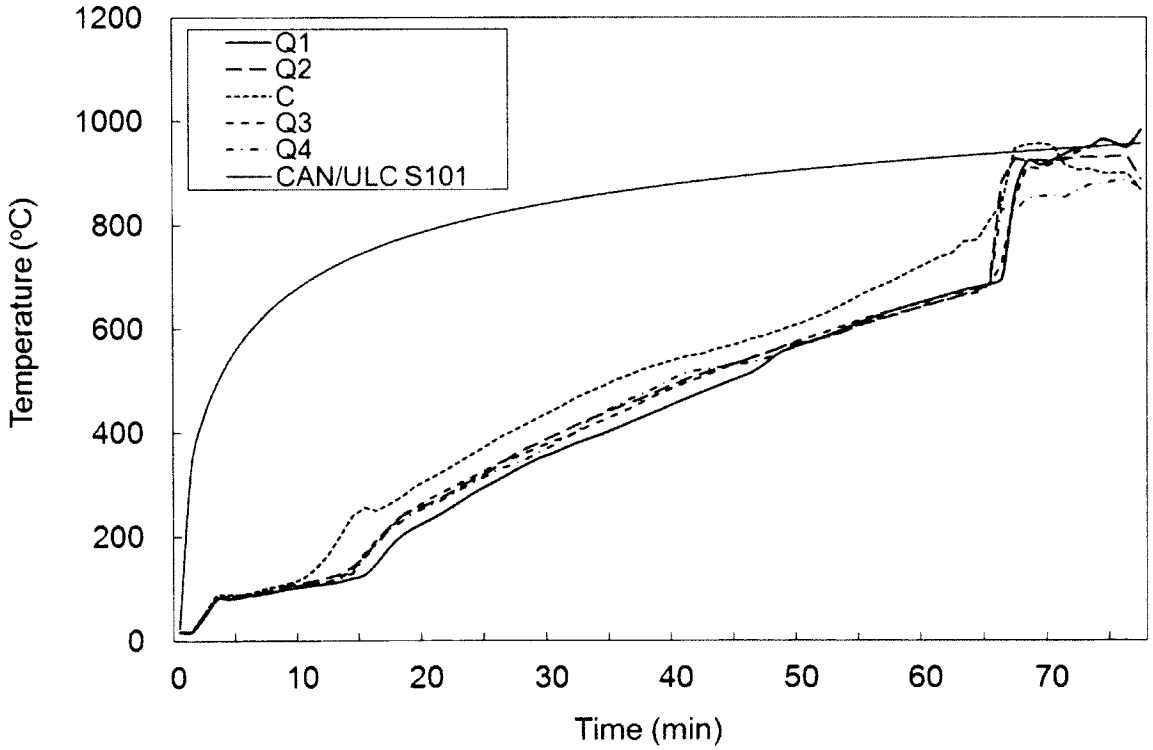

Figure 4-13: Temperatures between gypsum layers for full-scale 3-ply floor with 2 layers of ½" (12.7 mm) gypsum

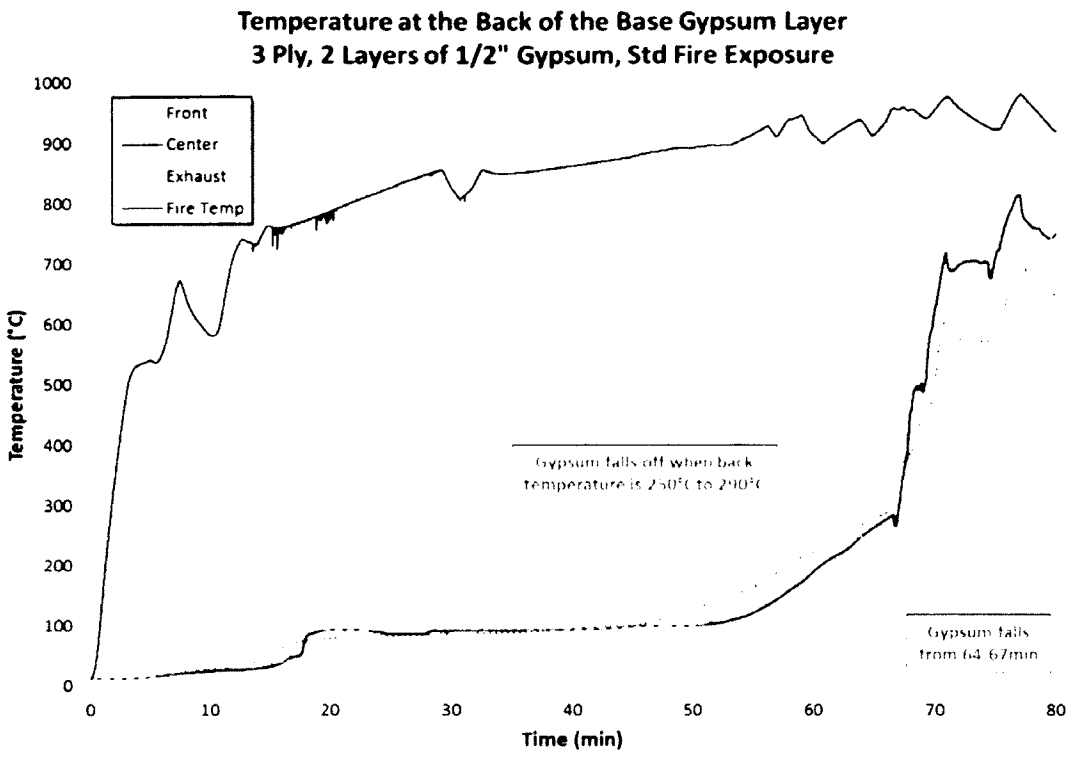

Figure 4-14: Temperatures behind base gypsum layer for medium-scale 3-ply floor with 2 layers of ½" (12.7 mm) gypsum

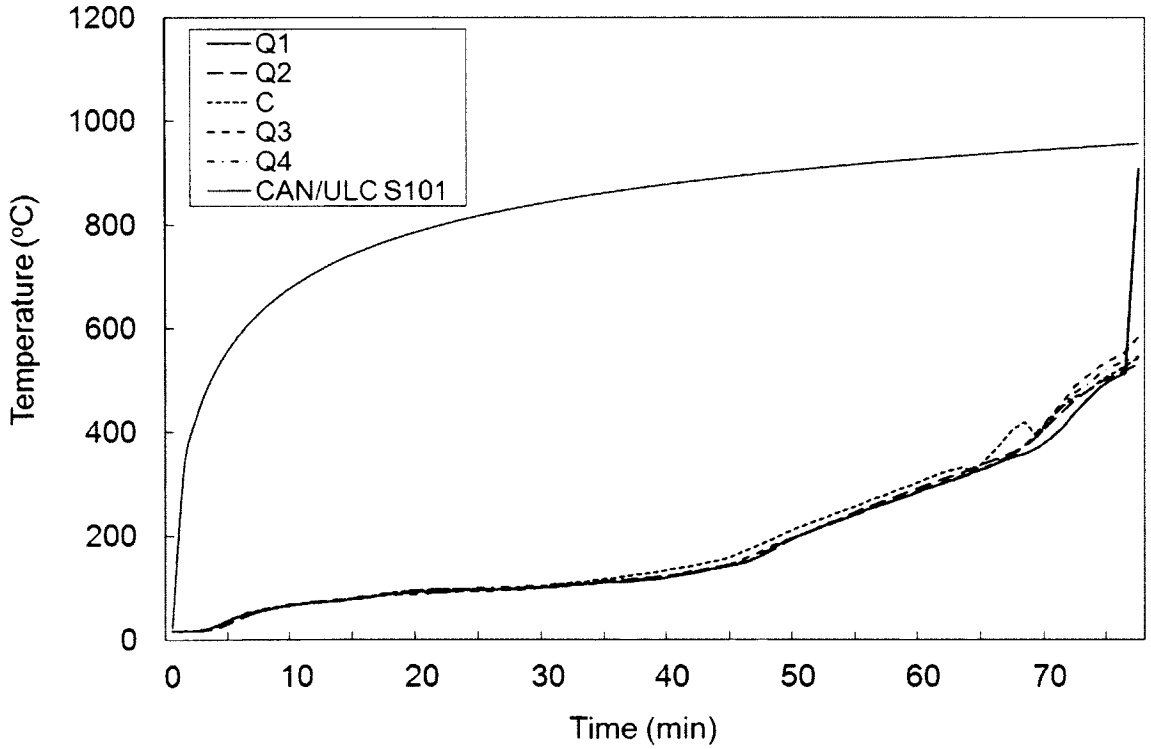

Figure 4-15: Temperatures behind base layer for full-scale 3-ply floor with 2 layers of ½" (12.7 mm) gypsum

4.1.1 Comparison of Standard and Non-Standard Fires

Gypsum boards exposed to the initially more intense non-standard fire, did not perform as well as the gypsum boards exposed to the standard fire. Boards exposed to the initial growth phase of the non-standard fire experienced shorter failure times and finish ratings, as well as lower fall-off temperatures. However, in the 3-ply double-layer test, the base board remained in place much longer in the non-standard fire than in the standard fire exposure, shown in Table 4-3. The base board in this test was not exposed to the fire until over an hour had passed. By this time the non-standard fire had entered the decay phase and the board was exposed to much lower temperatures than the standard fire, resulting in a slower calcination reaction rate, allowing it to remain in place much longer.

During non-standard tests, gypsum failure at one end of the furnace would occur around 15 minutes before it fell at the other end. This is explained by the non-uniform temperature observed across the length of the medium-scale furnace during non-standard fires. The furnace involved four burners in the front half and two burners in the exhaust half. When running all six burners at full capacity, as required for the design fire, the front of the furnace tended to have much higher temperatures, measured at up to 200°C higher than at the exhaust during the first 30 minutes of testing, as shown in Figure 4-16.

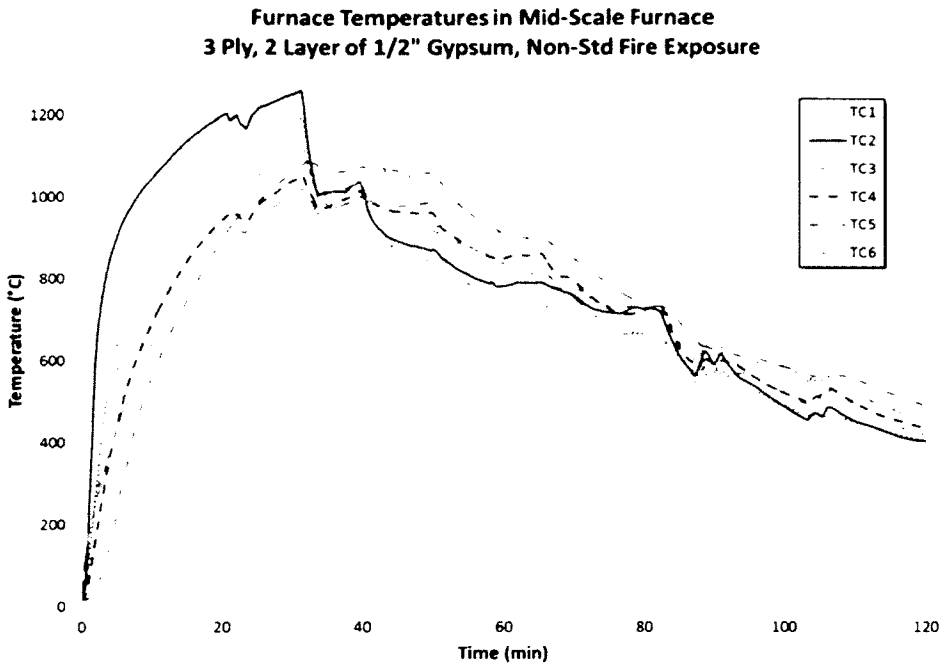

Figure 4-16: Furnace temperatures during non-standard fire exposure

This inconsistency caused gypsum at the front of the furnace (furnace thermocouples TC1 – TC3) to fail sooner than gypsum at the exhaust end of the furnace (TC4 – TC6), shown in Figure 4-17 and Figure 4-18.

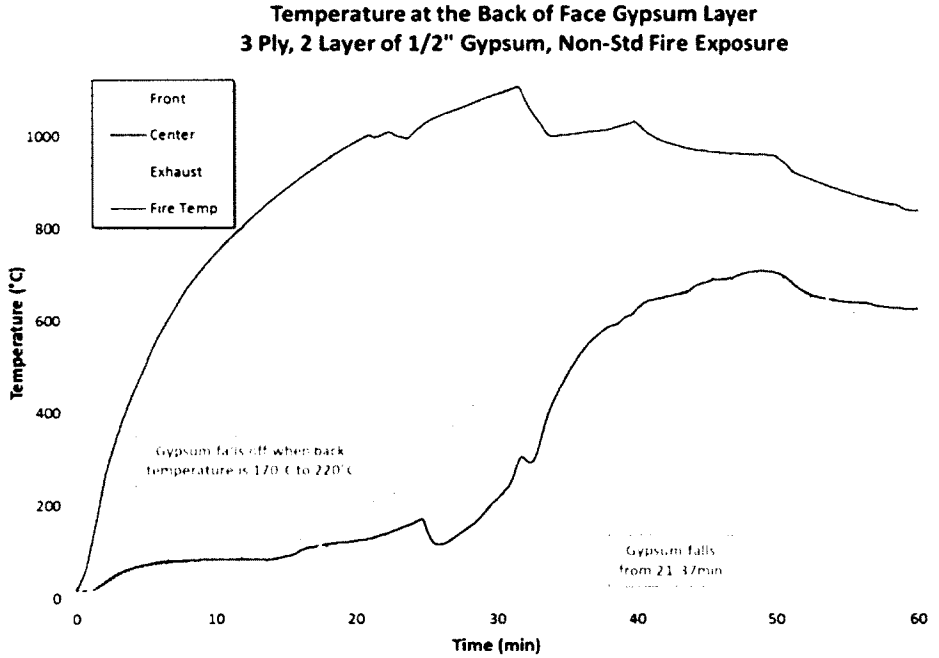

Figure 4-17: Temperature at back of face gypsum layer in 3-ply, 2-layer gypsum, non-standard fire test

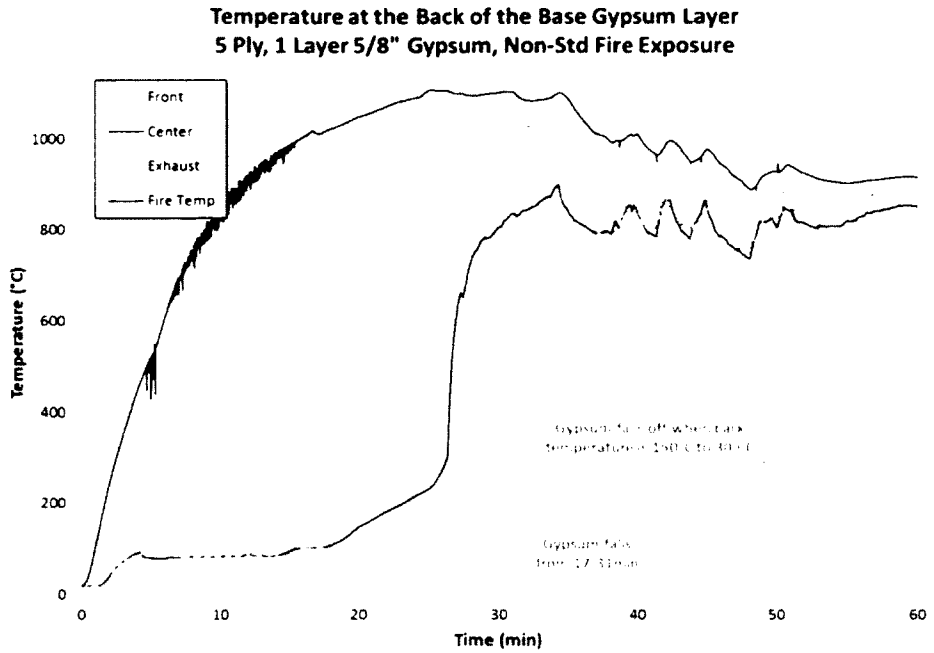

Figure 4-18: Temperature at back of base gypsum layer in 5-ply, 1-layer gypsum, non-standard fire tests

4.1.3 Gypsum Boards on CLT Panels

From data gathered by Sultan [38] regarding 80 full-scale, standard floor tests on a variety of floor assemblies; one layer of 15.9 mm Type X gypsum board typically endures around 40 minutes of exposure, while two layers of 12.7 mm Type X gypsum typically lasts around 65 minutes (though both of these times are subject to a large degree of variance, up to 20 minutes in extreme cases).

The average failure times of the gypsum boards during the standard fire tests fall within the normal spectrum of fall-off times found by Sultan, listed in Table 4-5. While test data from medium-scale gypsum lined CLT tests are not identical to full-scale CLT test data, it still provides some evidence that both sets of data appear to fall within times observed in common practices. Further, this demonstrates that gypsum boards fastened to CLT

floor panels are likely to behave very much the same as they do when fastened to other varieties of light frame floor assemblies.

Table 4-3: Average gypsum fall-off times in medium-scale tests

# of Plies	Type X Gypsum Protection	Fire	Face Gypsum Board Failure Time (min)	Base Gypsum Board Failure Time (min)
3	1x 5/8"	CAN/ULC	-	47
3	2x 1/2"	CAN/ULC	51	66
3	2x 1/2"	Non-Std	21-37	78-87
5	1x 5/8"	CAN/ULC	-	37
5	1x 5/8"	Non-Std	-	16-21

4.2 Ply Delamination

Adhesive failure and ply delamination were found to occur once the temperature at the back of each ply increased to around 200°C. Plies would not fall off as one layer all at once, but rather broke off in very small pieces at first, on the order of a few centimeters, which gradually increased in size as more pieces fell. This resulted in a period of time for each ply delamination that lasted several minutes. Ply delamination likely occurred in this way due to the lack of edge glue between individual pieces of lumber in Nordic constructions. Floors used in this test series incorporated face glue only, thus once the glue on the face of a specific piece of lumber failed, it was free to fall from the panel.

Ply fall-off was determined through visual monitoring via the video camera, shown in Figure 4-19, and temperature data recorded at three locations at the back of each ply.

Figure 4-19: Video snapshot of a 5-ply test without gypsum protection showing large pieces of the first ply layer falling off (circled)

Similar to gypsum failure, the time at which ply layers delaminated could also be associated with a sudden increase in temperature at the back of the ply due to thermocouples suddenly becoming exposed to the fire, shown in Figure 4-20.

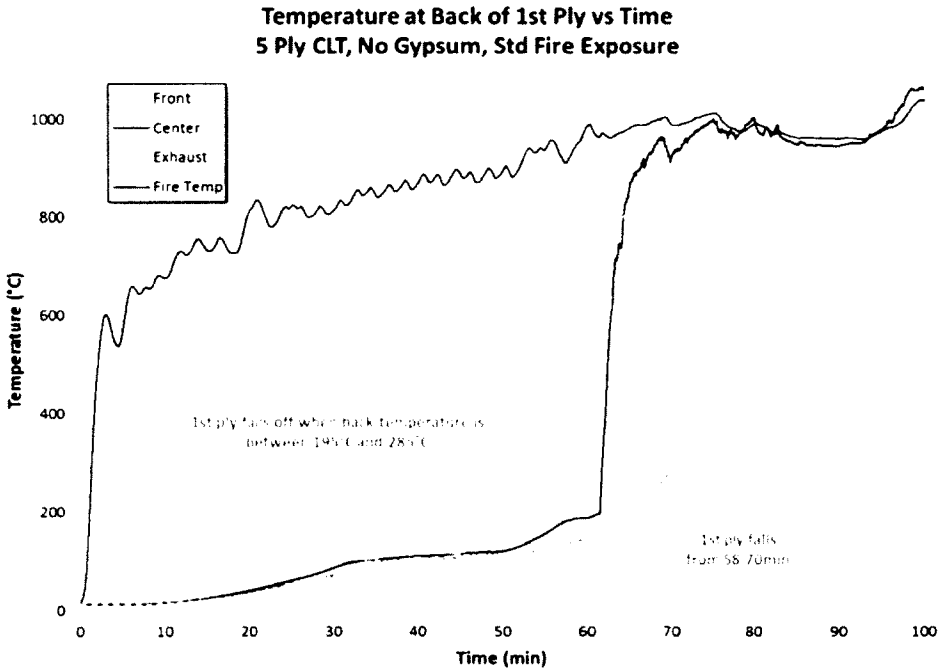

Figure 4-20: Temperature at the back of the first ply layer of a 5-ply panel without gypsum protection

The times and accompanying temperatures before a spike occurred at the back of each ply are summarised in the Table 4-6.

Table 4-6: Ply Layer Fall-Off Times and Temperatures

# of Plies	Type X Gypsum Protection	Fire	First Ply Fall-Off Time (min)	First Ply Fall-Off Temp (°C)	Second Ply Fall-Off Time (min)	Second Ply Fall-Off Temp (°C)
3	Unprotected	CAN/ULC	64-65	195-305	-	-
***3**	1x 5/8"	CAN/ULC	-	-	-	-
3	2x 1/2"	CAN/ULC	107-111	180-220	-	-
3	2x 1/2"	Non-Std	-	-	-	-
5	Unprotected	CAN/ULC	58-70	195-285	87+	205+
5	Unprotected	Non-Std	38-53	200-480	-	-
5	1x 5/8"	CAN/ULC	79-82	170-260	115+	140+
5	1x 5/8"	Non-Std	53-80	200-240	-	-

** Test was ended and burners turned off before any ply layers fell-off*
+ Indicates entire ply layer had not fallen off; complete data range was not found

In all tests, with the exception of the test marked with an (*), burners were left on to continue following the prescribed fire curve after the load was removed, in order to collect delamination data from ply layers still in place. In the non-standard 3-ply test with 2 layers of gypsum, no ply layer fell, since by the time both gypsum boards had fallen off, the fire temperature had decreased low enough that heat transfer to the adhesive was not sufficient to cause the first ply to delaminate.

4.2.1 Comparison of Medium- and Full-Scale Ply Delamination

Plies in all panels were 35 mm thick and used a one-part, polyurethane adhesive (PUR) between ply layers. The time that a ply layer was observed to begin falling off and the time when the layer had completely fallen off, are listed in Table 4-7 along with the associated temperature range measured at that interface. In the full-scale 3-ply tests

with 2 layers of gypsum, and the medium-scale 3-ply tests with 1 layer of gypsum, ply layers did not fall-off due to tests being ended prematurely. No standard full-scale, unprotected 3-ply test was conducted.

Table 4-7 Comparison of medium-scale and full-scale ply layer fall-off times and temperatures

# of Plies	Type X Gypsum	First Ply Layer				Second Ply Layer			
		Medium-Scale		Full-Scale		Medium-Scale		Full-Scale	
		t_f (min)	Temp (°C)	t_f (min)	Temp (°C)	t_f (min)	Temp (°C)	t_f (min)	Temp (°C)
3	-	64-65	195-310	-	-	-	-	-	-
3	1x 5/8"	-	-	78-81	160-200	-	-	-	-
3	2x 1/2"	107-111	180-220	-	-	-	-	-	-
5	-	58-70	195-285	60-65	195-280	87+	205+	92+	205+
5	1x 5/8"	79-82	170-260	73-87	190-235	115+	140+	107+	200+

t_f: *Time that ply began to fall off-time that layer had completely fallen off*
Temp: *Temperature range measured at interface over which ply layer fell off*
+ *Indicates entire ply layer had not fallen off; complete data range was not found*

Comparing equivalently protected 3-ply and 5-ply medium-scale and full-scale tests, both the first and second ply layers appeared to delaminate at roughly the same time. In all tests, first ply delaminations appeared to begin at around, or just before, the adhesive temperature had reached 200°C. Second ply delamination only occurred in the standard 5-ply tests. The adhesive between the second and third ply also failed at around, or just below 200°C. All four of these tests were ended before the entire second ply delaminated and the full time length and range of temperatures over which the delamination occurred was not able to be determined.

4.2.2 Ply Delamination in Unexposed Tests and Non-Standard Fires

Similar to gypsum board performance in the non-standard fire, plies began to delaminate earlier and over longer periods of time than plies observed in equivalent tests exposed to the standard fire. However, similar to standard tests, delaminations appear to begin at around, or just before, the adhesive temperature reaches 200°C. Small pieces of charred wood started to fall-off at the hotter front section of the furnace first in the non-standard fire tests due to a characteristic of the furnace. This is explained in greater detail in Section 4.1.2.

4.2.3 Ply Delamination in CLT

In all medium-scale and full-scale tests, a temperature plateau at the first ply interface was observed at 100°C and continued for about 15 minutes due to water evaporation in the surrounding wood. This occurrence was not as prominent at the second ply interface. Instead, a sudden decrease in the rate of temperature rise occurred once the temperature had reached 100°C, but the temperature then immediately began to climb again, rather than plateau. These incidents are displayed in Figure 4-21 and Figure 4-22. Most of the water around the second interface was likely driven off before the temperature had reached 100°C due to hygrothermal movement.

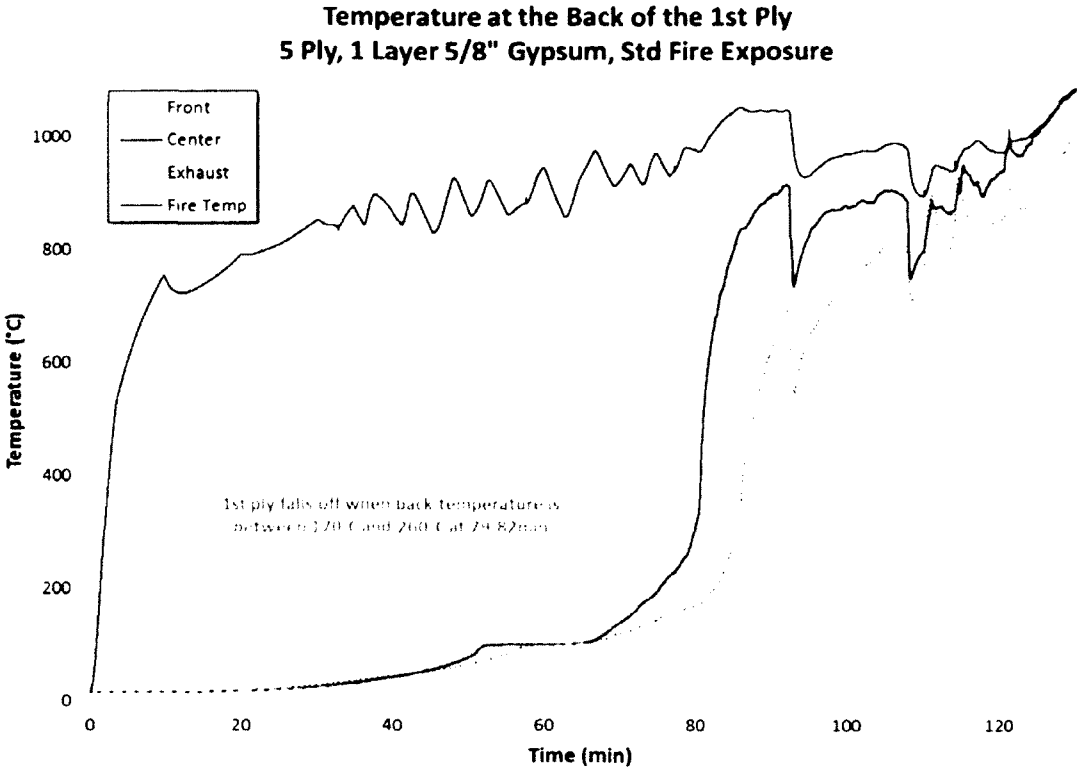

Figure 4-21: Temperature between 1st and 2nd ply in 5-ply, 1 layer gypsum standard test

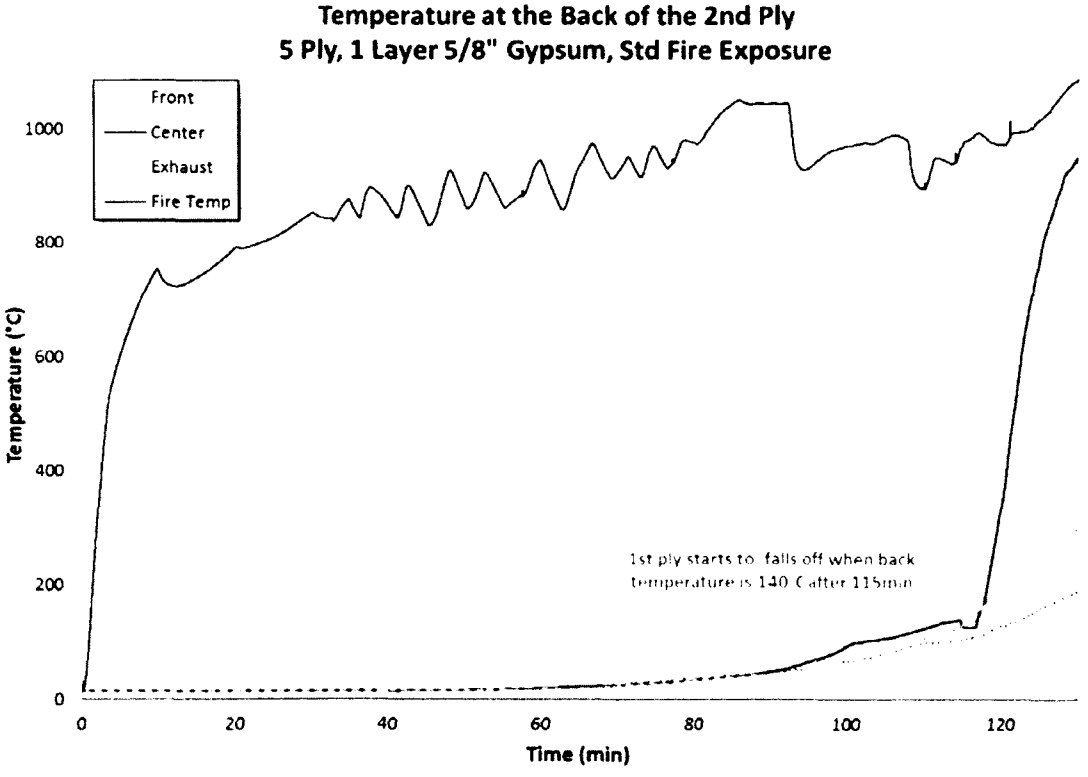

Figure 4-22: Temperature between 2nd and 3rd ply in 5-ply, 1 layer gypsum standard test

From observations in these experiments, it is evident that the polyurethane degradation was the underlying factor for ply delamination. In all tests, ply delamination began to occur at temperatures around 200°C. The average fall-off temperature calculated from temperatures found at the three thermocouple locations, in all tests, at both interfaces is 210°C.

4.3 Charring

Char is considered to have formed at a specific depth in the wood when the temperature reaches 300°C [8]. Thermocouples embedded at various depths in the panel provided time stamped temperature data, from which the time when charring began was determined. The average charring rate was calculated by dividing the depth to the exposed surface of each thermocouple by the difference in time from the start of charring at the surface of the panel, to when the temperature had reached 300°C at that depth. This is illustrated for a thermocouple 35 mm from the exposed surface in the equation below:

$$CR_{avg,35} = \frac{35}{t_{300,35} - t_{300,0}} \left[\frac{mm}{min}\right] \qquad \text{Eq. 4.1}$$

The average charring rates for every thermocouple depth in all tests are listed in Table 4-8. Panels exposed to the non-standard fire incorporated thermocouples at depth intervals of 8.75mm instead of 17.5mm to better capture the rapid heating that would occur from the growth phase of non-standard fire. Blank cells in the table indicate a depth for which there was either no thermocouple present or the temperature did not

reach 300°C. The onset of charring is the time at which charring began at the exposed surface of the panel after the burners had been ignited.

Table 4-6: Summary of Average Charring rate Calculated at Various Distances through Each Test

# of Plies		3	3	3	3	5	5	5	5
Type X Gypsum Protection		-	1x 5/8"	2x 1/2"	2x 1/2"	-	-	1x 5/8"	1x 5/8"
Fire		ULC	ULC	ULC	NonStd	ULC	NonStd	ULC	NonSta
Onset of Charring (min)		1.8	40	67	54	1.5	1.8	36	25
Avg. Charring rate at: (mm/min)	8.75 mm	-	-	-	0.86	-	0.89	-	1.66
	17.50 mm	0.37	-	0.96	0.90	0.46	1.10	0.90	1.23
	26.25 mm	-	-	-	-	-	1.10	-	0.87
	35.00 mm	0.57	-	0.81		0.57	0.93	0.74	0.77
	43.75 mm	-	-	-	-	-	0.78	-	0.79
	52.50 mm	-	-	-		0.72		0.79	-
	70.00 mm	-	-	-		0.76		0.77	-
	87.50 mm	-	-	-	-	-	-	0.93	-
Mean		0.47	-	0.88	0.83	0.63	0.88	0.83	1.08
σ		0.14	-	0.11	0.042	0.14	0.16	0.084	0.40

4.2.1 Comparison of Medium- and Full-Scale Charring Rates

Charring rates in full-scale tests were calculated in the same fashion as in medium-scale tests. Charring in the full-scale 3-ply test with two layers of gypsum did not continue long enough for the char front to reach the first thermocouple depth. However, after this panel was extinguished, the depth of char in the panel was measured and the charring rate was calculated by dividing by the length of the test minus the time to the onset of charring. Charring in this panel ranged from 0.50 to 0.72 mm/min, with an average of 0.59 mm/min [17]. This is lower than the equivalent medium-scale test, which had an average charring rate of 0.88 mm/min, although this may have been due to the different method used to calculate the charring rate in this test than in any other tests. The char depth was not measured until the panel was removed from the furnace

and extinguished, well after the test had ended. Therefore, it is likely that charring would have continued to advance past the time the test ended. This would have caused a larger char depth than was actually present at the end of the test, and resulted in a lower charring rate.

No unprotected, full-scale, 3-ply test was conducted. Charring rates for the three equivalent medium- and full-scale tests are listed in Table 4-9.

Table 4-9: Comparison of charring rates for equivalent medium- and full-scale tests

Scale		Medium	Full	Medium	Full	Medium	Full
# of Plies		3	3	5	5	5	5
Type X Gypsum Protection		1x 5/8"	1x 5/8"	-	-	1x 5/8"	1x 5/8"
Fire		ULC	ULC	ULC	ULC	ULC	ULC
Onset of Charring (min)		40	25	1.5	3	36	25
Average Charring rate at: (mm/min)	17.50 mm	-	0.43	0.46	0.52	0.90	0.55
	35.00 mm	-	0.42	0.57	0.55	0.74	0.42
	52.50 mm	-	0.62	0.72	0.64	0.79	0.53
	70.00 mm	-	-	0.76	-	0.77	0.59
	87.50 mm	-	-	-	-	0.93	-
Mean		-	0.49	0.63	0.57	0.83	0.52
σ		-	0.11	0.14	0.062	0.084	0.073

Charring began at the exposed surface sooner in all protected full-scale tests than in equivalent medium-scale tests. However, charring rates calculated in all full-scale tests are lower than those calculated in medium-scale tests. This discrepancy could be the result of many factors, one of which being the fact that full-scale test data was collected at one minute intervals while medium-scale test data was collected at one second intervals. The time at which each thermocouple measures a temperature above 300°C is taken as the time that the char front has reached that thermocouple. In full-scale tests,

this is measured at the first full minute with a temperature above 300°C, which would result in slightly longer times to charring and yield slightly lower charring rates at each thermocouple depth than in reality. This measurement inaccuracy can account for up to a 2% difference between charring rates, but differences of up to 60% are apparent between some equivalent medium- and full-scale tests.

The charring rate of wood is affected by several factors, such as density, moisture content, permeability, chemical composition and timber treatment [53]. Test panels in all medium-scale experiments were supplied by Nordic Wood. All were manufactured of spruce, pine or fir (SPF) lumber, with a density of ±560 kg/m^3, and moisture content of 12 ± 2 % at the time of production [47]. All full-scale test panels were made from the same manufacturer, except for two floors; the 3-ply panel with one layer of gypsum and the 5-ply panel with one layer of gypsum were manufactured by Structurlam. Structurlam CLT panels were also made from SPF lumber; however, they had a density of ±500 kg/m^3 and a moisture content of 12 ± 2 % at the time of production [54]. No treatment was applied to any test specimens, and given that they were all constructed of the same type of wood, of the possible factors, the density and moisture content are likely the only small influencing factors on the charring rates. A lower density typically gives rise to higher charring rates; however, the full-scale 5-ply panel with one layer of gypsum demonstrates a much lower charring rate than both the denser, medium-scale 5-ply panels. Moisture content may have been a small contributing factor in the variation of charring rates calculated, but was not measured immediately before any panels were tested and cannot be compared. Therefore, with only four tests to

compare, it is difficult to determine the reason for the discrepancy that occurs between medium-scale and full-scale charring rates. However, similar to the discrepancy found in gypsum performance between medium- and full-scale tests, it is possible that the source of error was caused by more heat transferring into the sides of the panel in the medium-scale furnace than in the full-scale furnace due to the larger perimeter to exposed surface area ratio of the specimens. Corner rounding observed on the edges of all panels tested in the medium-scale furnace is evidence that enough heat had impinged on the sides of the panel to cause charring. This was also an indication that heat had penetrated into the center of the panel, which would have increased the rate of char advancement into the panel from the exposed surface. While the charring rates in the medium- and full-scale furnace differ because of this, they still demonstrate similar trends as plies delaminated and charring rates spiked. However, charring rates from the medium-scale furnace are likely higher and not representative of one-dimensional charring.

4.3.2 Charring Rates in Standard and Non-Standard Fires

Charring rates calculated during the initial stages of the non-standard fire were found to be higher than charring rates found in equivalent assemblies exposed to the standard fire curve. This is expected due to the faster growth phase and higher temperatures of the non-standard fire. Similarly, charring rates observed during the decay period of the non-standard exposure were much lower than charring rates found in equivalent tests exposed to the standard fire. The non-standard 3-ply test with two layers of gypsum protection experienced significantly lower charring rates than all other tests due to the

gypsum taking the brunt of the fire exposure. By the time both layers of gypsum had fallen off, the fire temperature had decreased to around 600°C, causing char progression in the panel to proceed very slowly with a steadily decreasing charring rate. The char front did not advance to the 26.25 mm thermocouple in that test before the temperature of the fire had decreased below 300°C and the test was ended.

The depth of char at each individual thermocouple location is plotted at the time it was determined to occur for each test in Figure 4-23 to Figure 4-29. Charring rates calculated between each thermocouple are annotated on these graphs which compare tests of standard and non-standard exposures. Significant events that occur during each test, such as ply delamination and loss of gypsum protection, are also highlighted.

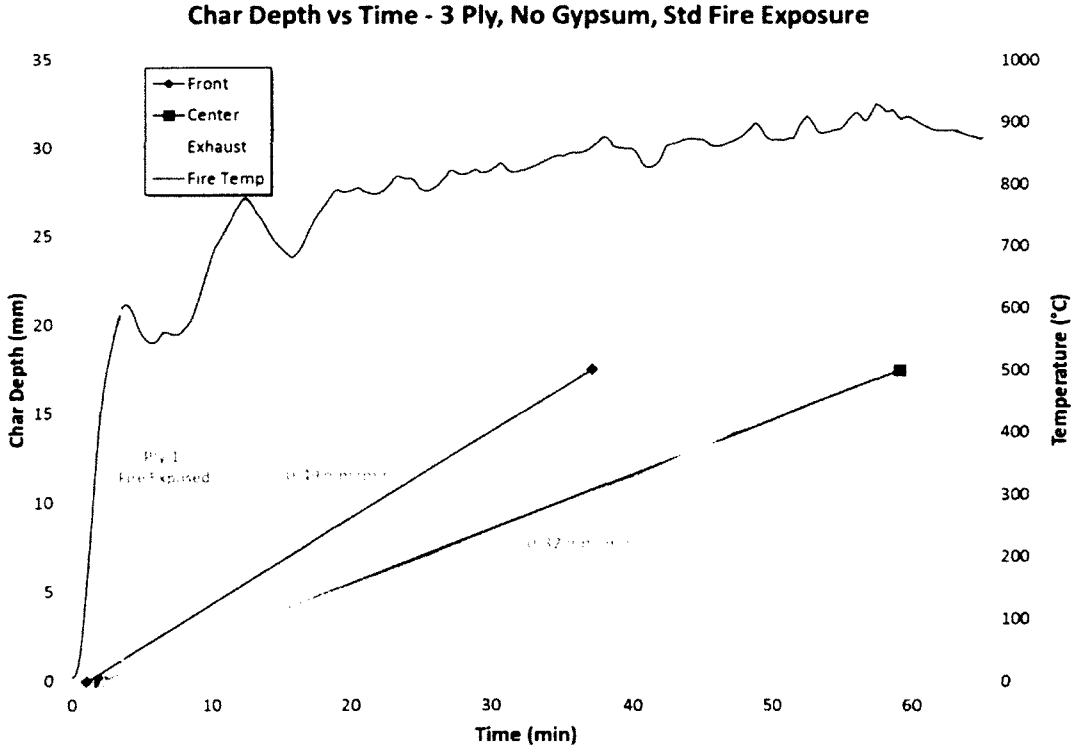

Figure 4-23: Char depth progression in a 3-ply panel without gypsum exposed to the standard fire

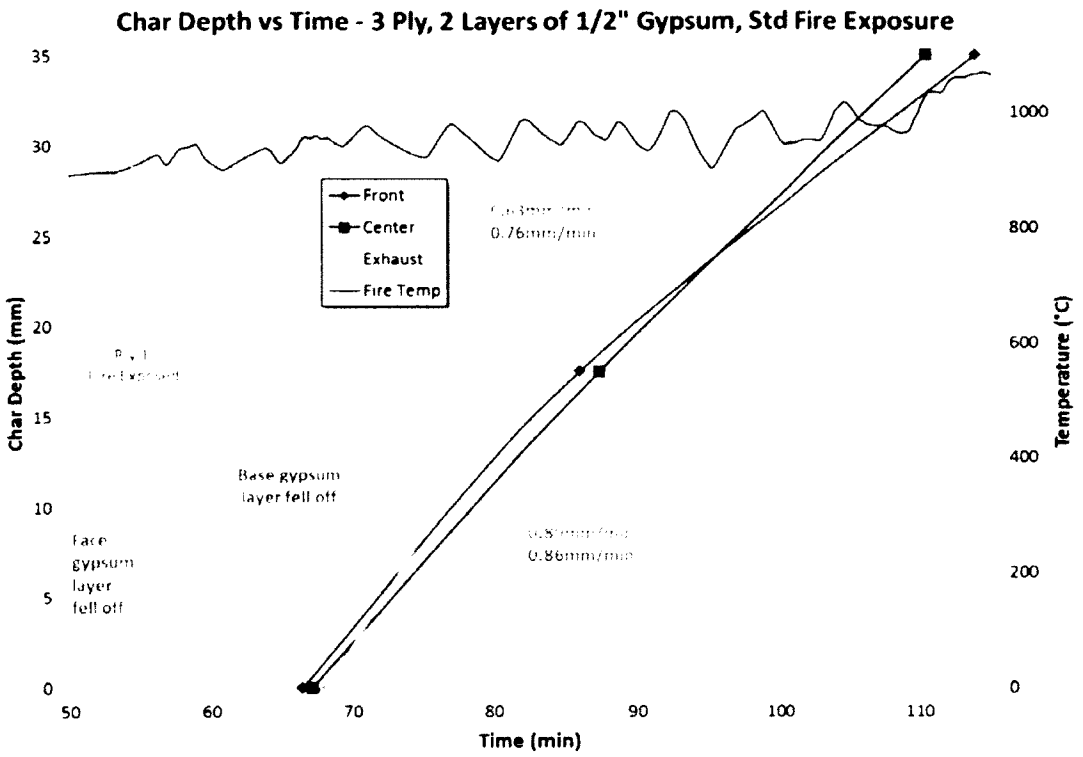

Figure 4-24: Char depth progression in 3-ply panel with 2 layers of gypsum exposed to the standard fire

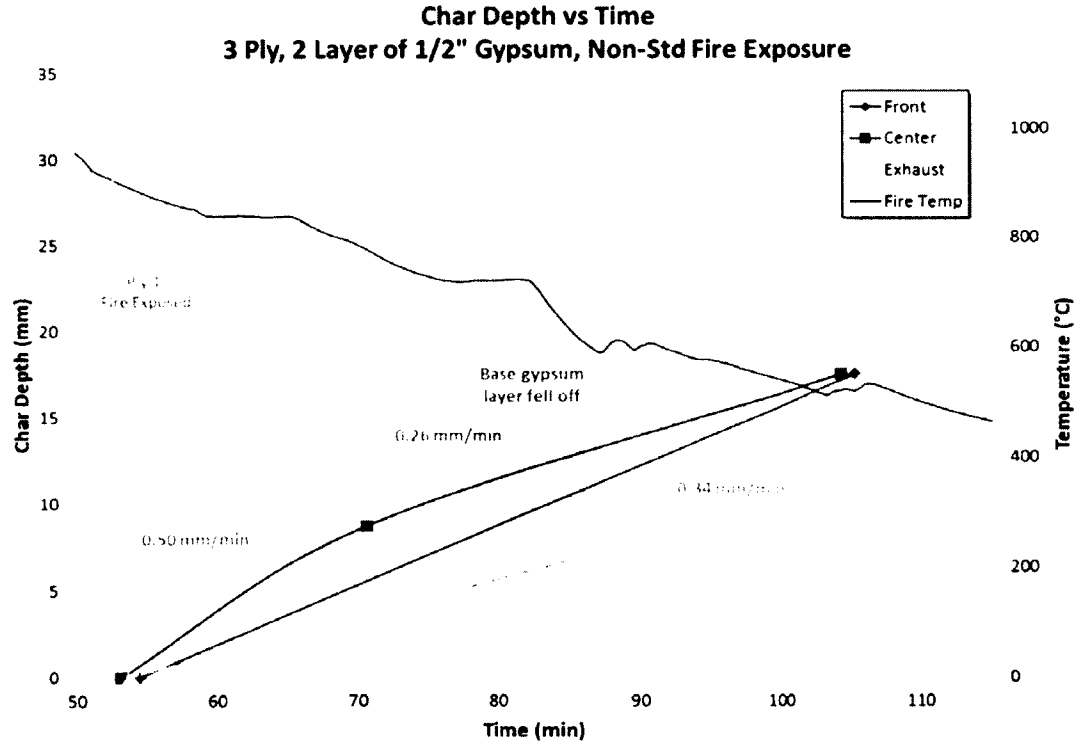

Figure 4-25: Char depth progression in 3-ply panel with 2 layers gypsum exposed to non- standard fire

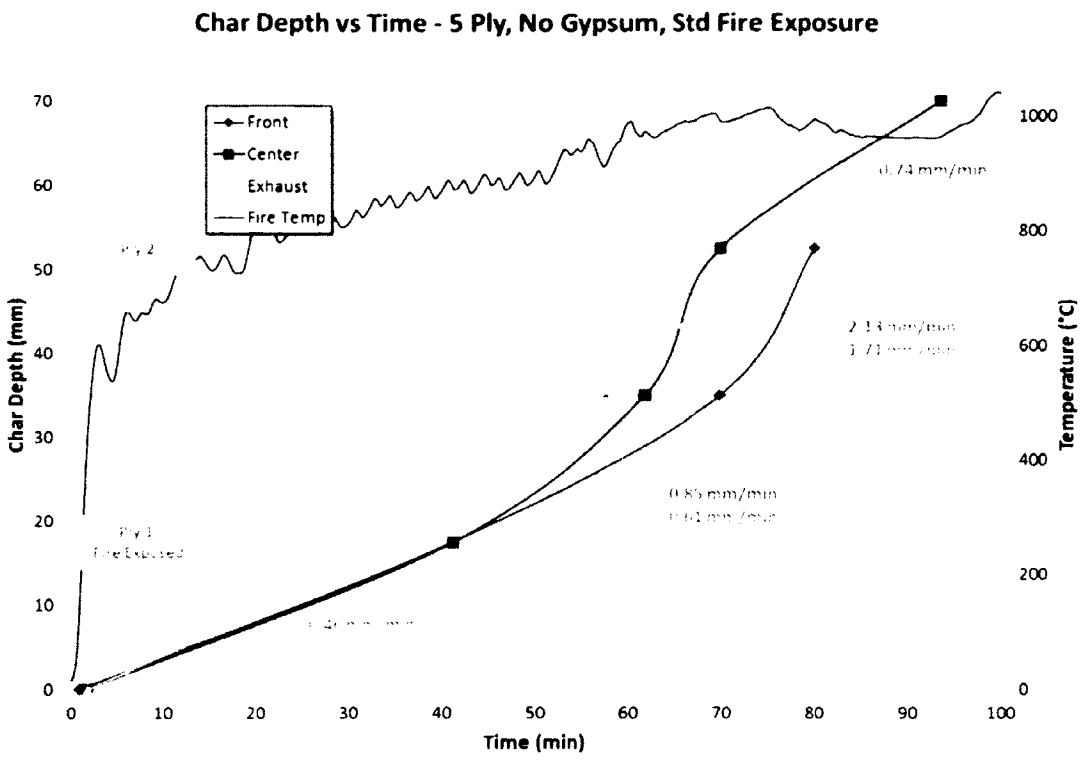

Figure 4-26: Char depth progression in a 5-ply panel without gypsum exposed to the standard fire

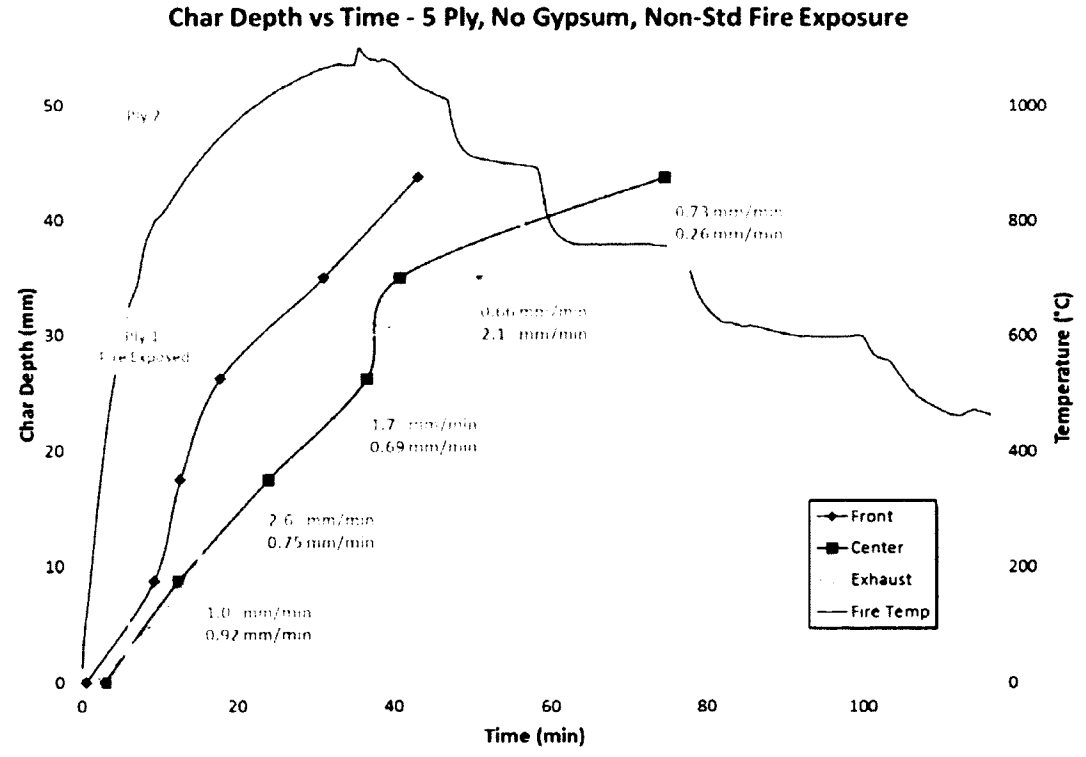

Figure 4-27: Char depth progression in a 5-ply panel without gypsum exposed to non- standard fire

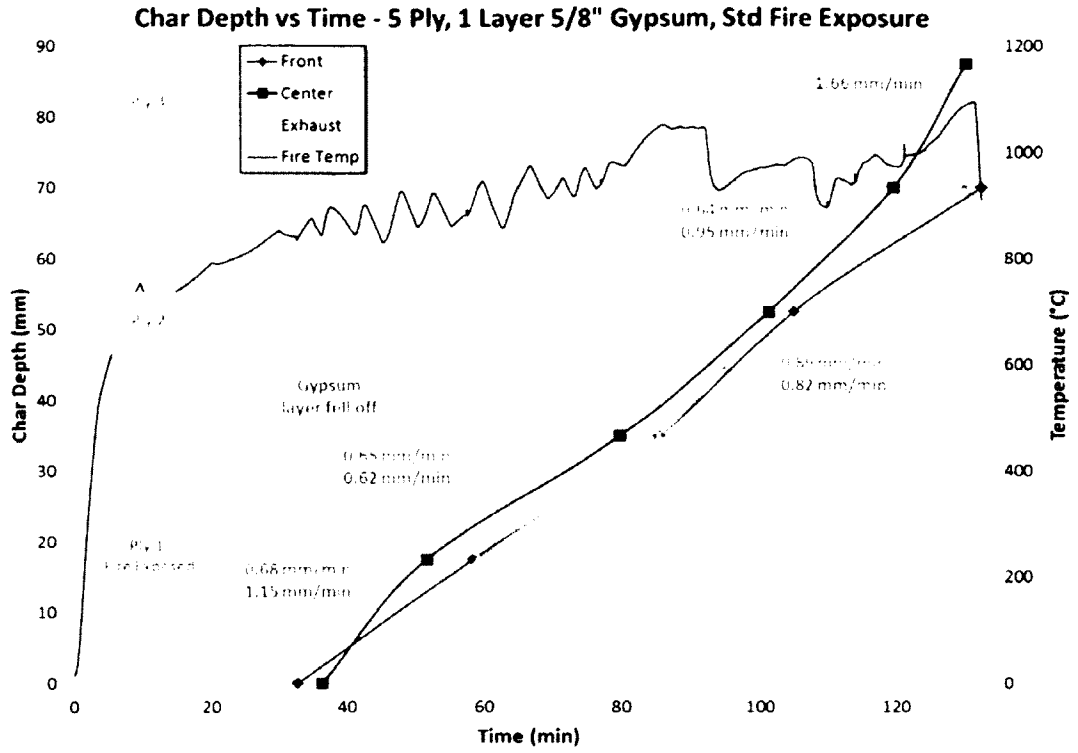

Figure 4-28: Char depth progression in a 5-ply panel with 1 layer of gypsum exposed to the standard fire

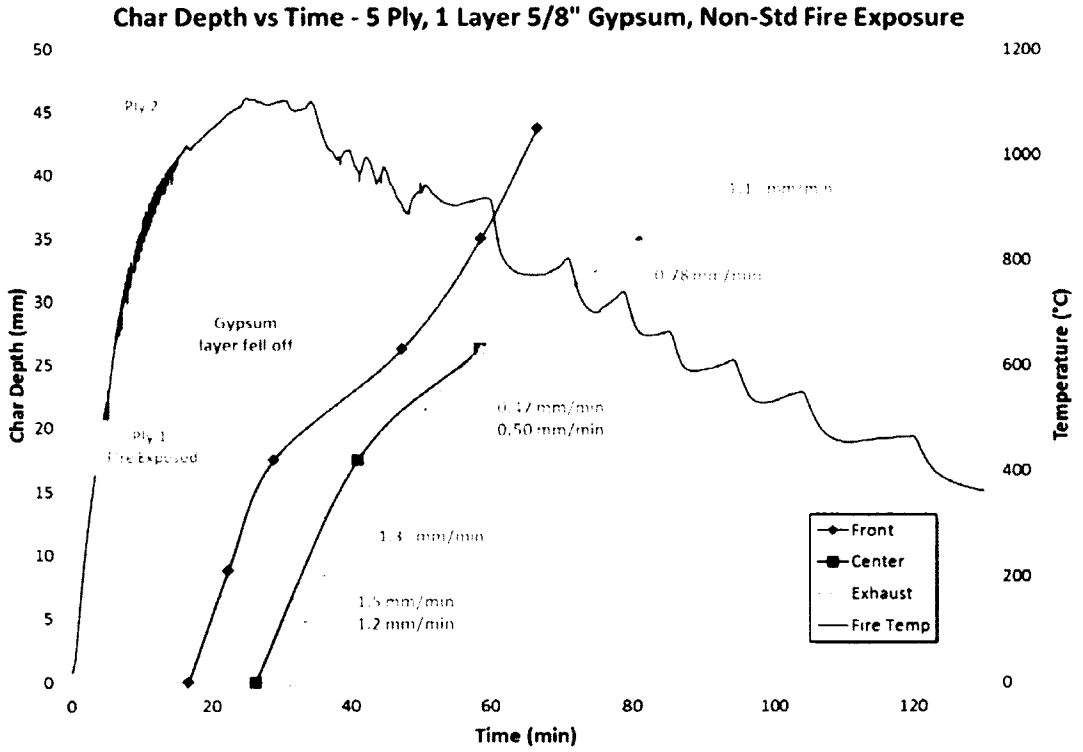

Figure 4-29: Char depth progression in 5-ply panel with 1 layer of gypsum exposed to non- standard fire

4.4.3 Charring Rate

A spike in the charring rate is typical when a ply delaminates as uncharred wood is exposed to the fire; however charring rates calculated between these points are not indicative of actual charring rates occurring. Plies in these experiments typically delaminate before the char front reaches the interface between layers, when its temperature is around 200°C, as shown in Figure 4-30.

Figure 4-30: Ply delamination showing uncharred wood between ply layers after a test

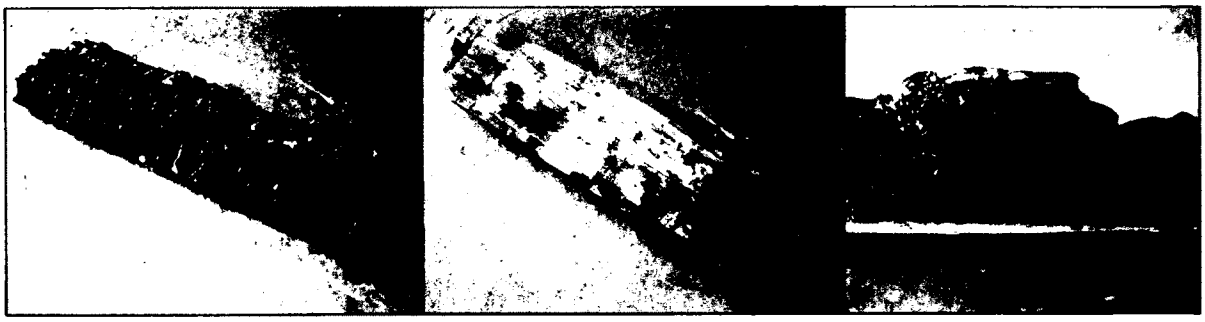

Figure 4-31: Piece of delaminated layer showing exposed charred side, uncharred adhesive side, and the few millimeters of uncharred wood in the ply

Once the layer delaminates, the thermocouple at the interface reads a sudden spike in temperature as it became exposed to the fire. Data analysis of this event places the char front at the newly exposed surface of the next ply at the time of delamination. However, as shown in Figure 4-31, there are a few millimeters of uncharred wood remaining in the fallen ply layer, which are accounted as having been charred in the charring rate calculation. Therefore, all charring rates calculated after such an event essentially represent a slightly higher *effective charring rate* of the panel, which incorporates ply fall-off, rather than the charring rate of just the solid timber itself.

For unprotected wood exposed to the standard fire exposure, EN 1995-1-2 [14, p. 23] uses a one dimensional charring rate, β_0, and a design charring rate to include the effects of corner rounding, β_n, as listed in Table 4-10.

Table 4-10: Design charring rates of timber from EN 1995-1-2 Eurocode 5

	β_0 (mm/min)	β_n (mm/min)
Softwood and beech		
Glued laminated timber with a characteristic density of ≥ 290 kg/m^3	0.65	0.7
Solid timber with a characteristic density of ≥ 290 kg/m^3	0.65	0.8

Examining the unprotected 3-ply and 5-ply panels exposed to the standard fire in Table 4-8, both exhibit a charring rate of 0.57 mm/min through the first ply (35 mm), which is lower than the Eurocode prescribed charring rate for solid timber of 0.65 mm/min. However, the Eurocode specifies a multiplication factor to design charring rates for wood with a density greater than 450 kg/m^3. The charring rate used for denser wood can be adjusted by multiplying the design rate by a density factor, $k_\rho = \sqrt{\frac{450}{\rho_k}}$, where ρ_k

is the characteristic density, in kg/m^3 [14, p. 22]. The density given by Nordic for CLT is 560 kg/m^3 [47]. Applying this factor to the one-dimensional charring rate, we get a characteristic charring rate of 0.58 mm/min, which offers a much closer fit to the charring rate found in the first ply. However, the overall charring rate through the first two plies of the 5-ply panel is 0.76 mm/min. This value incorporates the first ply delamination and is expectedly higher as it represents an effective charring rate.

When gypsum protection was present, panels exposed to both standard and non-standard fires exhibited much higher initial charring rates once the gypsum protection had fallen-off than were observed in unprotected panels. In standard fire exposures, the initial charring rate of the 5-ply panel with one layer of gypsum was double that of the unprotected panel, at 0.90 mm/min compared to 0.46 mm/min. The initial charring rate of the 3-ply panel with two layers of gypsum was more than double the rate of the unprotected panel, at 0.96 mm/min compared to 0.37 mm/min. In the 5-ply tests exposed to the non-standard curve, the panel with one layer of gypsum protection had an initial charring rate of 1.68 mm/min compared to 0.89 mm/min in the unprotected panel. Gypsum boards protect and delay the wood from initially charring, during which time the fire temperature becomes much hotter. When the gypsum fails and the wood is then initially exposed to a hotter fire than an unprotected and equivalently uncharred panel would be; a more rapid temperature rise occurs at the exposed surface from the significant amount of heat now penetrating the wood. This causes char to form quickly producing higher initial charring rates. These elevated charring rates were observed to continue until the char front had reached the thermocouple at the 17.5 mm depth. This

was not the case if the gypsum layers had fallen-off after the fire temperature had decreased, such as the case in the 3-ply panel with two layers of gypsum in the non-standard fire.

4.5.1 Comparison with Eurocode Method to Calculate Char Depth

The Eurocode EN 1995-1-2 [14] charring depth calculation method was compared with char depths measured in the medium- and full-scale tests to asses it's accuracy when applying it to CLT. The calculation method stipulates a constant charring rate of 0.65 mm/min be used for the wood used in this experiment. A density adjusted charring rate of 0.58 mm/min is also compared. For protected surfaces, a calculation to predict the time to gypsum failure is included and followed by charring at twice the standard rate for the first 25mm of char formed. After that point, the standard charring rate is then used. Char depths calculated using this method are graphed in Figure 4-32 to Figure 4-36. This method is intended for use in standard fire exposures only. Panels exposed to the non-standard fire in this test series were not included in this comparison.

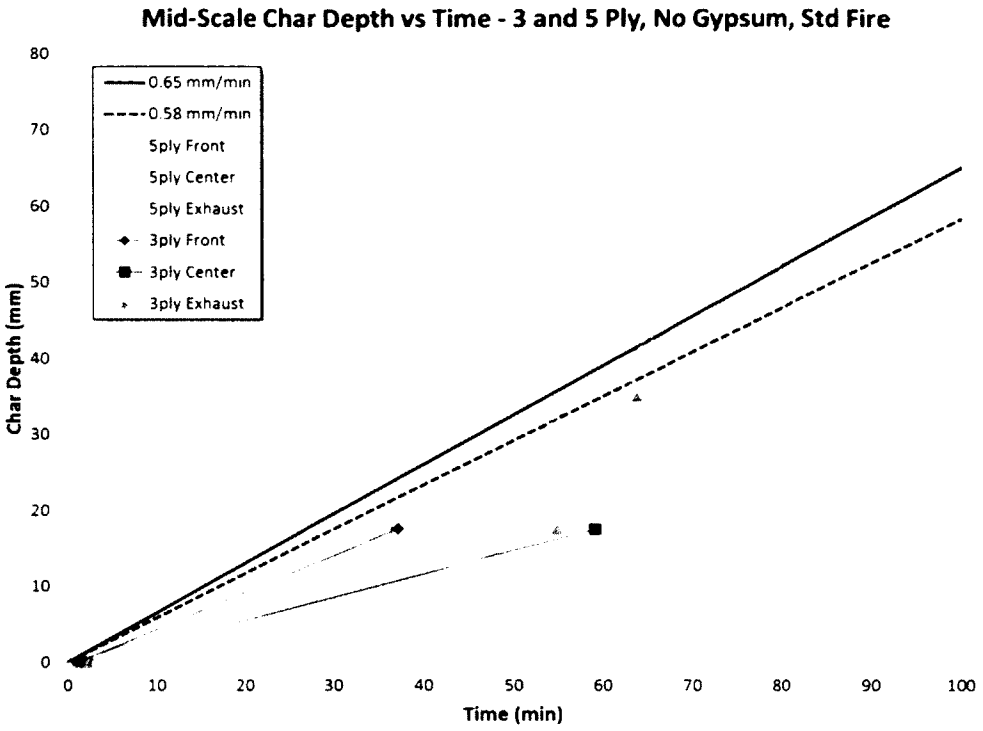

Figure 4-32: Char depth in medium-scale 3 and 5 ply unprotected panels exposed to the standard fire compared to Eurocode charring calculation method

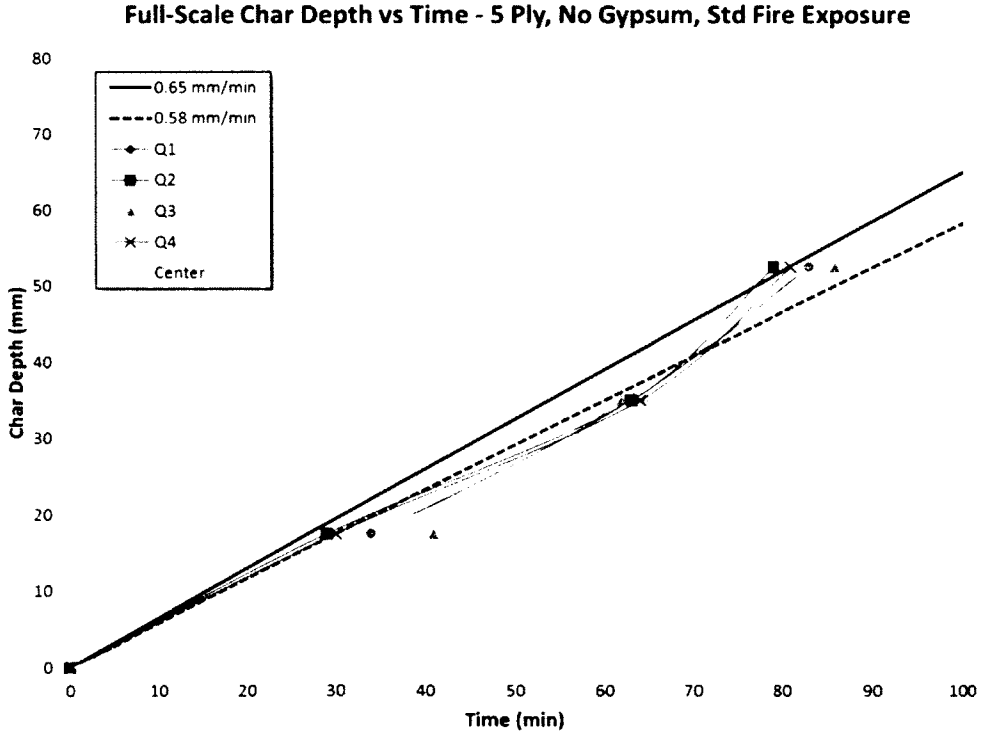

Figure 4-33: Char depth in full-scale 5 ply unprotected panel exposed to the standard fire compared to Eurocode charring calculation method

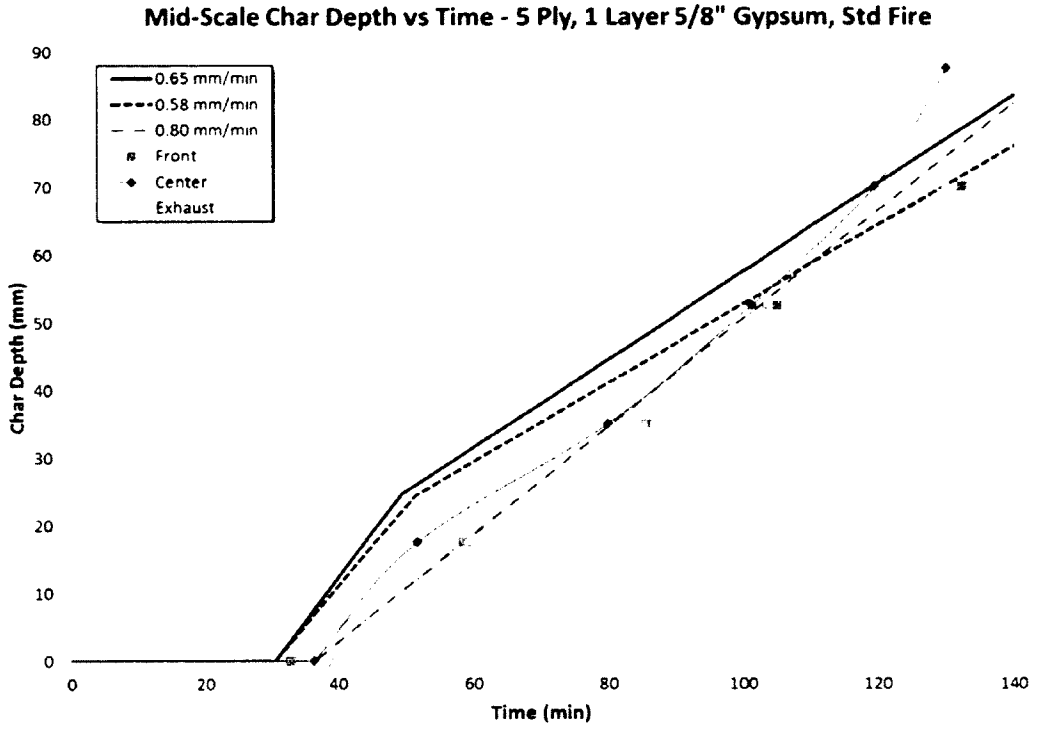

Figure 4-34: Char depth in medium-scale 5 ply panels with 1 layer of gypsum exposed to the standard fire compared to Eurocode charring calculation method

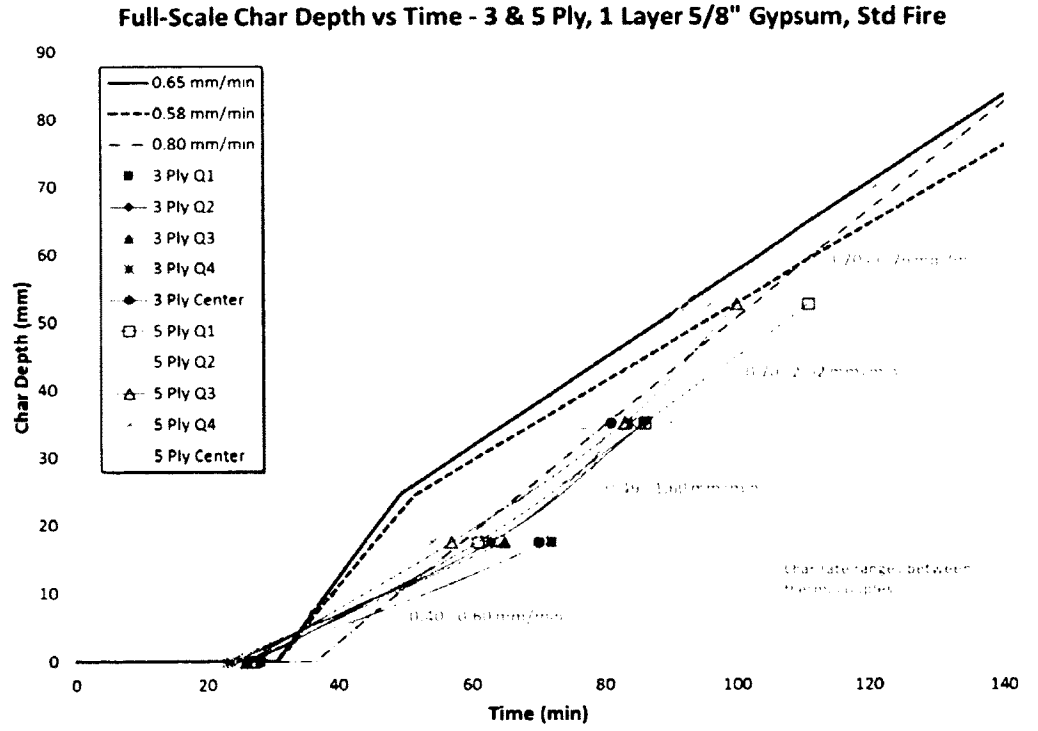

Figure 4-35: Char depth in full-scale 3 and 5 ply panels with 1 layer of gypsum exposed to the standard fire compared to Eurocode charring calculation method

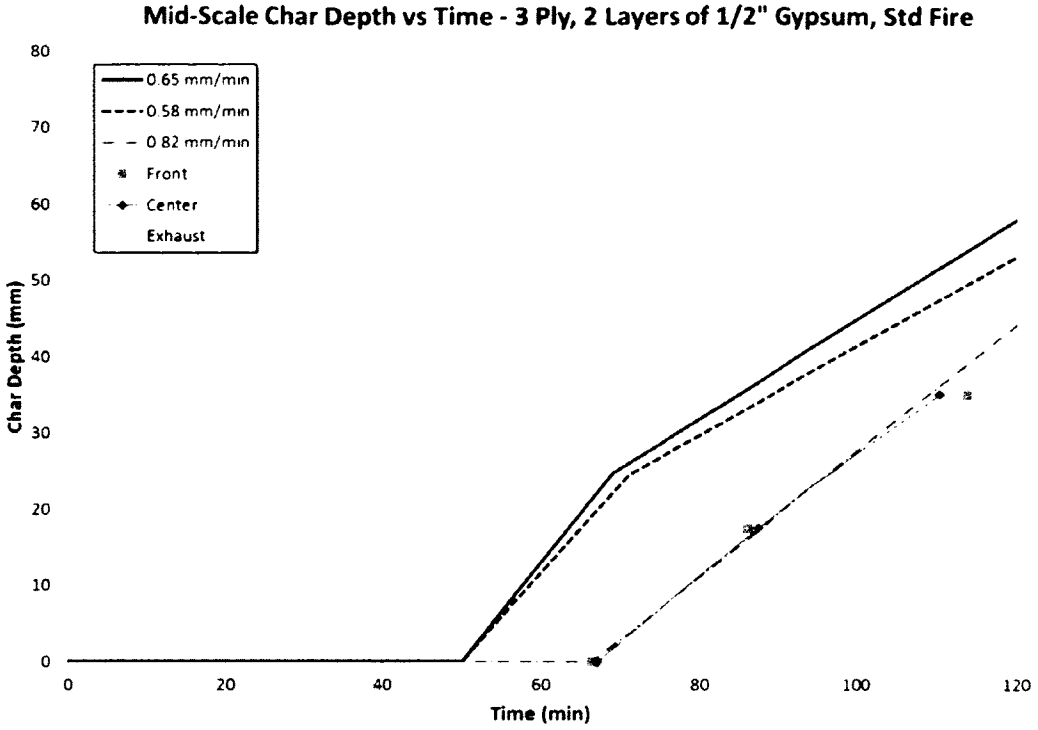

Figure 4-38: Char depth in medium-scale 3 ply panel with 2 layers of gypsum, exposed to the standard fire, compared to Eurocode charring calculation method

From these graphs it is apparent that the Eurocode char method does not offer a reliably accurate approach for estimating the char depth in CLT. While the predicted gypsum failure time is reasonably close to the actual failure times in single board tests, double board estimates predict a fall-off time nearly 20 minutes sooner than test results. Ply delamination tends to cause large variances in the charring rate, increasing drastically as new plies are exposed to the fire. This effect is not conventionally captured in the Eurocode beyond increasing the initial charring rate for a short period after gypsum failure. However, a creative interpretation of the Eurocode, assuming each ply layer as a layer of protection, could offer a closer approximation.

Since ply delamination is based on the failure temperature of the adhesive in these experiments, different adhesives will demonstrate different failure times, as shown by

Frangi [19]. Frangi also demonstrates ply thickness as a factor in delamination time and charring rates. Floors with thicker plies take much longer to delaminate and demonstrate a closer overall effective charring rate to that of solid timber. The adhesive in floors with thinner plies have less protection and delaminate more quickly as well as exhibit much higher overall effective charring rates.

A possible modification to this method to better model charring in CLT could involve the incorporation of an effective charring rate. However, this would also require the establishment of an empirical relationship for the effective charring rate based on variable inputs for ply thicknesses and adhesive failure temperatures to maintain universality of use. The formulation of such a relationship would require significant experimentation, which has not yet been completed. However, even with an established effective charring rate, a precise determination of the char depth in a CLT panel would not be possible. If the effective char depth is calculated at a time just after a delamination, it will yield a smaller char depth than the actual char depth. Whereas if the effective char depth is calculated at a time just before a delamination, it will yield a larger char depth. Given more experimentation, an average effective charring rate could be calculated, however since charring does not follow a linear pattern in CLT, it would not offer significant accuracy in its calculation.

A more accurate approach to predicting char depth in CLT is to treat each layer as an individual layer of protection, similar to recommendations made by Frangi [19], where he assumes a doubled charring rate of 1.3 mm/min to continue for 25 mm after a ply

delaminates. However, from the results in this research, this method is not fully representative of how charring continues. It is apparent from the results of Frangi's work and this research, that the amount the charring rate increases by is influenced by the ply thickness, adhesive properties, and whether or not gypsum protection was present. This method would require invoking a relationship based on ply thickness and adhesive properties to determine a distance of uncharred wood between the char front and the adhesive, at which the ply will delaminate. For example, an equation in the Eurocode, cited by Buchanan [8, p. 277], offers a calculation method for the temperature below the char layer in a wooden semi-infinite solid exposed to the standard fire. From this equation, when the char front is 8 mm away from the adhesive, it can be assumed that the temperature at the interface is around 200°C, and the ply will delaminate. Similar to gypsum failure in EN 1995-1-2, a multiplication factor can be applied to the standard charring rate when a ply delaminates. However, more experimentation to determine how ply thickness and gypsum protection affects this factor and for how long it should be applied before reverting back to the standard charring rate, is required.

Once the char front reaches the calculated distance from the adhesive, the ply would be considered fallen, the char front would then be taken at the surface of the next ply, and the multiplication factor would be applied as necessary. This method would offer a more accurate approximation for calculating the instantaneous char depth in a CLT panel at a given time during a standard fire exposure.

4.4 Temperature Profile and Heat-Affected Layer

A temperature profile throughout the depth of the panel is delineated using data from embedded thermocouples. A plot showing how the temperature profile changes every 10 minutes illustrates how heat penetrates the panel during a test, shown in Figure 4-37. Only temperature data that represents heated wood or char are included in the graph. Lines not extending to the fire exposed surface of the panel represent pieces of char that have fallen off, or plies that have delaminated.

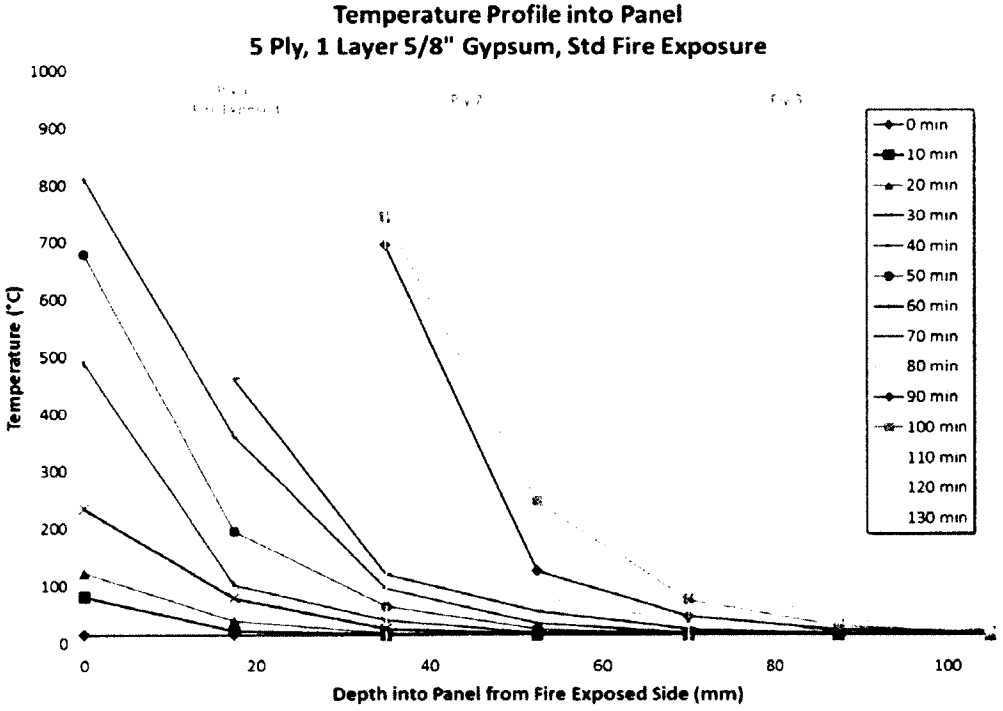

Figure 4-37: Temperature Profile of a 5-Ply Panel with 1 Layer of Gypsum Protection

The average heated zone in the wood is calculated by measuring the depth of wood with a temperature greater than 25°C (or ambient temperature, if it is higher than 25°C) and less than 300°C. This represents the heated layer of wood that has not yet been converted to char. The heat-affected layer is measured by making a linear approximation for temperatures between thermocouples, as demonstrated in Figure

4-37, and measuring the distance over which the temperature drops from 300°C to ambient. The average heated zone calculated in each experiment is listed in Table 4-11.

Table 4-11: Summary of Average Heat-Affected Layer

# of Plies	Type X Gypsum Protection	Fire	Avg. Heated Zone (mm)
3	Unprotected	CAN/ULC	46
3	1x 5/8"	CAN/ULC	45
3	2x 1/2"	CAN/ULC	50
3	2x 1/2"	Non-Std	66
5	Unprotected	CAN/ULC	40
5	Unprotected	Non-Std	42
5	1x 5/8"	CAN/ULC	41
5	1x 5/8"	Non-Std	49

4.4.1 Heat-Affected Layer in Standard and Non-Standard Fires

The heat-affected layer is much smaller during the initial growth phase of non-standard fires than in standard fires and is likely caused by the rapid growth phase of the non-standard fire exposure. Heat penetrating the wood is not able to advance into the wood much faster than the quickly progressing char front at the exposed surface. Once fire temperatures of around 800°C are attained and heat has had significant time to penetrate deeper into the wood, the heated zones in both standard and non-standard fires become more similar in size. During the decay phase of the non-standard fire, slow heating and lower temperatures cause the heated zone to increase in size significantly. As the fire temperature decreases, the charring rate decreases more than the rate at which heat continues to penetrate deeper into the panel. This creates a larger overall average heat-affected layer in panels exposed to the non-standard fire than that which is found in panels with equivalent gypsum protection exposed to the standard fire.

4.4.2 Heat-Affected Layer in CLT

For the same reasons stated in the previous section, it would be assumed that the presence of gypsum protection would create larger heated zones. However, no significant trend can be observed from these tests to demonstrate that effect. Without a larger sample size, it cannot be confirmed that gypsum boards have a substantial effect on increasing the size of the heated zone in both standard and non-standard fires.

As cited by Buchanan [8, p. 277], Eurocode 5 offers a calculation method for the temperature below the char layer in a wooden semi-infinite solid exposed to the standard fire. In this equation, the thickness of the heat-affected layer is taken as 40 mm. This provides a good fit with the average heat-affected layer found in both 5-ply tests exposed to the standard fire, at 40 and 41 mm. The average heated zone in 3-ply tests was slightly larger, at 47 mm.

4.5 Deflection

Once the preload has been applied and settled, deflection measurements were zeroed, the burners started, and deflection was recorded every second. Deflection data is plotted on graphs annotated with supplementary events that occur during the test, such ply and gypsum failure in Figure 4-38 to Figure 4-48.

4.5.1 Comparison of Deflection in Medium- and Full-Scale Tests

The LVDT's used to measure deflection in the first three tests had a maximum stroke of only 200 mm. Deflection in these panels exceeded the maximum stroke near the end of the tests and continued to deflect without showing an increase in the data. This can be

seen in Figure 4-38, where the center deflection reaches a maximum and stays there until the load is removed.

Deflection graphs from medium-scale tests display very similar values and trends to full-scale deflection graphs in three of the four comparable tests. The one exception is the full-scale 3-ply test with two layers of gypsum protection, shown in Figure 4-41. All tests with gypsum protection show a slow and gradual increase in downward deflection until the gypsum falls-off at which time deflection begins to increase rapidly. However, in the full-scale 3-ply test with two layers of gypsum, deflection steadily increases at a relatively constant rate throughout the entire test. A possible explanation for this may be the type of wood used in this panel. This was the only panel in both test series that used Nordic's SPF 1650F_b MSR lumber in the longitudinal plies, rather than the standard SPF 1950F_b MSR [17]. Although the modulus of elasticity and bending strength stated for SPF 1650F_b MSR plies are not substantially lower than that of SPF 1950F_b MSR, as listed in Table 4-12, manufacturing practices at Nordic were still in the early stages at the time of that test. It is possible that a problem may have occurred during the manufacturing of this panel. Material properties of the wood used in both medium- and full-scale tests are listed in Table 4-12.

Table A12 Summary of wood structural properties of eight full- and medium-scale panels

Plies	Type X Gypsum Protection	Full-Scale Wood Properties		Medium-Scale Wood Properties	
		Longitudinal Plies	Transverse Plies	Longitudinal Plies	Transverse Plies
3	1x 5/8"	**Structurlam** [54] SPF No.1/No.2 E = 9,500 MPa f_b = 11.8 MPa	**Structurlam** SPF No.1/No.2 E = 9,500 MPa f_b = 11.8 MPa		
3	2x 1/2"	**Nordic Wood** [17] SPF 1650F_b MSR E = 10,300 MPa f_b = 23.9 MPa	**Nordic Wood** SPF No.3/stud E = 9,000 MPa f_b = 7.0 MPa	**Nordic Wood** [47] SPF 1950F_b MSR E = 11,700 MPa f_b = 28.2 MPa	**Nordic Wood** SPF No.3/stud E = 9,000 MPa f_b = 7.0 MPa
5	-	**Nordic Wood** SPF 1950F_b MSR E = 11,700 MPa f_b = 28.2 MPa	**Nordic Wood** SPF No.3/stud E = 9,000 MPa f_b = 7.0 MPa		
5	1x 5/8"	**Structurlam** SPF No.1/No.2 E = 9,500 MPa f_b = 11.8 MPa	**Structurlam** SPF No.1/No.2 E = 9,500 MPa f_b = 11.8 MPa		

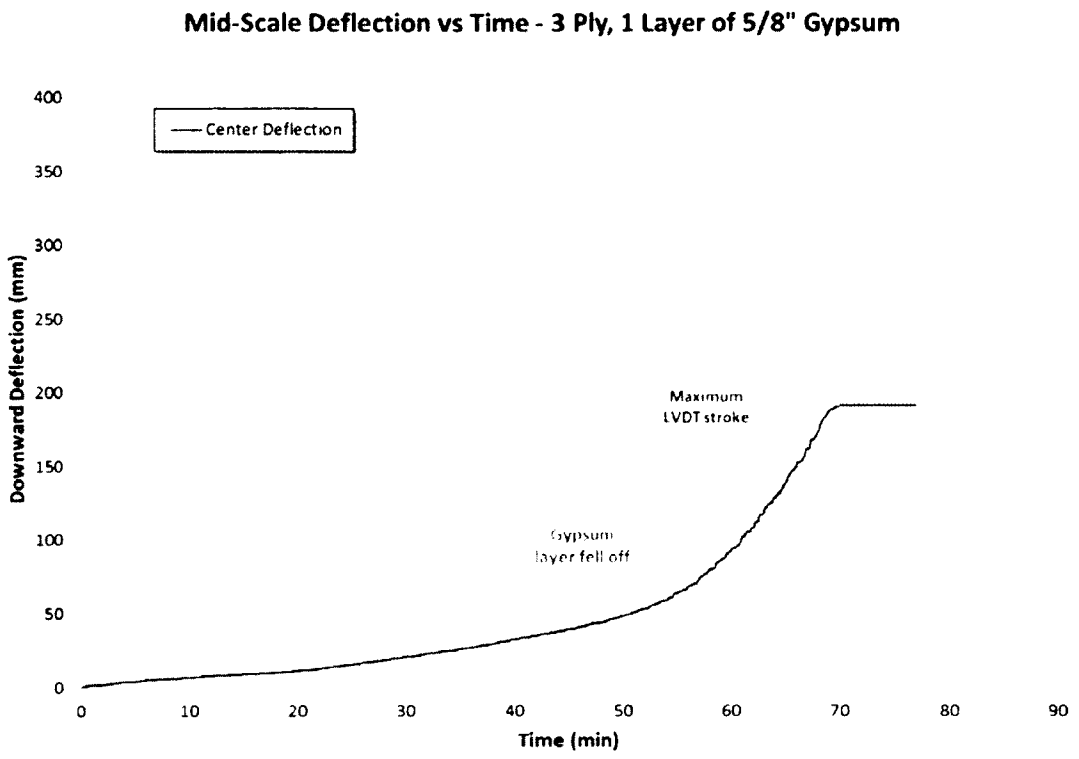

Figure 4-38: Mid-scale deflection versus time of a 3-ply panel with 1 layer of gypsum protection, std-fire

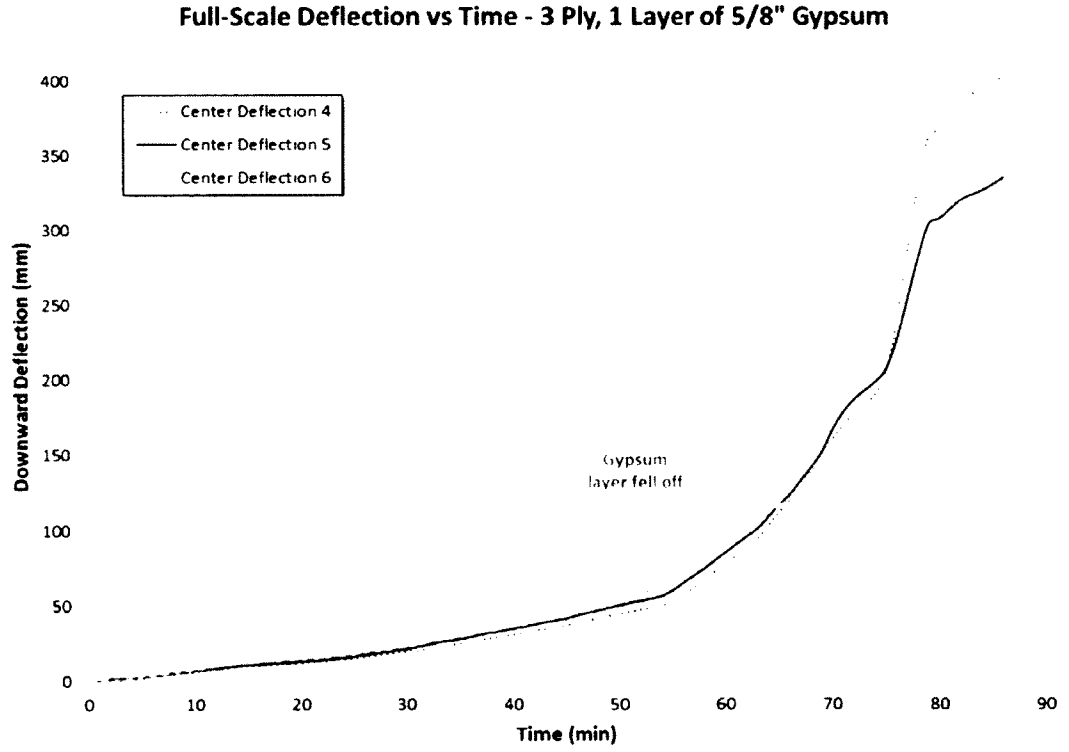

Figure 4-39: Full-scale deflection versus time of a 3-ply panel with 1 layer of gypsum protection, std fire

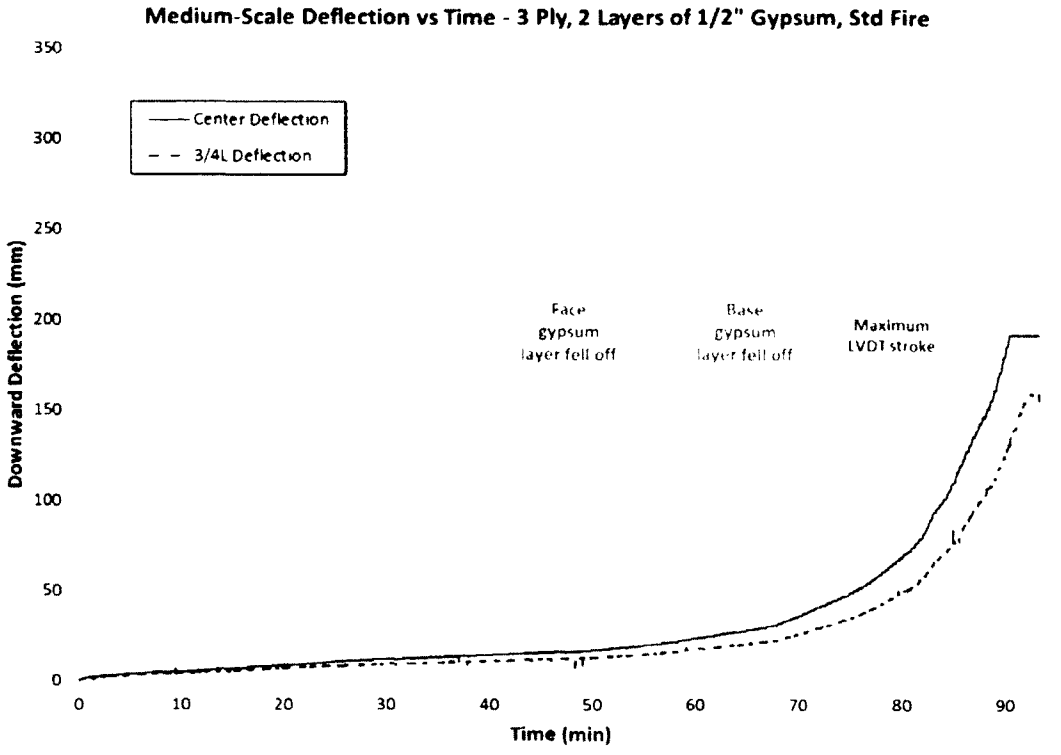

Figure 4-40: Medium-scale deflection vs. time of a 3-ply panel with 2 layers gypsum protection, std fire

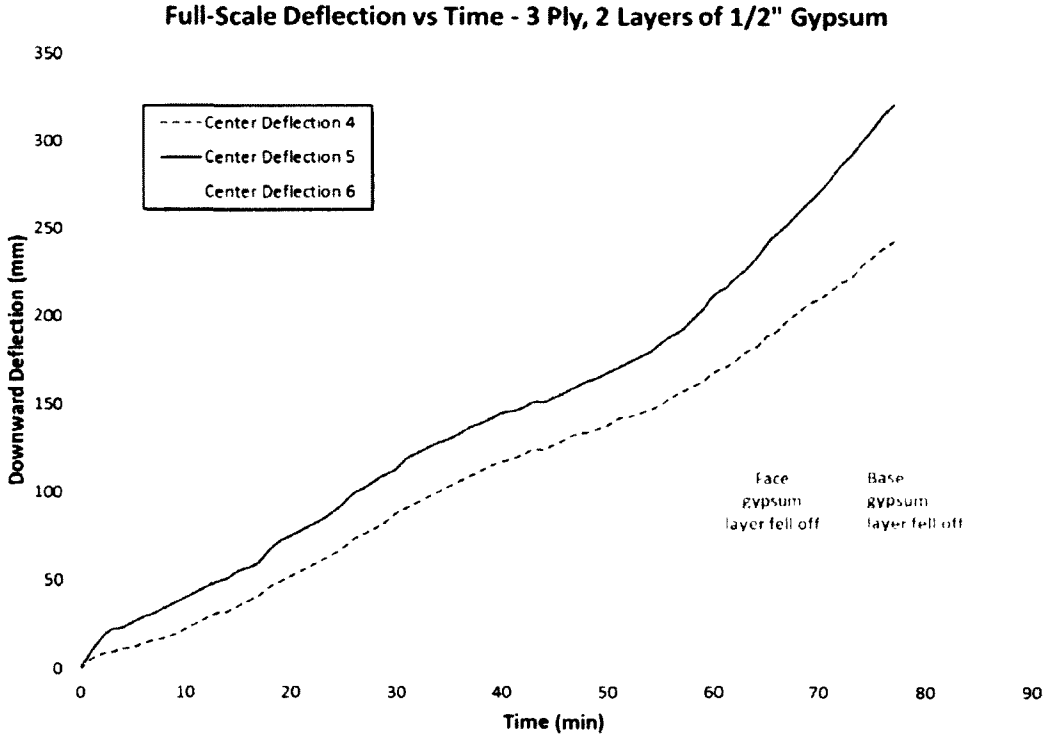

Figure 4-41: Full-scale deflection versus time of a 3-ply panel with 2 layers gypsum protection, std fire

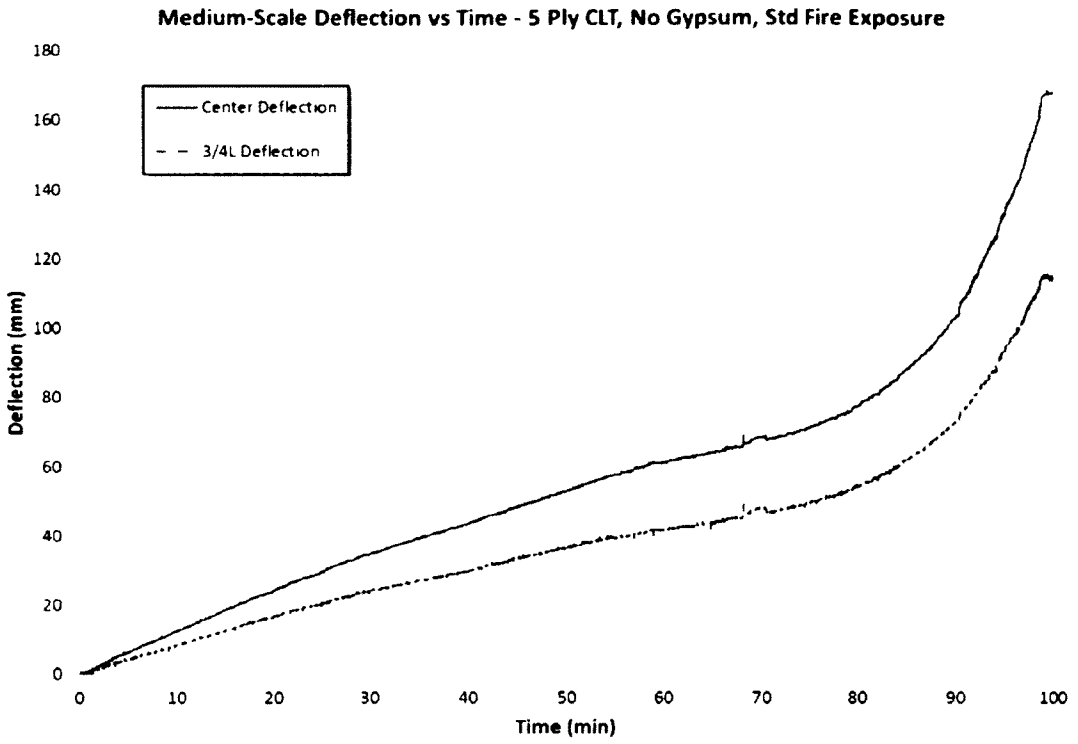

Figure 4-42: Medium-scale deflection versus time of a 5-ply panel without gypsum protection, std fire

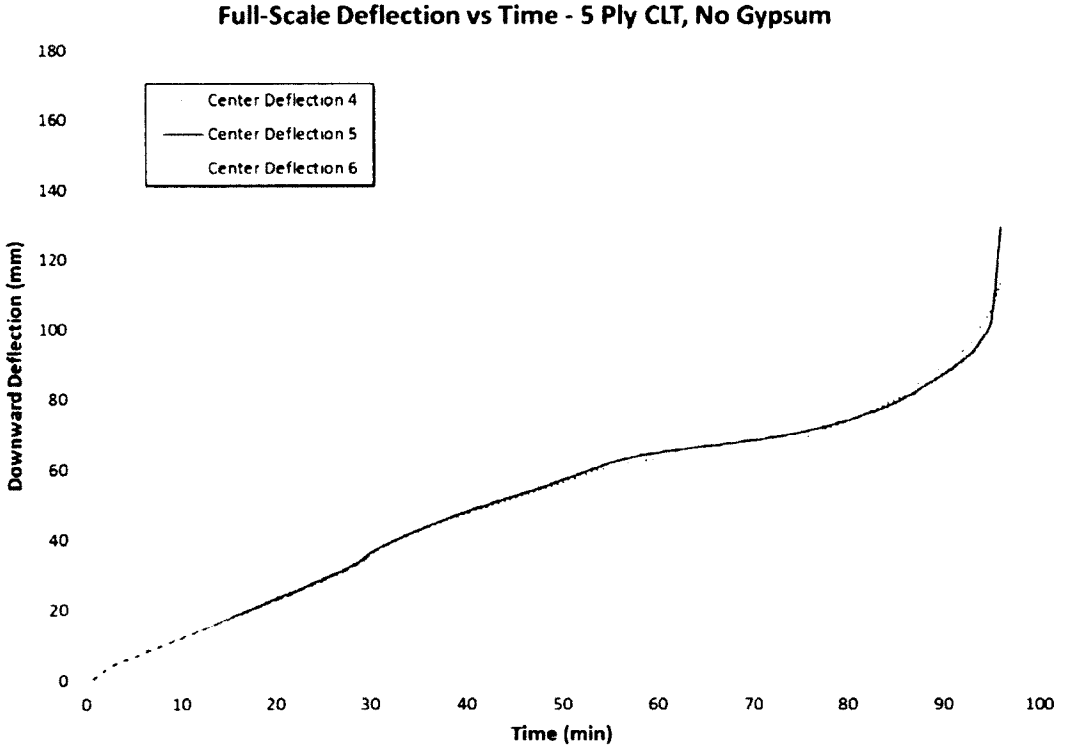

Figure 4-43: Full-scale deflection versus time of a 5-ply panel without gypsum protection, std fire

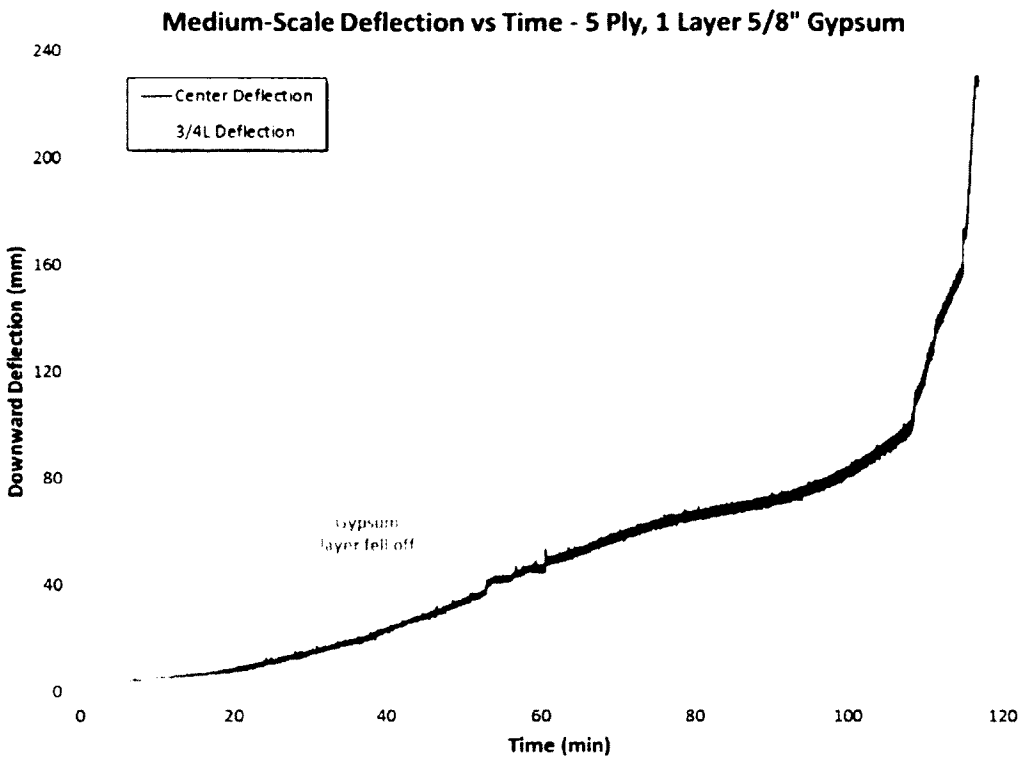

Figure 4-44: Medium-scale deflection vs. time of a 5-ply panel with 1 layer of gypsum protection, std fire

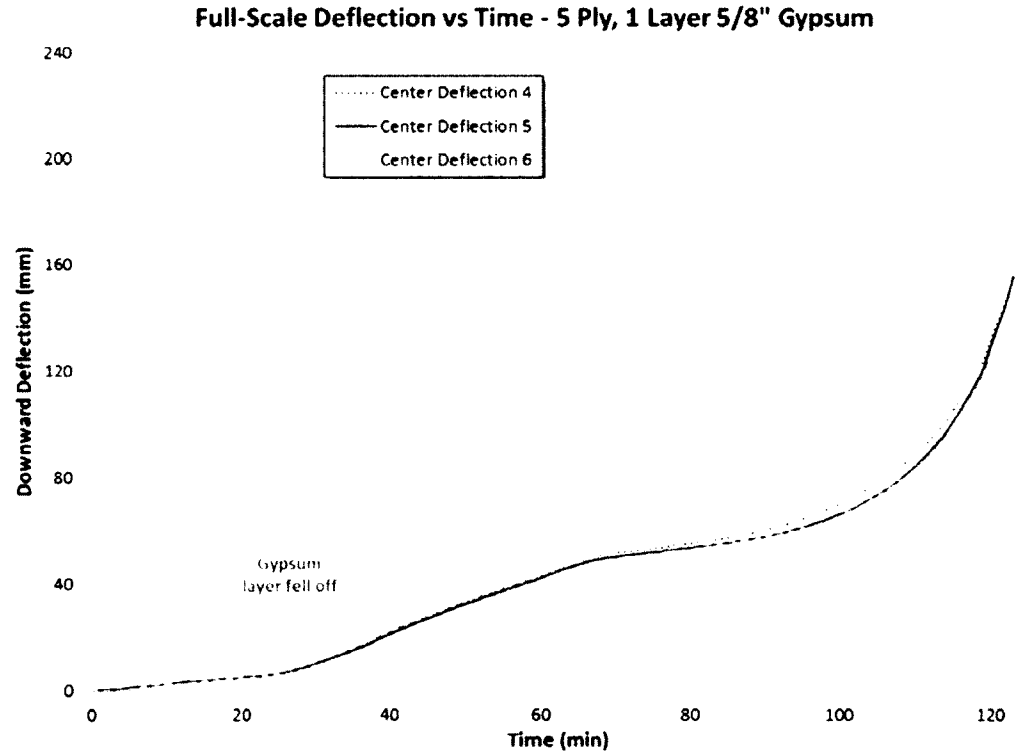

Figure 4-45: Full-scale deflection versus time of a 5-ply panel with 1 layer of gypsum protection, std fire

Loads applied in each test, along with the associated load ratios and the amount of deflection from preloads, are listed in Table 4-13. A description of how loading criteria were chosen and load ratios calculated are covered in Section 3.4.

Table 4-13: Summary of loading criteria and load ratios used in medium- and full-scale tests

Ply	Type X Gypsum	Full-Scale			Medium-Scale		
		Load Criteria	Load - Load Ratio	Preload Deflect (mm)	Load Criteria	Load* - Load Ratio	Preload Deflect (mm)
3	1x 5/8"	NBCC Office Live Load	2.4 kPa 62%	22.3	L/240 Deflection	2.75 kPa 29%	20.6
3	2x 1/2"	L/240 Deflection	2.7 kPa 30%	18.6	L/240 Deflection	2.68 kPa 29%	20.6
5	-	L/240 Deflection	11.75 kPa 47%	19.9	L/240 Deflection	11.7 kPa 47%	19.7
5	1x 5/8"	NBCC Live Load from $(1.5w_L + 1.25w_D)L^2/8 = M_r$	8.1 kPa 80%	17.4	L/240 Deflection	11.8 kPa 48%	20.1

NBCC: *National Building Code of Canada*
** 4-point load for L/240 deflection actually applied in tests; equivalent uniformly distributed load listed for comparison purposes*

4.5.2 Deflection in Standard and Non-Standard Fires

Gypsum failure and ply delamination during non-standard fires caused similar changes to the slope of deflection curves as those found in equivalent standard fire exposure deflection graphs. However, these events occurred at different times than in equivalent non-standard tests. Therefore, while these deflection graphs exhibited similar trends, they produced dissimilar shapes. The decreasing temperatures during the decay phase of the non-standard fire slowed the rate of heating into the wood, causing a more gradual loss of strength and slower rate of deflection change. Deflection graphs of the panels tested against the non-standard fire are included in Figure 4-46 to Figure 4-48.

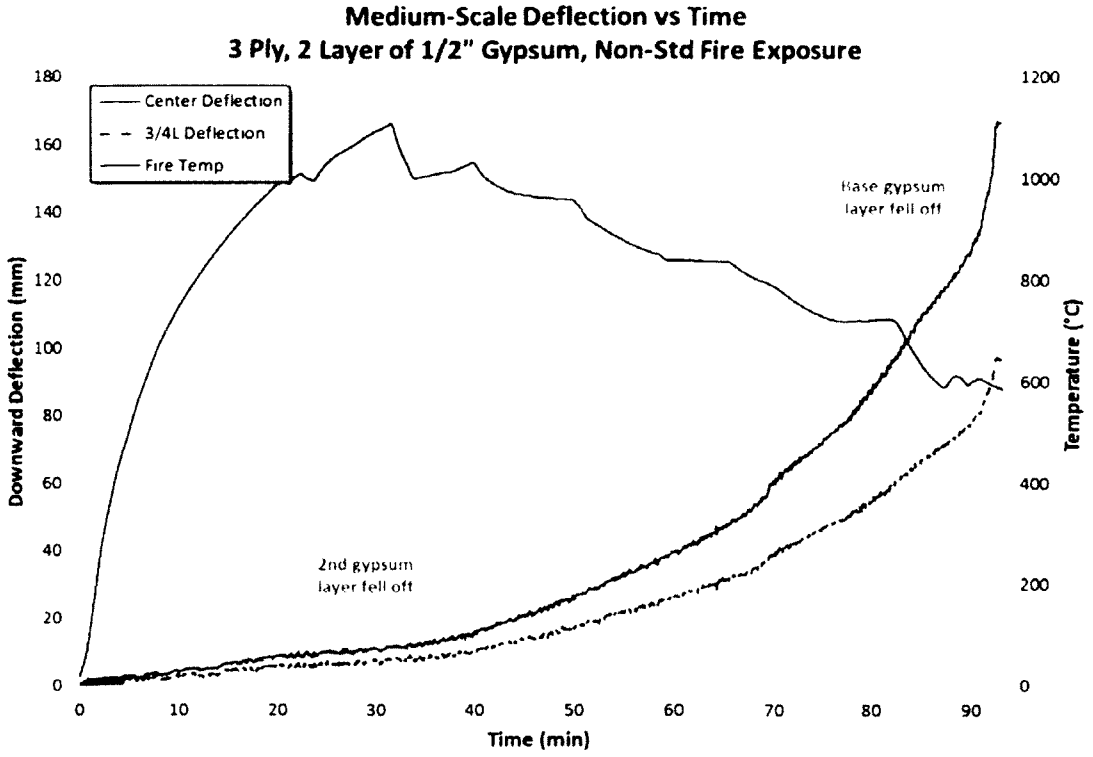

Figure 4-46: Medium-scale deflection versus time of a 3-ply panel with 2 layers gypsum, non-std fire

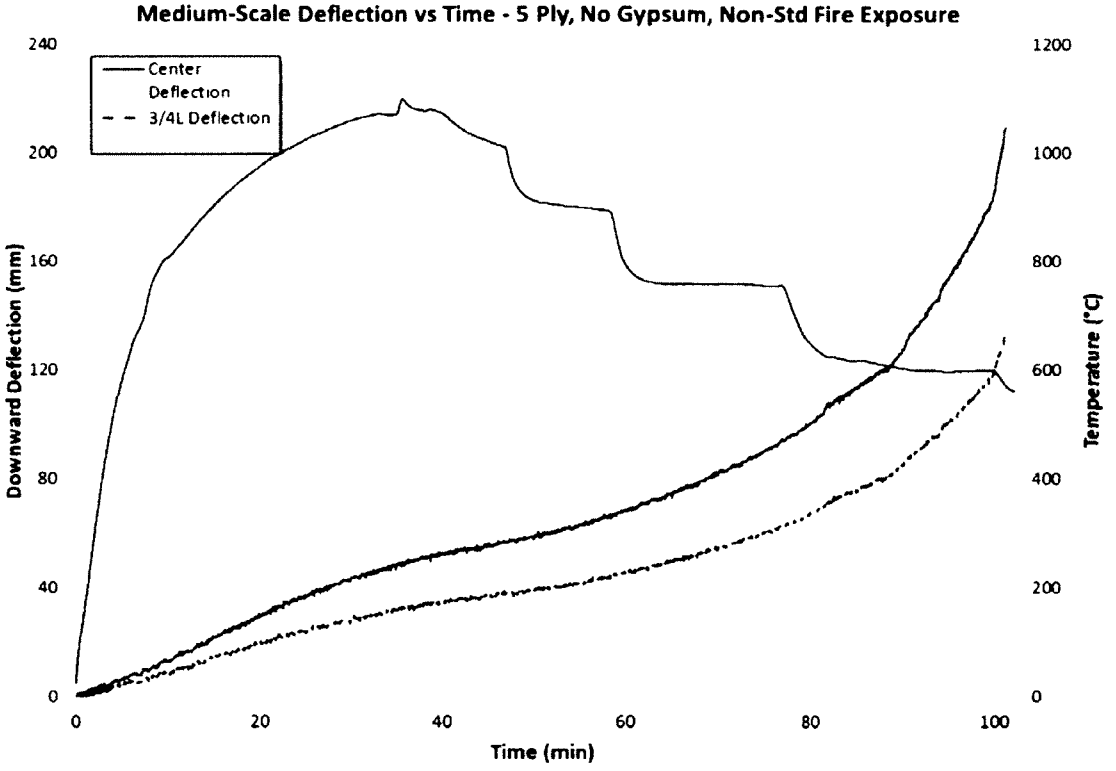

Figure 4-47: Medium-scale deflection vs. time of a 5-ply panel without gypsum protection, non-std fire

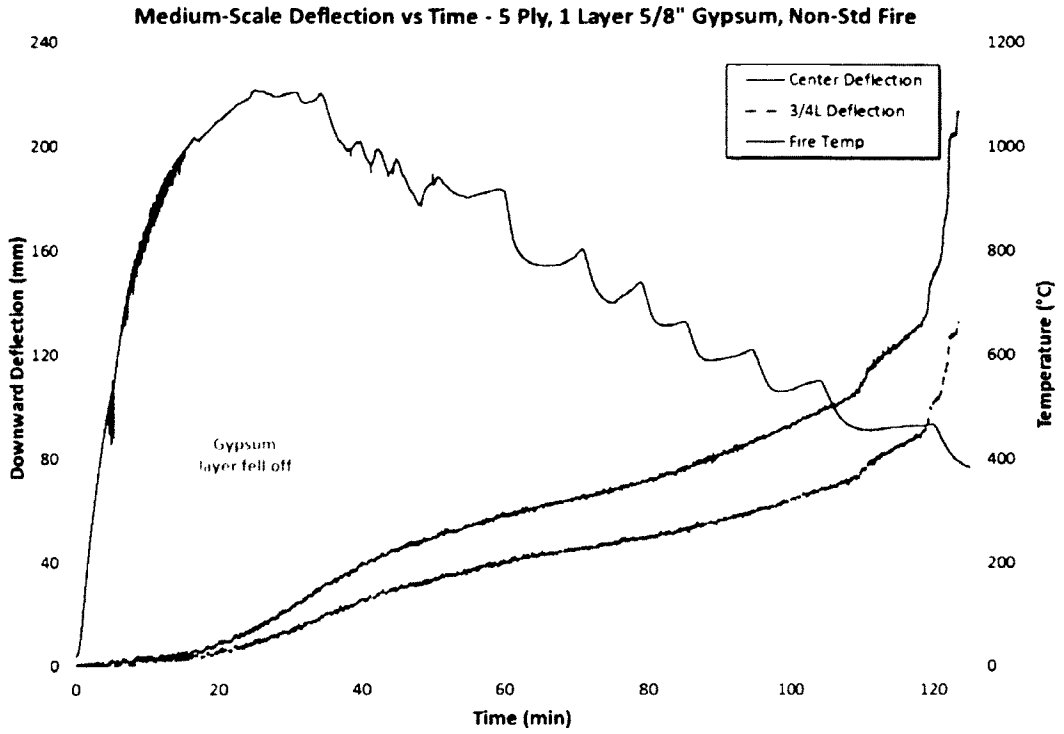

Figure 4-45: Medium-scale deflection versus time of a 5-ply panel with 1 layer of gypsum, non-std fire

4.5.3 Deflection in CLT

All floors in these experiments act in bending from the loads imposed on them. Therefore, in the 3-ply panel tests, the fire exposed, outermost ply provides nearly all the bending resistance to the load. The middle ply provides very little strength since it is oriented perpendicular to the direction of bending. Since the third ply alone cannot maintain the applied loads used in this test series, when the outermost ply delaminates, the panel structurally fails. Hence, all 3-ply tests were only loaded up until the first ply began to delaminate, in order to prevent damage to the lab equipment.

In the 5-ply panel tests, the load is taken up by the longitudinally oriented first, third, and fifth plies. Loading can continue beyond the failure of the first ply since the third and fifth ply are able to maintain the applied loads used in this test series. As the first

ply is heated, chars, and loses strength, deflection increases at a fairly high rate. This is demonstrated in the 5-ply deflection graphs from Figure 4-42 to Figure 4-45. This effective reduction of the first ply strength results in a large decrease in the overall bending resistance of the panel. Once the first ply had completely fallen off, the rate of increasing deflection noticeably decreases. This is because only the second ply, which does not provide much of the overall bending resistance to the panel, is now charring. However, about halfway between the time the first and second ply delaminate, the rate of deflection begins to accelerate again. At this point, the heat-affected layer has impinged on the third ply, causing it to begin to lose strength, thus beginning to remove the majority of the remaining bending resistance of the panel. When the second ply begins to delaminate and the third ply begins to char; deflection begins to run away dramatically. All 5-ply tests were only loaded until this severe increase in deflection was observed, to prevent structural failure that might have damaged lab equipment.

5 Numerical Model

5.1 Introduction

The literature review revealed that data from full-scale fire-resistance tests of CLT panels are limited. Predicting the performance of these panels can assist fire protection engineers when developing performance based CLT designs, and help researchers to plan future experiments. Current CLT models utilise complex two- or three-dimensional finite element software. This model uses numerical methods and empirical

temperature-dependent relationships based on previous research with wood and gypsum.

A one-dimensional, finite difference numerical model has been developed using Microsoft Visual Basic Express 2010 to predict the fire-resistance of CLT floor assemblies in both standard and non-standard fires. Layers of gypsum used to protect the CLT can also be included in the model. The purpose of the model is to provide an accurate prediction of the fire-resistance, along with detailed information of the assembly's temperature profile, deflection, bending resistance, char depth, charring rate and heated zone size throughout the entire simulation. Input parameters such as thickness, orientation and number of laminations, ambient properties of wood and gypsum, and the load imposed on the assembly can be modified as desired by the user.

The most common standard fires; ASTM E119, CAN/ULC-S101 and ISO 834, along with the Eurocode time-temperature curves for hydrocarbon fires, are included as options for the fire exposure selection. Unique non-standard fires can also be specified by inputting up to 30 temperatures points with associated times. To define all temperatures across an entire user specified non-standard fire curve, a linear interpolation is employed between known points.

The model solves the heat transfer equation for one-dimensional conduction described in Section 5.2 to calculate a temperature distribution throughout the depth of the assembly at each time interval. It was assumed that the temperature distribution found throughout the depth is identical across the entire length and width of panel. The

thermal and mechanical properties at each node are then reassessed based on the computed temperatures at each time step.

5.2 Heat Transfer Equations

The conduction equation for a one-dimensional, unsteady control volume is written as:

$$-kA\frac{\partial T}{\partial x}\Big|_x + \dot{q_G}A\Delta x = -kA\frac{\partial T}{\partial x}\Big|_{x+\Delta x} + \rho Ac\Delta x\frac{\partial T(x+\frac{\Delta x}{2},t)}{\partial t} \qquad \text{Eq. 5.1}$$

Where:

k = thermal conductivity, $W{\cdot}m^{-1}{\cdot}K^{-1}$

A = surface area through which heat is transferred, m^2

T = Temperature, K

x = node distance from surface, m

$\dot{q_G}$ = volumetric rate of heat generation, $W{\cdot}m^{-3}$

ρ = density of control volume, $kg{\cdot}m^{-3}$

c = specific heat capacity, $J{\cdot}kg^{-1}{\cdot}K^{-1}$

t = time, s

The second term is removed as no heat is generated in the wood or gypsum and the equation is divided by the area, *A*.

$$-k\frac{\partial T}{\partial x}\Big|_x = -k\frac{\partial T}{\partial x}\Big|_{x+\Delta x} + \rho c\Delta x\frac{\partial T(x+\frac{\Delta x}{2},t)}{\partial t} \qquad \text{Eq. 5.2}$$

In order to discretize the differential equation, the thickness of the panel is divided up into *N* small control volumes of height Δx (and $\Delta x/2$ at the boundaries), with nodes x_i, as shown in Figure 5-1.

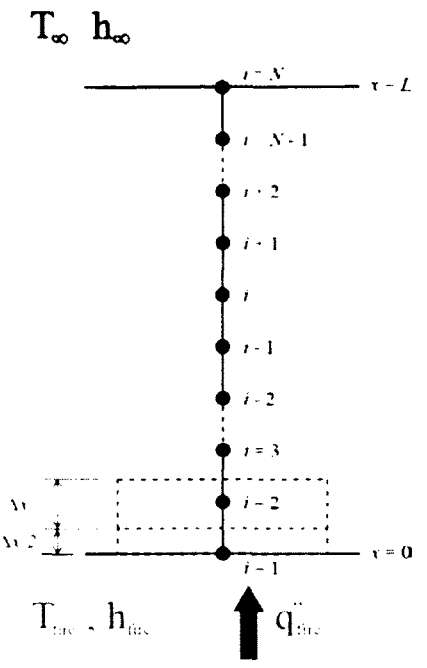

Figure 5.2: Discretization of CLT Panel for Numerical Analysis

Applying the control volume method and a discrete time step Δt, used by Kreith [55] we get the following equations:

$$t_m = m\Delta t \quad m = 0,1,2,\ldots \qquad \text{Eq. 5.3}$$

$$T_{i,m} \overset{\text{def}}{=} T(x_i, t_m) \qquad \text{Eq. 5.4}$$

$$-k\frac{T_{i,m} - T_{i-1,m}}{\Delta x} = -k\frac{T_{i+1,m} - T_{i,m}}{\Delta x} + \rho c \Delta x \frac{T_{i,m+1} - T_{i,m}}{\Delta t} \qquad \text{Eq. 5.5}$$

Rearranging Eq. 5.5 for the temperature at node *i*, in future time step of *m+1*, gives:

$$T_{i,m+1} = T_{i,m} + \frac{\Delta t}{\rho c \Delta x}\left\{\frac{k}{\Delta x}\left(T_{i+1,m} - 2T_{i,m} + T_{i-1,m}\right)\right\} \qquad \text{Eq. 5.6}$$

To avoid possible divergence, Eq. 5.6 is modified to its implicit [55] form by evaluating all of the temperatures in brackets at time step *m*+1 rather than at *m*. The equation is then simplified by defining the Fourier number, *Fo,* as follows:

$$\text{Fo}_i \overset{\text{def}}{=} \frac{k_i \Delta t}{\rho_i c_i \Delta x^2} \qquad \text{Eq. 5.7}$$

Substituting the Fourier number into the implicit form of the equation yields:

$$a_i T_{i,m+1} = \mathrm{b}_i T_{i+1,m+1} + c_i T_{i-1,m+1} + d_i \qquad \text{Eq. 5.8}$$

Where:

$$a_i = 1 + 2\mathrm{Fo}_i \qquad \text{Eq. 5.9}$$

$$\mathrm{b}_i = \mathrm{Fo}_i \qquad \text{Eq. 5.10}$$

$$c_i = \mathrm{Fo}_i \qquad \text{Eq. 5.11}$$

$$d_i = T_{i,m} \qquad \text{Eq. 5.12}$$

This equation can be solved to find the temperature at all nodes ($1 < i < N$); however, boundary conditions must be defined in order to solve for the temperature at the top and bottom surfaces of the panel. At the bottom surface the conduction term from the fire to node 1 in Eq. 5.5 is replaced with the convective and radiative heat transfer terms from the fire (subscript *f*), as shown in Eq. 5.13 below:

$$h_f\left(T_{f,m} - T_{1,m}\right) + \epsilon\sigma\left(T_{f,m}^4 - T_{1,m}^4\right) = -k\frac{T_{2,m} - T_{1,m}}{\Delta x} + \rho c\frac{\Delta x}{2}\frac{T_{1,m+1} - T_{1,m}}{\Delta t} \qquad \text{Eq. 5.13}$$

where h_f, ϵ, and σ are the convective heat transfer coefficient, emissivity factor, and the Stefan–Boltzmann constant, respectively.

Solving Eq. 5.13 for $T_{1,m+1}$ in its implicit form and substituting the Fourier number into the equation yields:

$$a_1 T_{1,m+1} = \mathrm{b}_1 T_{2,m+1} + d_1 \qquad \text{Eq. 5.14}$$

Where:

$$a_1 = 1 + 2\mathrm{Fo}\left[\frac{\Delta x}{k}\left(h_f + \epsilon\sigma T_{1,m+1}^3\right) + 1\right] \qquad \text{Eq. 5.15}$$

$$\mathrm{b}_1 = 2\mathrm{Fo} \qquad \text{Eq. 5.16}$$

$$d_1 = T_{1,m} + 2Fo\frac{\Delta x}{k}T_{f,m+1}\left(h_f + \epsilon\sigma T_{f,m+1}^3\right) \qquad \text{Eq. 5.17}$$

The term, $T_{1,m+1}^3$ in the coefficient a_1 represents the temperature at the bottom surface one time step into the future. This temperature is being solved for, and is therefore unknown. To avoid the complexity of having to solve a fourth order equation, an approximation is made for this term. The surface temperature at the next time step can be estimated by taking the average of the fire temperature at the next time step and the surface temperature at the current time step. This gives a coefficient for a_1 of:

$$a_1 = 1 + 2\text{Fo}\left[\frac{\Delta x}{k}\left(h_f + \epsilon\sigma\left[\frac{T_{f,m+1} + T_{1,m}}{2}\right]^3\right) + 1\right] \qquad \text{Eq. 5.18}$$

At the top surface, the conduction term from node *N* to the ambient air in Eq. 5.5 is replaced with the convective heat transfer term to the air (subscript ∞). Radiation can be neglected at this boundary since the top surface was found to never increase more than a few degrees above the ambient temperature in all experiments. The boundary condition at the top surface is then written as:

$$-k\frac{T_{N,m} - T_{N-1,m}}{\Delta x} = h_\infty\left(T_{N,m} - T_{\infty,m}\right) + \rho c\frac{\Delta x}{2}\frac{T_{N,m+1} - T_{N,m}}{\Delta t} \qquad \text{Eq. 5.19}$$

Solving for $T_{N,m+1}$ in the implicit form and substituting the Fourier number into the equation yields:

$$a_N T_{N,m+1} = c_N T_{N-1,m+1} + d_N \qquad \text{Eq. 5.20}$$

Where:

$$a_N = 1 + 2\text{Fo}\left[\frac{\Delta x}{k}h_\infty + 1\right] \qquad \text{Eq. 5.21}$$

$$c_N = 2\text{Fo} \qquad \text{Eq. 5.22}$$

$$d_N = T_{N,m} + 2Fo\frac{\Delta x}{k}T_{\infty,m+1}h_\infty \qquad \text{Eq. 5.23}$$

The initial condition applied at t = 0 assumes that all nodes of the wood and gypsum are at ambient temperature, such that; $T_{i,0} = T_\infty$ for $1 \le i \le N$.

In order to determine the temperatures at all nodes in the assembly at the next time step, Eq. 5.14 for $i = 1$, Eq. 5.8 for $1 < i < N$, and Eq. 5.20 for $i = N$ are rewritten in matrix form using the previously defined coefficients a_i, b_i, c_i and d_i, such that:

$$\boldsymbol{A} = \begin{bmatrix} a_1 & -b_1 & 0 & 0 & & & & \\ -c_2 & a_2 & -b_2 & 0 & \cdots & & 0 & \\ 0 & -c_3 & a_3 & -b_3 & & & & \\ & \vdots & & \ddots & & & \vdots & \\ & & & -c_{N-2} & a_{N-2} & -b_{N-2} & 0 & \\ & 0 & & \cdots \; 0 & -c_{N-1} & a_{N-1} & -b_{N-1} & \\ & & & 0 & 0 & -c_N & a_N & \end{bmatrix} \quad \text{Eq. 5.24}$$

where,

$$\boldsymbol{A} \times \begin{bmatrix} T_{1,m+1} \\ T_{2,m+1} \\ T_{3,m+1} \\ \vdots \\ T_{N-2,m+1} \\ T_{N-1,m+1} \\ T_{N,m+1} \end{bmatrix} = \begin{bmatrix} d_1 \\ d_2 \\ d_3 \\ \vdots \\ d_{N-2} \\ d_{N-1} \\ d_N \end{bmatrix} \quad \text{Eq. 5.25}$$

Since all the coefficients in matrix $\boldsymbol{A}$ are known along with all values of d_i, the system can be solved to find all new temperatures. The program takes advantage of the *tridiagonal matrix algorithm* [55] in order to solve the system efficiently. New temperatures calculated at each time step are used as the current temperatures in the next time step, which are then used to update the thermal and mechanical properties of both the gypsum and wood based on temperature-dependent relationships established in the literature.

5.3 Gypsum Boards

One of the important aspects of modelling gypsum protection, aside from protecting the wood from the fire exposure, is to effectively simulate the time that it remains in-place

on the specimen. This is comprised of two main components; an accurate representation of the thermal properties as a function of temperature, and defined criteria to determine when gypsum boards fall off. Gypsum boards incorporated into the model do not provide any structural strength to assemblies and therefore no mechanical properties for the boards were included.

Equations of the thermal properties of gypsum such as density, conductivity and specific heat capacity are garnered from the literature [38] [39] [40] [41] [56]. Graphs of the temperature-dependent relationships for the thermal conductivity (Figure 2-17), specific heat capacity (Figure 2-20), and density (Figure 2-23) of gypsum used in the model can be found in Section 2.7: Thermal Properties of Gypsum. These are very important features of the model as they define how the board heats up throughout the test and in particular, how the dehydration reaction [56] in gypsum will be accounted for. When the temperature of a node in the gypsum board is between 100°C and 150°C, a drastic change in the specific heat capacity occurs. In this temperature range, the SHC increases up to 18 times higher than its original value, before decreasing back down to just below its original value at 150°C. This spike represents the energy absorbed during the dehydration reaction and subsequent evaporation of the liberated water molecules. This is an important part of modelling gypsum as it represents a significant period of time during which the temperature of the board is held at around 100°C, effectively delaying heat transfer to the assembly it is protecting. A similar, yet less severe, process occurs in nodes of wood for temperatures between 100°C and 120°C.

Although there is plenty of information available regarding how gypsum performs on light frame wood structures, there is very little research regarding criteria at which gypsum panels fall off CLT floors when exposed to either standard or non-standard fires. Therefore the gypsum board fall-off criteria built into the model was designed to best match the fall-off times that were observed in the full-scale CLT tests done by FP Innovations [17]. FPInnovations' work was compared to fall-off times found by Sultan [38] for wood-frame assemblies and found to be reasonably similar. Although FPInnovations tests are a small sample size to base the model on, Sultan's work provides some validation in its usage. However, as more research on the subject is completed, the model will be updated accordingly.

5.4 Charring and Heated Zone

Char formation in the wood is determined by all nodes with a temperature greater than or equal to 300°C, as is the commonly accepted value in the literature. The char depth is determined during the simulation by following the 300°C isotherm as it progresses throughout the panel at each time step [14]. This information is then used to calculate the charring rate.

Once a node is considered to be converted to char, it remains in place for subsequent heat transfer calculations unless the ply it is in delaminates, just as any other node in the assembly. The properties of wood and char are based on information from the literature [8] [24] [25] [26] [27] and are continuously updated as the temperature of a charred node increases. Graphs of the temperature-dependent relationships for the

thermal and mechanical properties of wood can be found in Section 2.6: Wood Properties. These include graphs for the modulus of elasticity (Figure 2-7), thermal conductivity (Figure 2-10), specific heat capacity (Figure 2-12), and density (Figure 2-14). The model does not incorporate char fall-off or regression, since information of this nature was unavailable in the literature. However, as temperatures in nodes increase beyond 300°C, they continually provide less and less thermal protection to the uncharred wood above. Thermal property relationships built into the model cause density and heat capacity values to significantly decrease while thermal conductivity increases. By the time a node reaches 1200°C it will possess 7.5% of its original density, zero heat capacity and a continually increasing conductivity, thus providing an approximation of heat transfer through a regressed or fallen charred node.

The heated zone is determined by adding the distance between all nodes from the char front to the unexposed side of the panel that have a temperature greater than 22°C.

3.5 Failure Criteria

The CAN/ULC-S101-07 standard fire-resistance test [5] has three failure criteria; structural, insulation and integrity. The structural criterion states that the assembly must support the load applied for the duration of the test. Insulation failure occurs when the unexposed side of the panel exceeds an average temperature increase greater than 140°C from its original temperature or 180°C at any one location on the assembly. The integrity of the panel is considered to have failed if the passage of flame or gases hot enough to ignite a cotton pad occurs on the unexposed side.

Integrity failure was observed to occur in full-scale experiments at the lap joint between two panels, but never through a solid section of the panel. Joints are not included in the model, as they would require a two- or three-dimensional analysis to simulate the geometry and widening of a lap joint as it chars. Therefore integrity failure could not be assessed by the model.

The model assesses the structural capacity of the assembly as well as the insulation failure criteria at each time interval. The temperature at the unexposed side of the panel never raised more than a few degrees, and as a result, in only very rare and unrealistic cases would insulation failure cause a CLT test to be terminated. Therefore, the fire resistance of the assembly in the model is essentially determined by the weakening of the structural resistance as the panel chars.

5.5.1 Moment Resistance Calculation

Following the Canadian Standard for Engineering Design in Wood (CSA O86) [24], the factored bending moment resistance and shear resistance of the panel are calculated. When various loads are applied and the required bending and shear strength are calculated, it is clear in the vast majority of cases of CLT floor assemblies, aside from unrealistically short spans, that structural failure due to fire exposure will occur in bending long before shear failure occurs. Thus the governing factor in the model when determining the fire resistance of the panel is the bending moment resistance.

As a CLT panel chars, the cross sectional area decreases, effectively reducing its mechanical strength. The bending strength of the panel is calculated at each time step

using a slightly modified version of the procedure described in the CLT Handbook [57]. The CLT Handbook proposes calculating the char depth by using a fixed charring rate of 0.65 mm/min as specified in Eurocode 5 Part 1-2, Table 3.1 [14, p. 23]. It also instructs using a heat-affected zone of 10.5 mm after 20 min which, along with the charred layer, contribute zero strength to the assembly. To attempt to increase the accuracy of this method, the numerical model instead utilises a temperature-dependent relationship for the modulus of elasticity of wood, illustrated in Figure 5-2. Temperatures calculated at each discrete node from the heat transfer model described in Section 5.2 are used to evaluate the reductions in strength that occur.

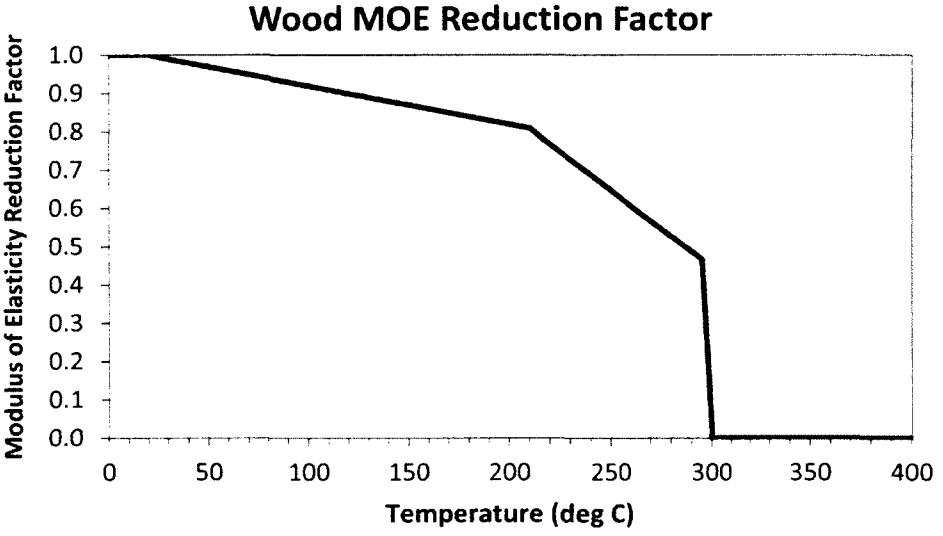

Figure 5-2: Reduction in wood modulus of elasticity multiplication factor used in numerical model

All control volumes and their accompanying modified modulus of elasticity are then used following the steps outlined in the CLT Handbook [57] to calculate an effective neutral axis, an effective stiffness and an effective section modulus (S_{eff}) for the entire panel. These parameters are used to calculate the factored bending moment resistance at each time step using Eq. 5.26, as stipulated in CSA O86 [24].

$$M_r = \phi F_b S_{eff} K_{zb} K_L \qquad \text{Eq. 5.26}$$

Where the resistance factor, $\phi = 0.9$ and

$$F_b = f_b(K_D K_H K_{Sb} K_T) \qquad \text{Eq. 5.27}$$

where f_b is the specified bending strength. K_{zb}, K_L, K_D, K_H, K_{Sb} and K_T are the size factor in bending, are the lateral stability factor, load duration factor, system factor, service condition factor and treatment factor, respectively. By default, all are set to equal 1, but can be changed in the user interface developed for the model, as shown in Figure 5-3.

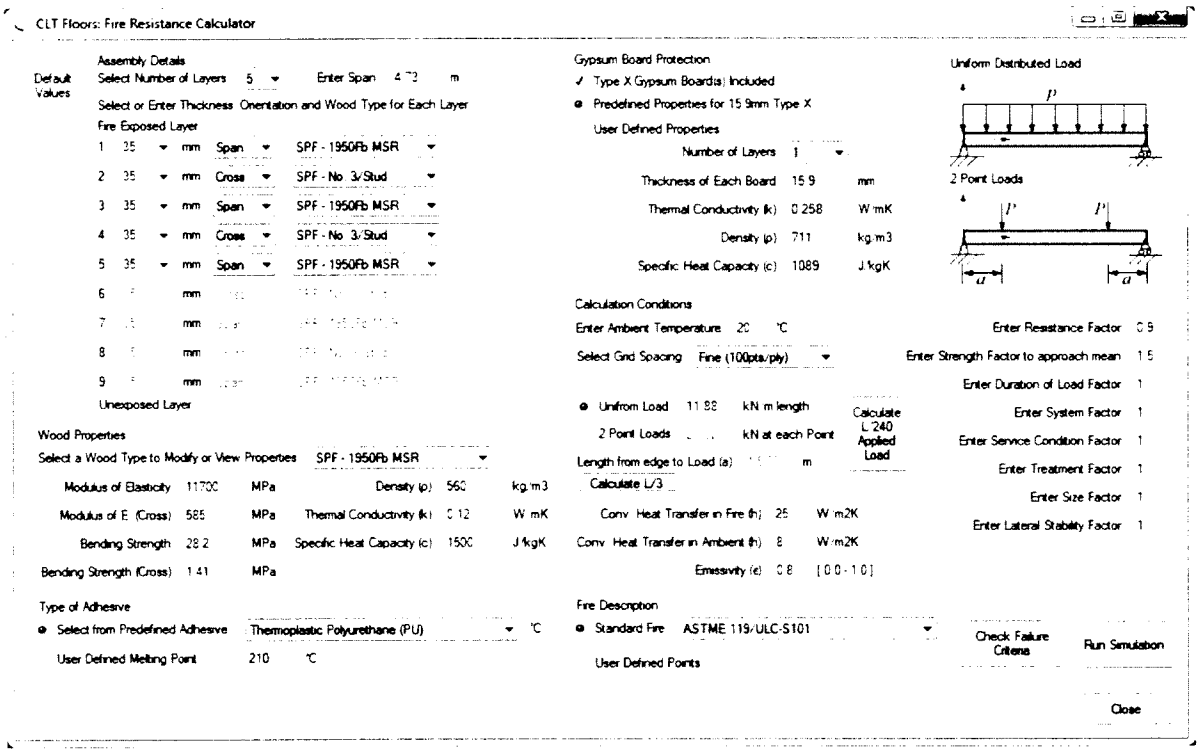

Figure 5-3: Graphical User Interface for Numerical Model to Calculate the Fire Resistance of CLT

The structural model is based on an ultimate limit state approach. In this scheme, the factored bending moment resistance (M_r) from Eq. 5.26, that the remaining cross section of the panel can produce, must be greater than the bending moment (M_f) that is required to support the load, as shown in Eq. 5.28.

$$M_r \geq M_f = \frac{wL^2}{8} \qquad \text{Eq. 5.20}$$

The simulation is terminated once this condition is no longer met.

5.6 Delamination of Plies

Ply delamination was observed to occur when temperatures at the adhesive bond line had reached around 210°C in both the medium- and full-scale experiments conducted in this study. This effect is simulated in the model when the thermoplastic polyurethane adhesive is chosen in the graphical user interface. When other adhesives are chosen from the predefined list, an estimated melting point appears in the box below the adhesive name. This temperature represents the bond line temperature required to trigger a delamination event during the simulation. Alternatively, the failure temperature of the adhesive being modelled can be inputted by selecting the "User defined melting point" option. It should be noted that if a melting point greater than 300°C is chosen, the model assumes a thermoset adhesive is used and delamination events do not occur, as per Frangi [19]. Rather plies remain in place and simply char through as temperatures increase.

Ply delamination during experiments is described in greater detail in Section 4.2.

5.7 Input Parameters

5.7.1 Loads

The type of loading applied to the panel can be selected from two options; a uniformly distributed load, or two point loads, as illustrated in the two diagrams at the top right

corner of the program window (Figure 5-3). If the two point loads are chosen, the distance (*a*) from the end of the panel to the point of loading must be entered. A button to automatically calculate one-third the distance of the span is available, which is typical when applying two concentrated loads. Regardless of whether the uniformly distributed load or two point loads are selected, a button to calculate the L/240 deflection can be used to determine the load required to satisfy this criterion. Once all assembly details have been entered, pressing this button will calculate the strength and weight of the assembly to determine the applied load necessary in order to produce an initial deflection equal to the span of the floor divided by 240.

5.7.2 Check Failure Criteria

A button is available to assess the strength and failure criteria of the assembly prior to running the simulation. This button calculates the maximum moment the currently defined panel assembly can resist, as well as the minimum moment required to support the specified applied load. The initial deflection the specified applied load will produce is also displayed.

5.7.3 Strength Factor to Approach Mean

The characteristic values listed for solid sawn lumber and many other engineered wood products are typically representative of the 5th percentile as a safety and reliability factor. This means that the strength found in 95 percent of a significantly large enough sample of timber would be expected to be greater than the stated value. To better represent the typical strength that would be found in real timber, an option is available to include a multiplication factor to the bending strength to provide a closer match to

the mean strength value of the lumber. This value is set to 1.5 by default, since this value was found to produce data similar to that which was observed in the real tests, but can be changed as desired in the user interface.

5.7.4 Numerical Model Process and Flow Chart

The process that the model follows when a simulation is run is outlined in the flow chart in Figure 5-4. This process is described in greater detail in this section.

When the program is executed, the graphical user interface appears and all assembly and test parameters are required to be input prior to running the simulation. After all parameters have been entered and the simulation is run, the model will first use the entered ambient temperature to calculate the initial material properties of the gypsum and wood in the defined assembly. Based on the temperature of the all nodes in the assembly, the model will then determine if any control volumes have been converted to char, along with the distance and rate that the char front has advanced from the last time step, as well as the size of the heat-affected zone. During the first time-step, these calculations will result in nil values, assuming that the ambient temperature is reasonably defined (i.e. less than 300°C). Next the model will calculate the maximum bending moment the panel is capable of resisting and compare that to the minimum bending moment required from the applied load. If the panel is not capable of supporting the load, the results are tabulated, the simulation is terminated, and all data and results are sent to an excel file for the user to review. If the panel is capable of supporting the load, the simulation continues and checks if gypsum protection is

present. If gypsum is included, the temperature at the back of each board is compared to the fall-off criteria set in the model. If the fall-off temperatures have not been reached, the gypsum board(s) will remain in place. If the fall-off temperature has been reached, the gypsum board in question is then considered to have fallen off in this time step. The model will then disregard all nodes in that board for future time steps and continue as if they are no longer present in the assembly. The model then determines if a ply delamination event has occurred by comparing the temperature at the adhesive bond line between each successive ply layer, to the adhesive failure temperature specified in the user interface. If a bond line temperature is greater than the defined adhesive failure temperature, the ply is considered to have delaminated in that time step and all nodes below that bond line will be disregarded in future calculations. Next the fire temperature, defined at the current time step, along with the previously calculated thermal properties at each node and corresponding control volume, are used to determine the new temperatures for each node throughout the entire remaining assembly. Once this calculation is complete, the program then loops to the next time step and, using the new temperatures, repeats this entire process. Once the maximum moment the panel is capable of resisting is no longer adequate support the moment required from the loads, the program is terminated and all data and results are tabulated and sent to an excel file. If the no failure criteria is met after eight hours have been simulated, the model is automatically terminated and all data and results are tabulated and sent to an excel file.

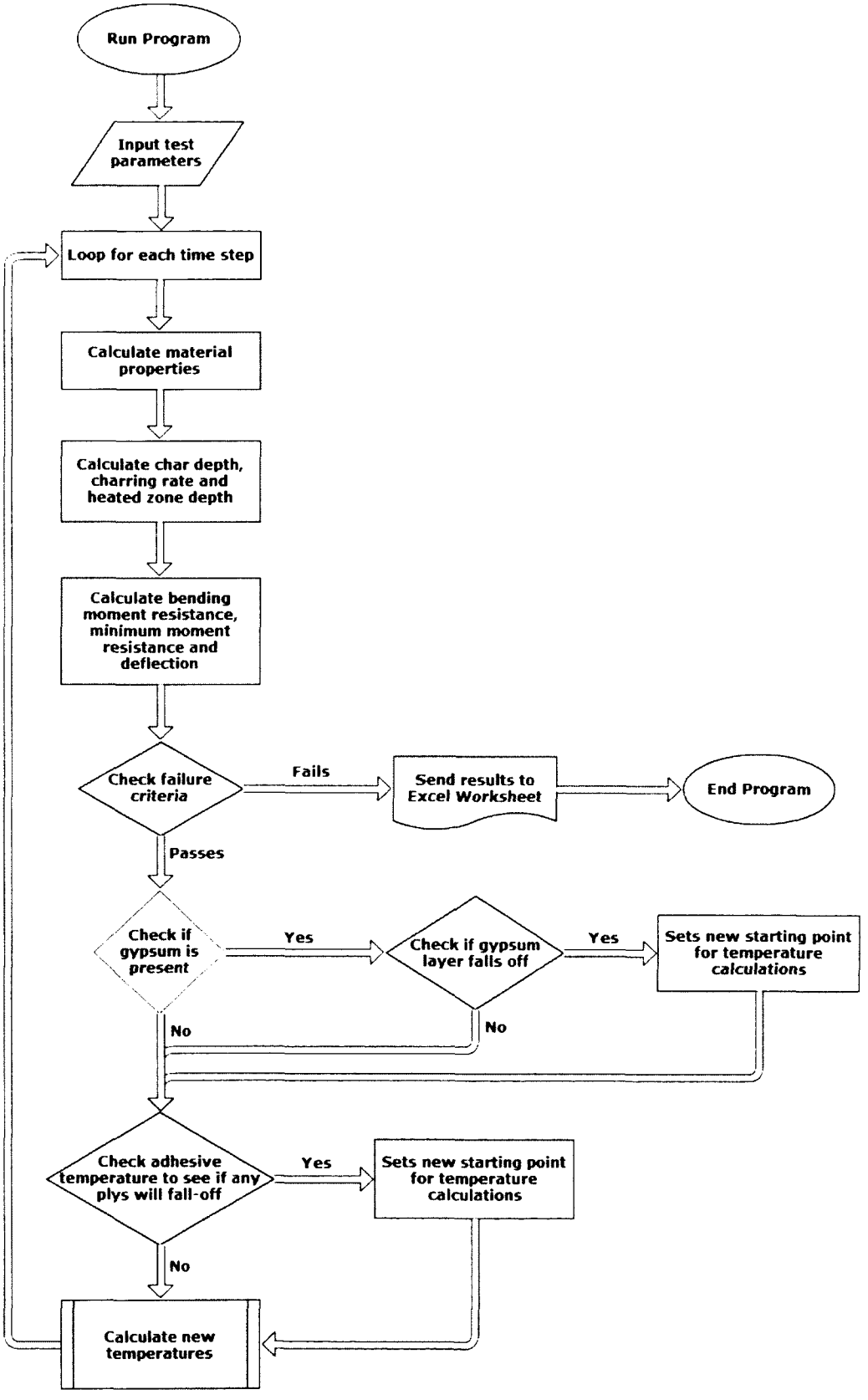

Figure 5-4: Process completed by numerical model to calculate fire resistance of CLT

6 Comparison of Model Predictions with Test Results

Each test conducted in this series was simulated using the numerical model. The results of these simulations are outlined and compared with experimental test results in the following sections.

6.1 Gypsum Boards

Gypsum boards were integrated into the model based on information from full-scale test results found in the literature and the full-scale tests conducted by FPInnovations. Accordingly, gypsum performance in the model displays a closer fit to full-scale test results than to medium-scale test results, as shown in Table 6-1 and Figure 6-1.

Table 6-1: Gypsum fall-off times from numerical model and experiments

# of Plies	Type X Gypsum Protection	Fire	Face Gypsum Board Failure Time (min)	Face Gypsum Board Finish Rating (min)	Base Gypsum Board Failure Time (min)	Base Gypsum Board Finish Rating (min)
3	**1x 5/8"**	**CAN/ULC**	-	-	**55 (47) {52}**	**23 (24) {21}**
3	**2x 1/2"**	**CAN/ULC**	**60 (51) {65}**	**17 (28) {15}**	**76 (66) {76}**	**47 (55) {46}**
3	2x 1/2"	Non-Std	40 (28)	13 (21)	Did not fall (82)	37 (42)
5	**1x 5/8"**	**CAN/ULC**	-	-	**54 (37) {26}**	**22 (23) {22}**
5	1x 5/8"	Non-Std	-	-	30 (26)	17 (17)

No parentheses indicate model results
( ) parentheses indicate medium-scale results
{ } parentheses indicate full-scale results

Gypsum properties vary significantly depending on the manufacturer as well as the time of production. This typically results in a low level of repeatability when conducting

gypsum experimentation. It is therefore difficult to precisely simulate gypsum performance in the model. However, gypsum temperatures produced from the model still follow trends similar to those observed in full-scale experimentation, as demonstrated in Figure 6-1.

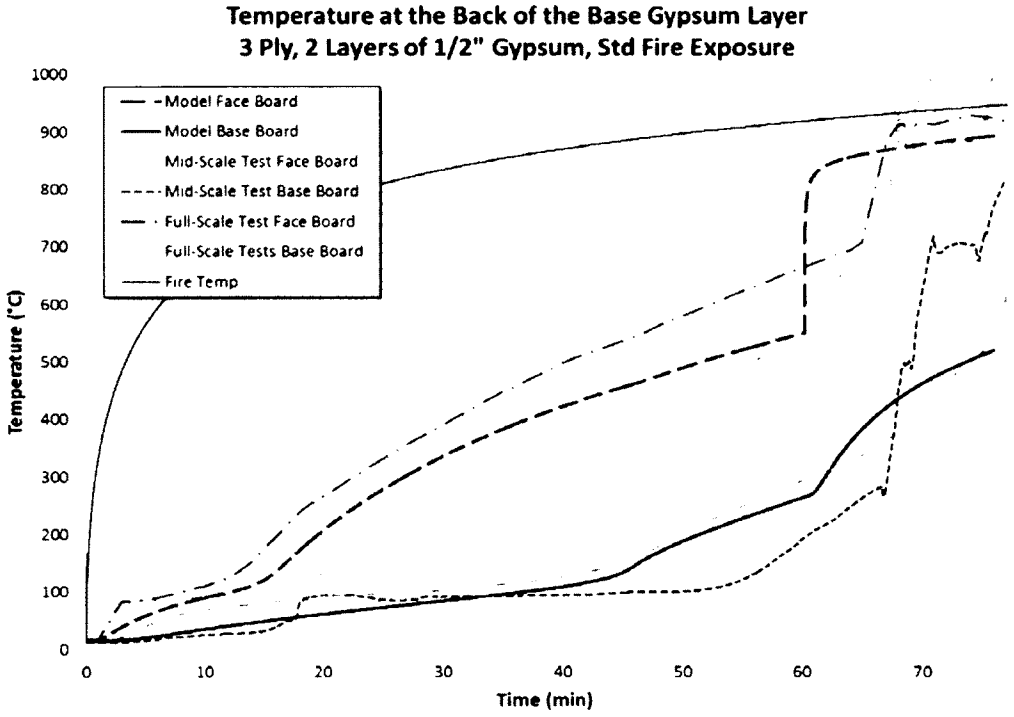

Figure 6-1: Comparison between model and experimental temperatures found at the back of gypsum layers from a 5-ply panel with 1 layer of gypsum standard fire test

6.2 Ply Delamination

Unlike real tests, once the delamination criteria has been triggered in the model, an entire ply will fall-off all at once, as opposed to over a span of several minutes. Despite this limitation, ply delamination performed very well in the model; falling off at times within, or very close to, the ranges of both medium-scale and full-scale delamination times, listed in Table 6-2.

Table 6-2: Summary of Model Predictions and Experimental Results

# of Plies	Type X Gypsum Protection	Fire	First Ply Failure (min)	Second Ply Failure (min)
3	Unprotected	CAN/ULC	57 (64-65)	-
3	1x 5/8"	CAN/ULC	86 {80+}	-
3	2x 1/2"	CAN/ULC	107 (107-111)	-
3	2x 1/2"	Non-Std	89 (-)	-
5	Unprotected	CAN/ULC	55 (58-70) {60-65}	90 (87+) {92+}
5	Unprotected	Non-Std	41 (38-53)	88 (-)
5	1x 5/8"	CAN/ULC	85 (79-82) {75-81}	117 (115+) {107+}
5	1x 5/8"	Non-Std	69 (54-80)	- (-)

No parentheses indicate model results; ( ) parentheses indicate medium-scale results; { } parentheses indicate full-scale results

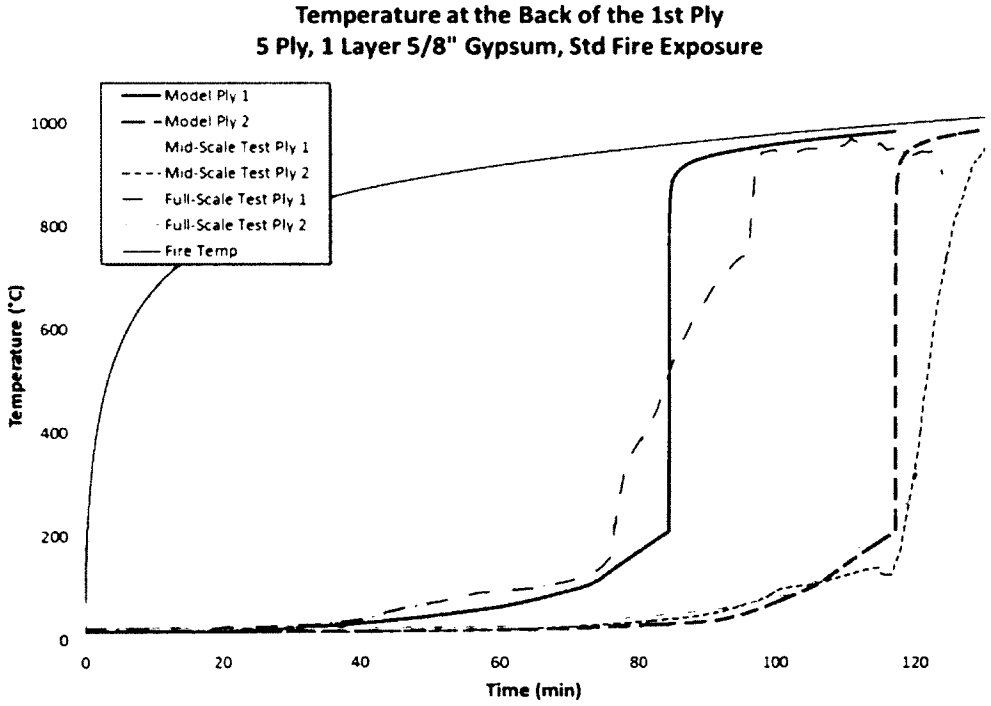

Figure 6-2: Comparison between model and experimental temperatures found at the back of ply layers from a 5-ply panel with 1 layer of gypsum standard fire test

Figure 6-2 compares average temperatures found at the first and second ply interfaces in the medium- and full-scale tests to delamination temperature curves produced by the model. The figure shows the experimental data and numerical results are in good agreement.

6.3 Charring

Char depth and charring rate calculations were determined every second at a grid resolution of 0.35 mm in the model, while experimental data were measured at intervals of 8.75 mm or 17.5 mm. This allowed for a much more detailed analysis of how charring proceeded in simulations than in the experimental tests. Comparable results from the model are listed in Table 6-4.

Table 6-3: Summary of average charring rates calculated at various depths from numerical model

# of Plies		3	3	3	3	5	5	5	5
Type X Gypsum Protection		-	1x 5/8"	2x 1/2"	2x 1/2"	-	-	1x 5/8"	1x 5/8"
Fire		ULC	ULC	ULC	NonStd	ULC	NonStd	ULC	NonStd
Onset of Charring (min)		2.7	31	62	44	2.5	1.5	31	21
Avg. Charring rate at: (mm/min)	8.75mm	0.87	0.44	0.64	0.50	0.90	1.51	0.45	0.91
	17.50mm	0.66	0.59	0.84	-	0.69	1.04	0.60	1.00
	26.25mm	0.55	0.55	0.70	-	0.57	0.82	0.56	0.68
	35.00mm	0.54	0.54	0.66	-	0.56	0.76	0.55	0.74
	43.75mm	0.77	0.76	0.93	-	0.79	1.05	0.78	0.86
	52.50mm	0.80	0.81	0.96	-	0.82	1.05	0.82	0.74
	70.00mm	-	-	-	-	0.75	0.81	0.76	-
	87.50mm	-	-	-	-	0.87	-	0.88	-
Mean		0.70	0.62	0.79	0.50	0.74	1.01	0.68	0.82
σ		0.14	0.14	0.14	-	0.13	0.26	0.15	0.12

Model results demonstrated similar charring trends to those observed in medium-scale tests, although the exact charring rate values produced by the simulation are not perfectly comparable to experimental values. Differences between experimental and

simulated charring rates are present due to the variability of the fire and wood in real tests, in combination with the high level of sensitivity embodied in the calculation itself. A far better method of comparing charring rates generated from the model with those found in experiments, is to plot the char depth against time, as shown in Figure 6-3.

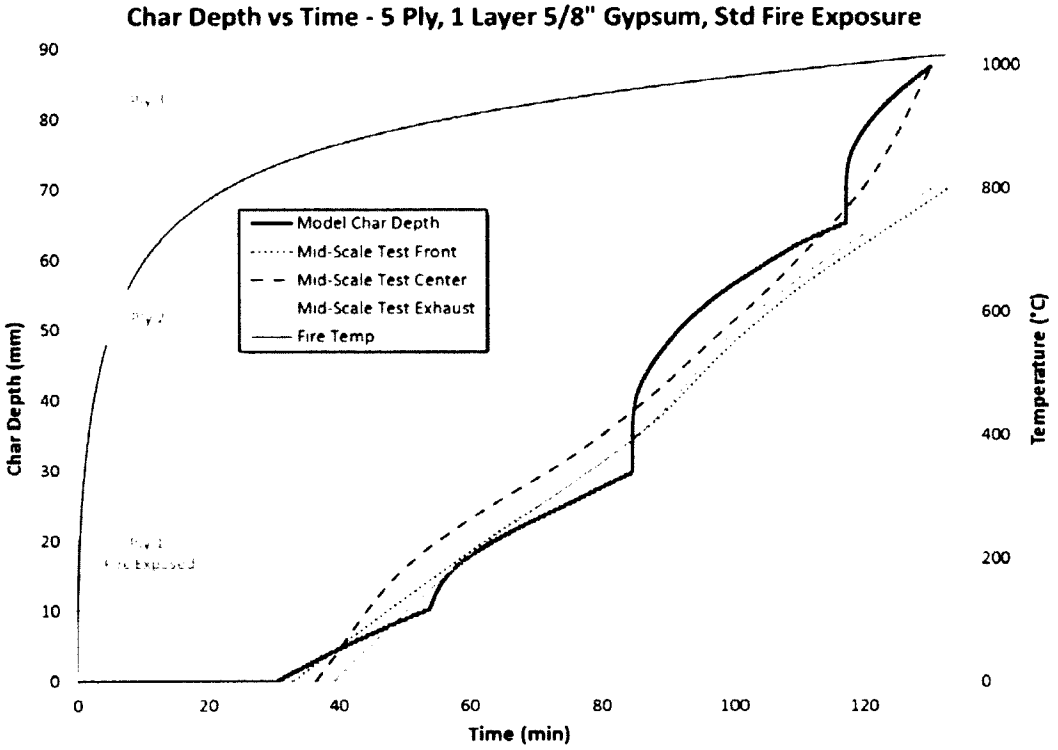

Figure 6-3: Comparison between model and experimental char depth in a 5-ply panel with 1 layer of gypsum

From the graph, it is easier to see that the overall trend of char progression produced by the model is very similar to that found in test results. However, due to the high frequency of measurements of the char depth and the uniform nature of the wood properties used in the model; a much more pronounced jump in char depth occurs when a ply delaminates.

Charring rates can be calculated on a significantly finer scale in the model than in experiments and the time it takes for the char front to advance to the next node in the

model can be used to calculate a nearly "instantaneous charring rate" in the panel. While the "effective charring rate" is the char depth divided by the time difference between when charring began at the surface and the time until the current char depth was reached. The effective charring rate could be calculated in the model with the same intermittency as the instantaneous charring rate. Information regarding how the charring rate changes in CLT panels can offer helpful insight in creating a simpler calculation method for determining char depth. A plot of the char depth, effective charring rate, and instantaneous charring rate produced from the model is presented in Figure 6-4.

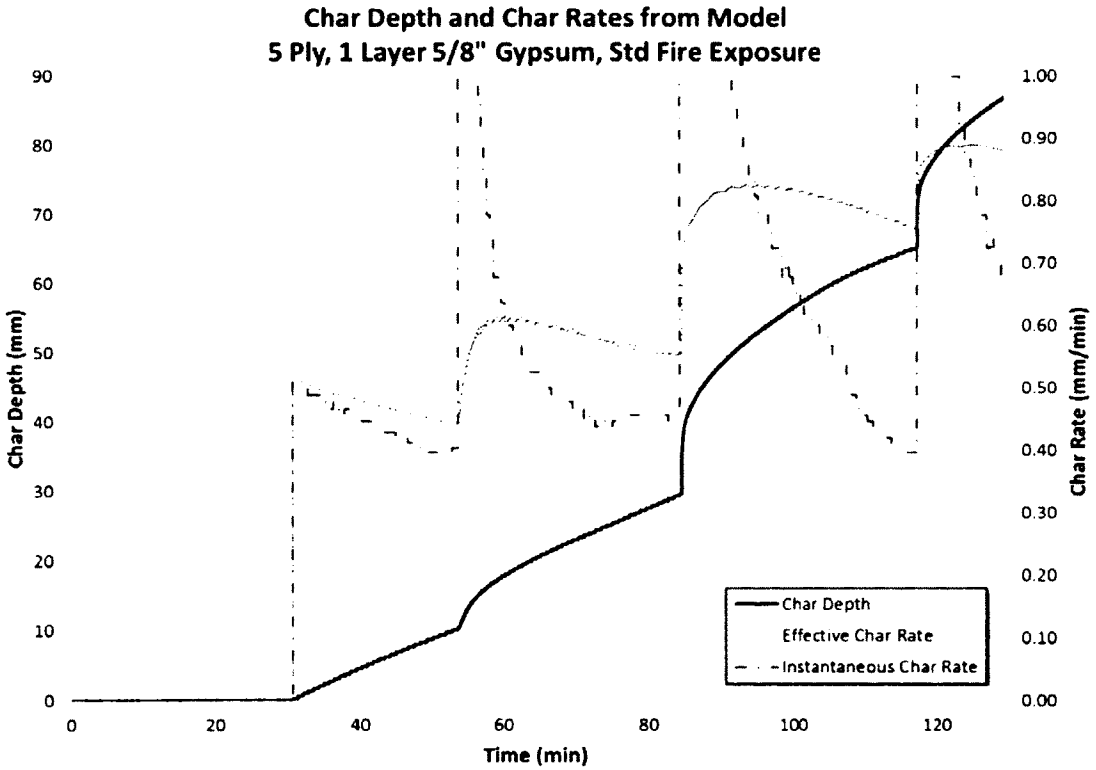

Figure 6-4: Char depth, effective charring rate and instantaneous charring rate determined by the model in a 5-ply panel with 1 layer of gypsum during a standard fire test

From this graph, spikes in the instantaneous charring rate, up to 100 mm/min are caused when gypsum fails or each time a ply delaminates. This kind of detailed

information was not possible to observe in the test series and illustrates how quickly heat transfers into the panel after such an event. The effective charring rate and how it changes throughout the course of the simulation provides an understanding into how char in CLT cannot be simply modelled for practical design purposes. The graph illustrates that a single effective charring rate would not provide a suitable substitute for the dynamic changes observed.

6.4 Temperature Profile and Heat-Affected Layer

The heat-affected layer calculated by the model exhibits a fairly close correlation with experimental results, as shown in Table 6-4. More interestingly, a clear trend that was assumed would occur in experiments, given more tests completed, is visible in model results for the heat-affected layer thickness. That is, that the presence of gypsum board protection causes the overall average size of the heated zone to increase. This trend is evident in the 3-ply results listed in Table 6-4.

Table 6-4: Summary of average heat-affected layer from numerical model

# of Plies	Type X Gypsum Protection	Fire	Avg. Heated Zone (mm)
3	**Unprotected**	**CAN/ULC**	**33 (46)**
3	**1x 5/8"**	**CAN/ULC**	**36 (45)**
3	**2x 1/2"**	**CAN/ULC**	**47 (50)**
3	2x 1/2"	Non-Std	54 (66)
5	**Unprotected**	**CAN/ULC**	**40 (40)**
5	Unprotected	Non-Std	51 (42)
5	**1x 5/8"**	**CAN/ULC**	**40 (41)**
5	1x 5/8"	Non-Std	51 (49)

( ) *parentheses indicate medium-scale results*

The size of the heated-zone generated in the numerical model is tracked throughout each simulation and shown in Figure 6-5. Interestingly, it appears that the heated-zone would continually grow in size if it were not for ply delamination, which allows the char front to catch up to the fast advancing heat penetration into the panel.

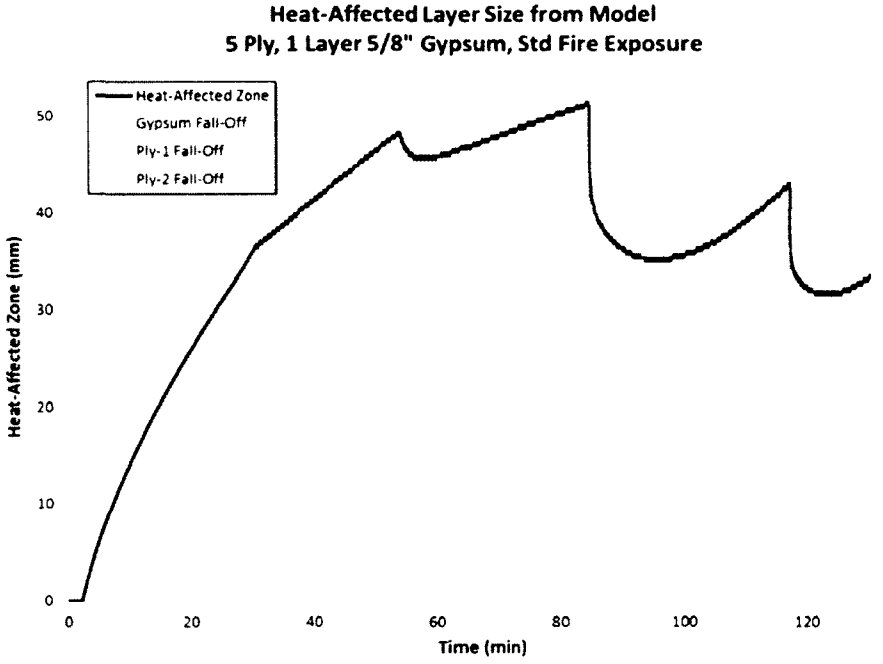

Figure 6-5: Heat-affected layer size determined by model in a 5-ply panel with 1 layer of gypsum standard fire test

6.5 Deflection

During the experiments, localised cracking was heard as panels deflected. These small cracks allowed stresses in the panel to redistribute more evenly, resulting in a more steady increase in deflection. This phenomenon was not captured in the model. The anisotropic, yet perfectly uniform properties of wood used in the model, produced smaller deflections and more abrupt increases when a ply delamination occurred, than was observed in experiments. This is illustrated in the 5- and 3-ply panel deflection graphs in Figure 6-6 and Figure 6-7.

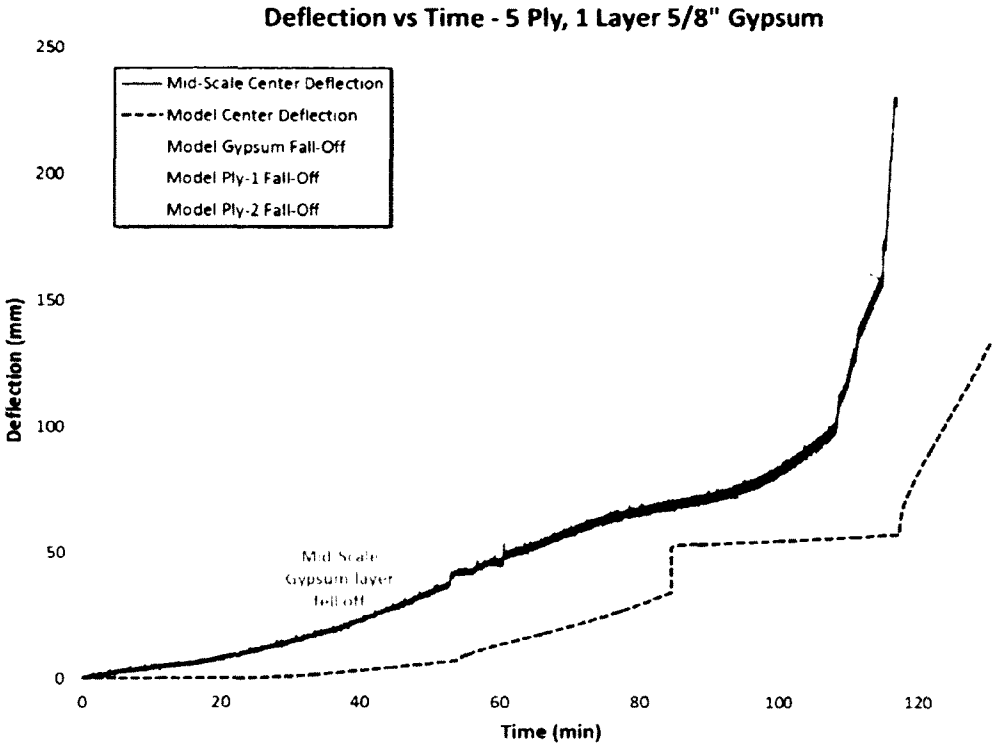

Figure 6-6: Comparison between model and experimental deflection in a 5-ply panel with 1 layer of gypsum

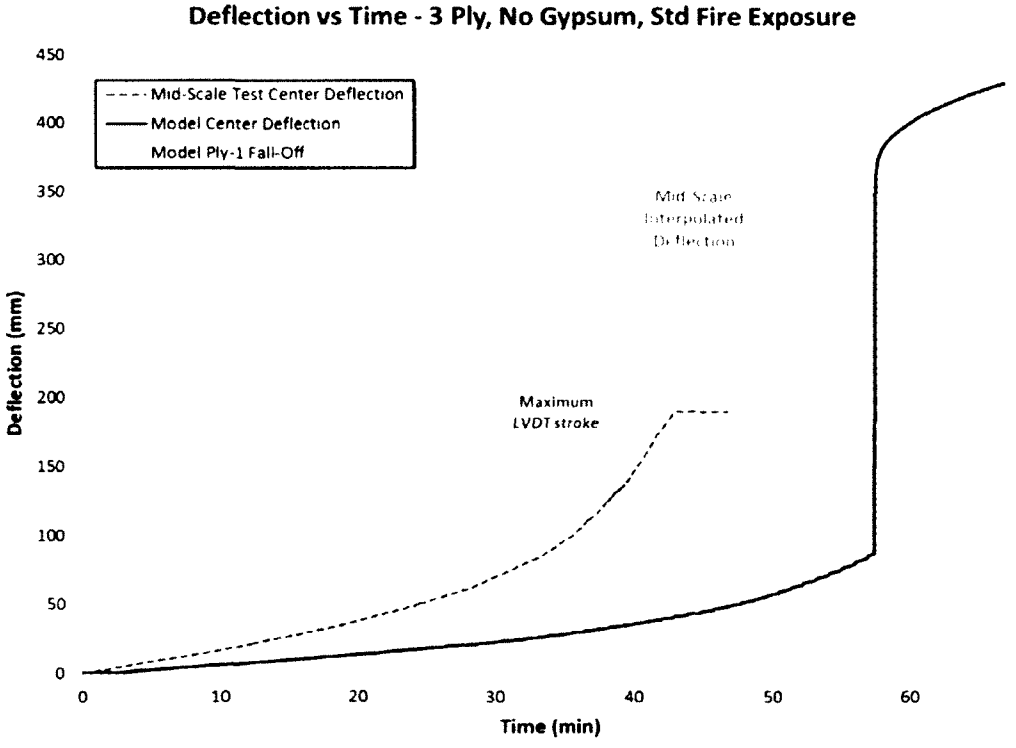

Figure 6-7: Comparison between model and experimental deflection in a 3-ply panel

The graph of the 3-ply panel in Figure 6-7, demonstrates how much of the bending resistance of the whole floor is contingent on the outmost spanning ply. Once the first ply delaminates, deflection in the panel increases drastically and the floor fails soon after.

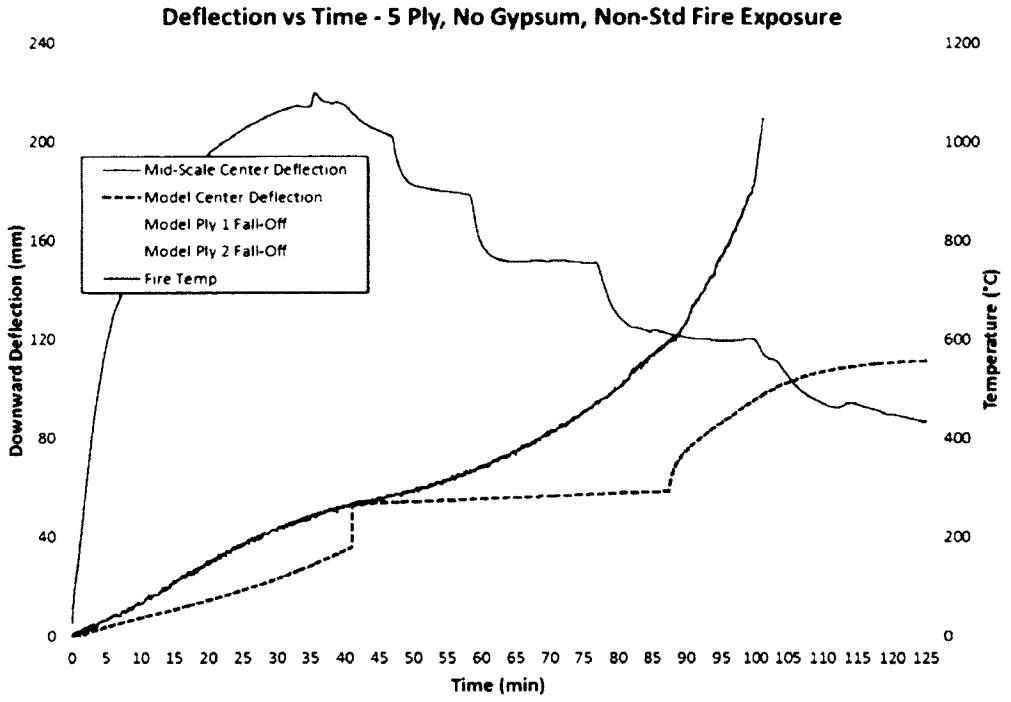

Figure 6-8: Comparison between model and experimental deflection in a 5-ply panel exposed to the non-standard fire

Non-standard fire simulations produce similar deflection predictions, although once the fire begins to cool in the decay phase, deflection begins to slow considerably, as illustrated in Figure 6-8. In the experiments using non-standard fires, deflection constantly increases throughout the test regardless of the decreasing fire temperature. This is likely caused by smouldering or flaming wood in the panel continuing to generate heat, char and degrade the strength of the floor. A heat generation term is not included in the model and the temperature of the wood is based solely on the temperature of

the fire. Therefore the effect of flaming and smouldering wood is unaccounted for and evident from the slowing of charring and deflection in panels as fire temperatures in non-standard fire simulations decrease.

6.6 Fire Resistance

The fire resistance determined by the model is the time until structural failure occurs. However, experimental tests were not permitted to continue until structural failure occurred. Thus times noted for all experimental test in Table 6-5, are shorter than those calculated by the model.

Table 6-5: Comparison between numerical model and experimental fire resistance

# of Plies	Type X Gypsum	Fire	Numerical Model†	Medium-Scale	Full-Scale
3	-	CAN/ULC	67 min	46 min	-
3	1x 5/8"	CAN/ULC	96 min	74 min	86 min
3	2x 1/2"	CAN/ULC	116 min	92 min	77 min*
3	2x 1/2"	Non-Std	83 min'	93 min	-
5	-	CAN/ULC	104 min	99 min	96 min
5	-	Non-Std	111 min'	101 min	-
5	1x 5/8"	CAN/ULC	130 min	115 min	124 min
5	1x 5/8"	Non-Std	98 min'	122 min	-

† *Numerical model results indicate time to structural failure, rather than integrity failure*

* *Test was stopped prematurely due to safety concerns after base gypsum layer failed*

' *Tests did not finish, indicates time that charring into the panel stopped*

In all standard 3-ply tests, the model predicted structural failure to occur roughly 10 minutes after the first ply delaminated, while experimental tests were ended just before the first ply fell-off. Predictions of first ply delamination from the numerical model correlate very closely with the first ply delaminations observed in experiments. It is likely that structural failure of real 3-ply panels would have also occurred around 10 minutes after the first ply fell off; however, from observations made in full-scale tests,

failure is likely to occur from integrity failure, i.e. flame passage, before structural failure occurs.

Model predictions of structural failure in both standard 5-ply panel tests occur around 14 minutes after second ply delamination. In physical experiments, the tests were ended when deflection began to increase dramatically, indicating structural failure was imminent. Model predictions of structural failure in these panels were only a few minutes after experimental tests were ended, and therefore also likely represent a good prediction of failure times. However, from the full-scale test results, the 5-ply panels also failed due to flame passage, prior to structural failure.

Since the model is not capable of predicting when flames will penetrate the assembly which, from the full-scale test series, appears to be the primary source of failure, the fire-resistance ratings determined from structural failure are likely longer than actual fire-resistance ratings of these floors.

Floors exposed to non-standard fires, both in the model and during physical tests, did not fail structurally. As the design fire temperature decreased, charring and deflection slowed and eventually stopped altogether. The times at which charring into the panels had stopped completely are listed in Table 6-5.

During the experiments using non-standard fires, the first ply did not fall-off during the 3-ply test, and the second ply did not fall off during the two 5-ply tests. Thus structural failure was deemed unlikely to occur. However, retrospective analysis of the data shows that deflection in all three floors continued to increase. This is believed to be caused by

residual flaming and smouldering of the wood in the panel. Despite retaining the last integral structural ply, deflections in these panels increased to a point where they were approaching damaging thermocouples in the furnace, and tests were ended. However, if tests were continued, it is probable that the first ply would have continued smouldering until it fell-off, causing structural failure. This amount of deflection was not observed in model predictions.

While the model seems to predict comparable results to the standard fire tests, it did not perform well when compared with the non-standard fire tests. This is mostly due to the fact that the model is based entirely on empirical temperature-dependent relationships derived from standard fire tests. This information does not encompass the effects of decreasing fire temperatures on material properties. The current model simply uses the material properties calculated from the highest past temperature attained at each point in the assembly. However, residual heat from flaming and smouldering in the wood may cause properties to continue to degrade as fire temperatures drop during the decay phase of a real fire. In order to incorporate a set of material properties intended for the decay phase of a fire, significantly more research in this area is required.

6.6.1 CLT Handbook Fire Resistance Calculation

The CLT Handbook [15] produced by FPInnovations, offers a simplified method of calculating the fire resistance of CLT panels exposed to the standard fire. This method involves the use of design values from the CSA O86 [24], and is based on the Eurocode's

reduced cross section method [14, p. 30]. This method is very similar to the approach used in the numerical model described in this report in Chapter 5. However, as opposed to calculating temperatures via a method of one-dimensional heat transfer in order to determine the char depth and charring rates, a constant charring rate of 0.65 mm/min from EN 1995-1-2 [14] is used.

The method stipulated in the CLT Handbook was used to calculate the fire-resistance of a 3-ply and 5-ply panel without gypsum protection. The results are compared with identical panels simulated in the numerical model, shown in Figure 6-9 and Figure 6-10. Based on a load criterion that initially produces an L/240 deflection in the panel, these graphs illustrate the maximum moment resistance capacity each panel is capable of, and how it reduces as the panel chars. The minimum required moment to maintain the load is depicted by a horizontal line. Once the moment resistance of the panel is lower than the minimum required moment resistance, structural failure is assumed to occur.

The sudden increase in the resistance of the 5-ply panel is a result of the calculation method. When the first ply falls off, the load is transferred to the third ply, since the second ply contributes no strength to the panel. This results in a large reduction in the distance from the neutral axis to the outermost uncharred edge of the bending ply, which has now moved from the first to the third ply. This causes the effective section modulus to increase, and by extension, increases the moment resistance. In reality this would not occur in this manner, since the load would gradually transfer to the third ply even as the first ply was still nearly completely intact. This scenario is not as simple to

model and requires finite element analysis software to simulate. This kind of high level detail was avoided to maintain simplicity and speed in the model. A model that did include this kind of analysis in the moment resistance calculation would show a more shallow slope as the first ply charred, connecting smoothly with the nearly horizontal line, shown in Figure 6-9, indicating the second ply is charring.

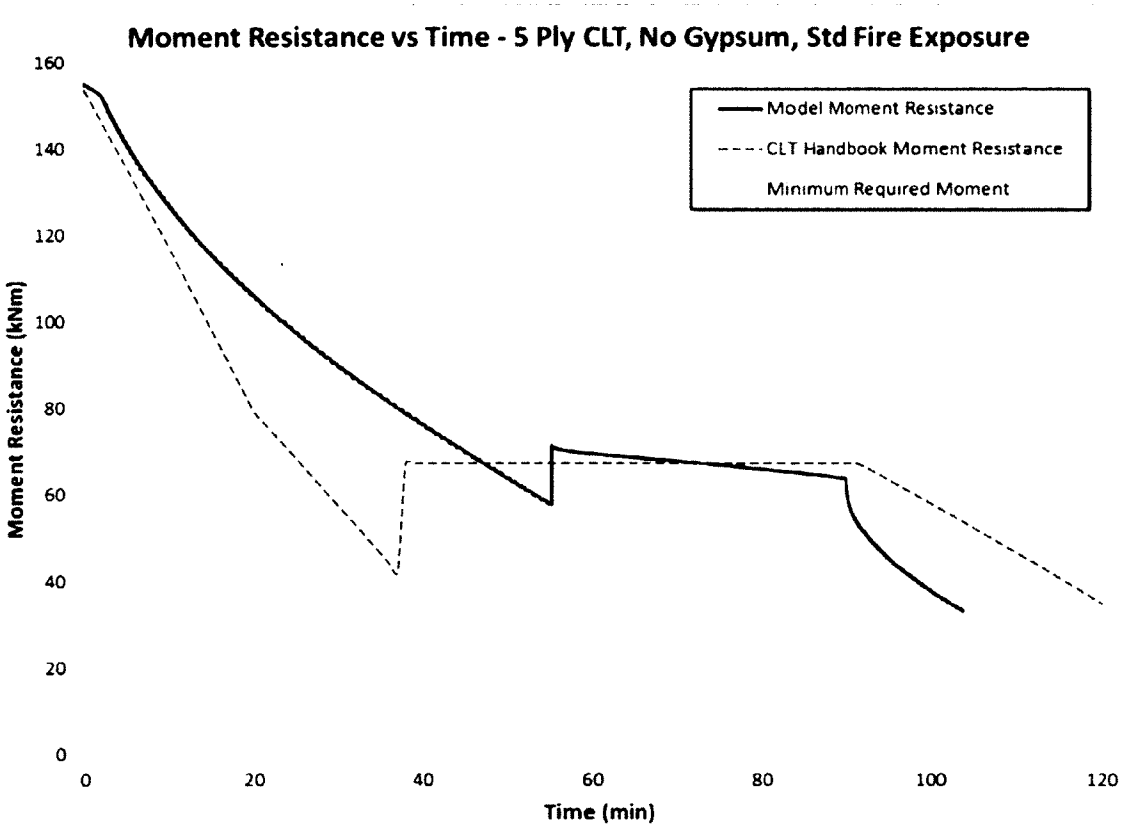

Figure 6-9: Comparison between model and CLT Handbook prediction for structural failure of a 5-ply panel without gypsum exposed to the standard fire

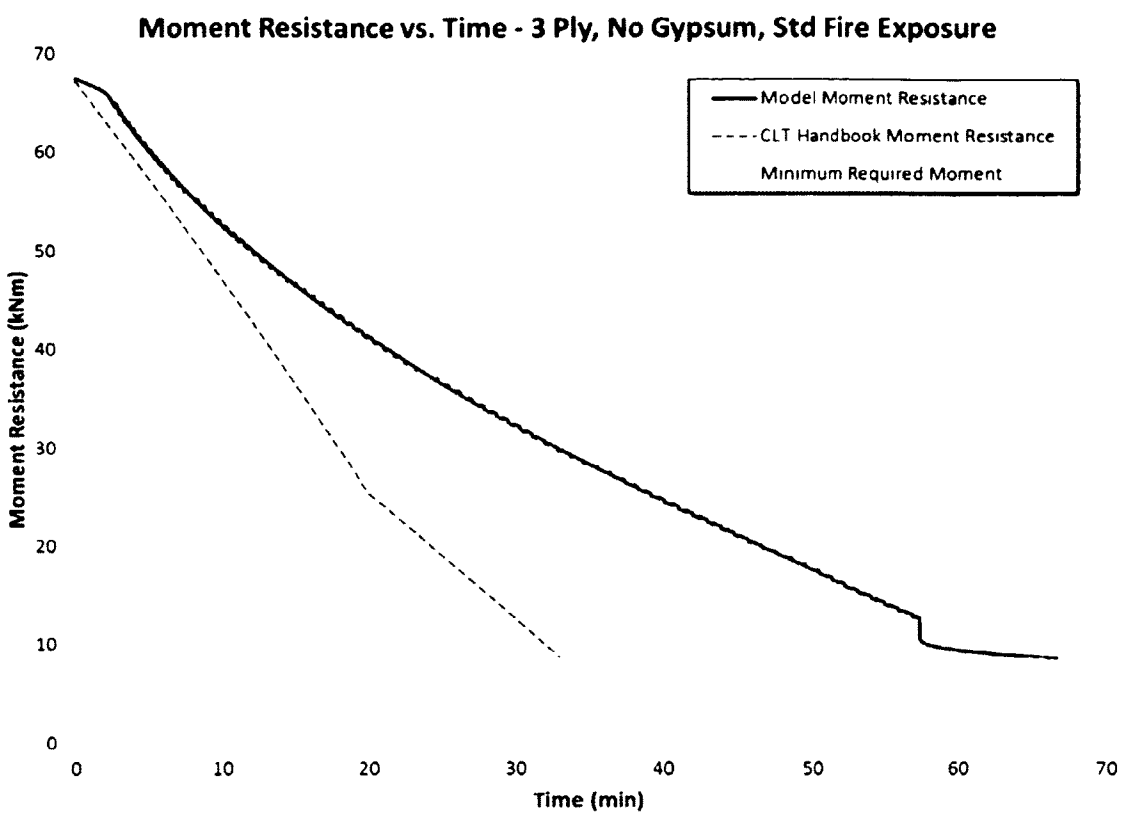

Figure 6-10. Comparison between model and CLT Handbook prediction for structural failure of a 3-ply panel without gypsum exposed to the standard fire

From these graphs it is clear that the results of the two methods are not consistent with each other, especially in the 3-ply panel. The handbook depicts a faster initial decrease in strength than the model due the constant charring rate (0.65 mm/min) used. This charring rate is higher than initial charring rates found in the model and real experiments, and causes the 3-ply panel to fail much quicker than the model prediction, at 33 minutes compared to 67 minutes.

It is important to note that the CLT Handbook method used to produce these graphs does not incorporate ply delamination in the calculation, but rather chars through plies completely with the inclusion of a 10.5 mm zero strength layer ahead of the char front. In the 5-ply panel, the first ply is considered to contribute zero strength before it is

predicted to fall-off in the model; however the char front and zero-strength layer take far longer to reach the second ply bond line than it takes for the second ply to delaminate in the model. While the charring rate used by the handbook is initially higher than charring rates produced by the model, later in the test when the fire temperature increases, the charring rate in the model increases to greater than the constant charring rate used in the handbook. This causes the 5-ply panel to fail after the predicted failure time from the model, unlike the 3-ply panel.

To include ply delamination into the CLT Handbook calculation, it is recommended to assume that a ply has fallen off once the remaining ply thickness between the char front and the adhesive is 12 mm. This distance corresponds to a temperature of 150°C at the bond line, based on the equation from Janssens and White cited in the Handbook [15]. In order to better compare with the model and experimental results, a thickness of 7 mm, which corresponds to a temperature of 210°C at the bond line, would be required instead of 12 mm for more accurate approximation of the real tests. Since the zero strength layer thickness is already larger than 7 mm, at 10.5 mm, the results of the Handbook calculation using a 7 mm delamination criterion would be identical to those presented in Figure 6-9 and Figure 6-10.

For floors with gypsum protection, the Handbook [15] recommends a simple addition of 30 minutes to the fire resistance rating be made for one layer of 15.9 mm type X gypsum board and 60 minutes for two layers of 12.7 mm type X gypsum. Alternatively, the calculation outlined in the Eurocode [14, p. 23] for gypsum protection can be used.

From this limited comparison, the method outlined in the CLT Handbook provides somewhat similar results as the model in a 5-ply unprotected panel. However, results are not in agreement for a 3-ply unprotected panel. It is assumed that this method would be most compatible with CLT floors with no less than 5 plies. However, modifications to the charring rate to more accurately simulate slower charring at the beginning of the test and increased charring later on, would likely improve the accuracy of using this method for both 3 and 5-ply panels. Although as it stands, the numerical model developed in this thesis provides a more robust method of predicting the response of different types of CLT configurations and adhesives.

7 Conclusions and Recommendations

7.1 Summary

The main objectives of this research were to:

1. Provide a better understanding of the fire performance and characteristics of CLT floors when exposed to both standard and non-standard fires.
2. Compare the performance of CLT panels when tested in medium-scale and full-scale fire resistance tests using standard fire exposures.
3. Develop a numerical model to predict the fire resistance of CLT floors.

The summarised results of the medium- and full-scale floor tests are listed in Table 7-1.

Table 7-1 Results from CLT Fire Resistance Tests

# of Plies	Type X Gypsum	Fire	Medium-Scale	Full-Scale
3	-	CAN/ULC	46 min	-
3	1x 5/8"	CAN/ULC	74 min	86 min
3	2x 1/2"	CAN/ULC	92 min	77 min*
3	2x 1/2"	Non-Std	93 min	-
5	-	CAN/ULC	99 min	96 min
5	-	Non-Std	101 min	-
5	1x 5/8"	CAN/ULC	115 min	124 min
5	1x 5/8"	Non-Std	122 min	-

** Test was stopped prematurely due to safety concerns after base gypsum layer failed*
Tests did not finish; indicates time that charring into the panel had nearly stopped

All medium-scale tests were stopped when deflection began to increase rapidly, indicating that structural failure was imminent. All full-scale tests were ended when flames penetrated at the edges or center lap-joint in the floors. Flame penetration in medium-scale tests was not used as the primary criteria for failure, due to the narrow width of the floor and inability to apply protection around the edges of the panel as

thoroughly as in full-scale tests. This caused charring at the edges to occur in medium-scale tests, creating a small opening and allowing flames to pass out of the furnace before any rapid increases in deflection began. Flaming was covered with insulation as it occurred and tests were continued, since terminating tests when flaming was observed would result in significantly less data. According to CAN/ULC S101 [5], "The area exposed to fire shall be not less than 16.8 m^2, with neither dimension less than 3660 mm", therefore all medium-scale test results are not officially recognised fire-resistance times. However, the overall comparison of equivalent medium- and full-scale test assembly results revealed several very similar trends and the fire resistance times of medium-scale tests were in fact closely representative of the full-scale fire resistance times.

However, not all of the trends which appeared in medium-scale tests were completely similar to those observed in full-scale tests. Higher charring rates and slightly shorter gypsum failure times were observed in all medium-scale tests. Despite the fact that temperatures in both furnaces followed the same standard curve, higher charring rates may have been caused by a lower moisture content in the medium-scale floors than in the full-scale floors, although this would not fully account for the difference observed. Discrepancies in gypsum board performance may have been caused by a number of different factors, although it is assumed that heat penetrating the sides of the panels in the medium-scale furnace caused earlier gypsum board failure and was also assumed to be the largest contributing factor for the higher charring rates. The early gypsum failure times are reflected accordingly in the fire resistance times of medium-scale tests.

Ply delamination times and temperatures compare favourably in all tests. Adhesive failure was observed to begin at around 200°C for all medium- and full-scale tests.

Identical floor assemblies were subjected to non-standard and standard fire exposures and results were compared. The non-standard fire showed a somewhat similar overall severity to the standard fire over exposure times of about 100 minutes. This statement is based on the similarity of the fire resistance times attained by equivalent assemblies exposed to both fires, which were around 100 minutes each. This was true despite the non-standard fire involving a faster initial growth phase and very high peak temperature, reaching 1100°C much earlier in the test than the standard fire. During the initial phase of the non-standard fire, gypsum protection did not perform as well, failing sooner, at lower temperatures and displaying lower finish ratings than equivalent boards exposed to the standard fire. Charring rates were also higher and ply delamination occurred sooner. However, once the decay phase of the non-standard fire began, all these trends reversed. Any remaining gypsum, such as the base board in the double layer test, remained in place much longer than its equivalent board exposed to the standard fire. Charring rates dropped significantly and ply delamination took much longer to occur in comparison, although the adhesive failure temperature did not change from 200°C in any of the experiments.

7.2 Numerical Model

A numerical model was developed based on information in the literature along with results from this test series with the intent of predicting the fire resistance of various CLT constructions. The model performed very well when compared to specific trends observed in tests using the standard fire, such as charring and ply delamination. Gypsum failure was more in line with that which was observed in full-scale tests than in medium-scale tests. The fire resistance predicted by the model signifies the time at which structural failure from the load occurs, unlike the results of the experimental tests, which were terminated before structural failure. This was reflected in the results, and fire resistance times predicted by the model were slightly longer than the times determined in real tests. However, based on the similarity of charring and ply fall-off found between the model and experiments exposed to the standard fire, these times are likely close predictions of when structural failure would occur in these floors.

The model did not perform as well in non-standard fires. This model is based entirely on empirical temperature-dependent relationships derived from standard fire tests; it does not accurately encompass the effects of decreasing fire temperatures on material properties. The current model uses material properties calculated based on the highest past temperature attained at each point in the assembly. In reality, residual heat from flaming and smouldering in the panel itself may cause wood properties to continue to degrade even as fire temperatures drop during the decay phase of the non-standard fire. An update to the model to include heat generation due to combustion of the panel itself would be a valuable contribution to its application in engineering practices.

Main Conclusions

The following conclusions can be drawn from this test series on CLT floor assemblies exposed to fire:

- Gypsum boards fastened to CLT floor panels behave very much the same as they do when fastened to other varieties of floor assemblies.
- Adhesive failure is the underlying factor in ply delamination. In all tests in this series, ply delamination begins to occur at temperatures around 200°C and occurs before the char front reaches the ply interface.
- Experiments without gypsum protection, exhibit an initial charring rate of 0.57 mm/min through the first ply of a standard fire exposure, which is lower than the Eurocode [14] prescribed charring rate for solid timber of 0.65 mm/min. This is likely due to the higher density wood used in these experiments. The Eurocode density adjustment factor applied for the density of wood used in this test series yields a charring rate of 0.58 mm/min.
- When gypsum protection is present, panels exposed to the standard fire exhibit approximately double the initial charring rates observed in unprotected panels once all gypsum layers have fallen off. This occurs for, roughly, the next 17 mm of char penetration, although this measurement is subject to high degree of variance since thermocouple spacing is in the order of 9 – 17 mm, depending on the test. Charring rates immediately after gypsum protection fails in panels exposed to the non-standard fire are also higher than the initial charring rates in similarly exposed unprotected panels, but by only a small amount.

- Due to ply delamination, for simple calculation purposes, a single effective charring rate would not provide a suitable substitute for the dynamically changing effective charring rate that is witnessed in CLT. As a result of this, the Eurocode [14] char method does not currently offer a reliably accurate approach to estimating the char depth in CLT.
- A spike in the charring rate is typical when a ply delaminates, as uncharred wood is exposed to the fire. Charring rates after a delamination in unprotected panels exposed to both the standard fire and non-standard fire would increase an average of about twice as high as previous charring rates. Panels with one layer of gypsum exposed to both the standard fire and non-standard fire would increase an average of about one and a half as high as previous charring rates after a delamination. Panels with two layer of gypsum protection did not produce enough delamination and char data to evaluate.
- The average heat-affected layer found in both 5-ply tests exposed to the standard fire, was 40 and 41 mm. The average heat-affected layer in 3-ply tests was slightly larger, at 47 mm. In non-standard fire tests, the average heat-affected layer is larger than in comparable standard fire exposure tests and is more pronounced with each additional layer of gypsum present.
- Deflection in CLT does not follow a linear trend as char progresses through the panel, nor is the rate of deflection proportional to the corresponding charring rate. Deflection increases dramatically when one of the load carrying, spanning

plies, chars and loses strength; and only increases slightly as a perpendicular ply chars.

7.4 Recommendations for Future Research

As building codes change and the practice of CLT constructions becomes more widely accepted across Canada, a more accurate way to approach predicting char depth in CLT is required. From the current work, charring rates found in CLT panels are largely affected by the time at which plies fall-off during a test. The time until ply delamination is primarily driven by two factors; ply thickness and adhesive failure. Further research conducted on CLT floors examining how ply delamination is affected by the use of different adhesives and ply thicknesses would provide the necessary data to precisely quantifying how these factors relate to the charring rates observed in CLT panels. More research is required to accurately determine how much charring rates increase after a delamination, and for how long it remains high. In addition, how other factors such as the presence of gypsum boards influence this spike in charring. A more accurate char model combined with the current fire resistance calculation outlined in the CLT Handbook [57] would be of significant importance to designers and fire protection engineers in being able to simply calculate alternative solutions and performance-based designs for CLT constructions. This information would also be of great support in further refining and validating the numerical model developed in this thesis.

Currently, the numerical model cannot accurately predict the results of CLT exposed to real fires due to the unknown nature of material properties during the decay phase of

the fire. In order to incorporate a set of material properties intended for the decay phase of real fires, significantly more research in this area is required. This may involve work to develop hysteresis loops of the thermal and mechanical properties of wood through various temperature cycles. Knowledge of this nature properly integrated into the model would vastly improve its range of function, and allow many types and configurations of CLT assemblies to be analysed using a wide variety of design fires. As an extension of this, continued testing of CLT floors exposed to real fires would provide valuable information to help validate such future iterations of the model.

7.3 Final Remarks

A significant target for CLT constructions in Canadian applications is to possess a two hour fire resistance rating. This rating would give CLT constructions a much wider coverage of applications in building constructions. From this test series, it is apparent that a two hour rating is possible with a 5-ply, 35 mm per ply, floor panel with one layer of 15.9 mm type X gypsum protection, as demonstrated in the full-scale experiment. However, based on observations made during non-standard fire exposures, in real scenarios it would be wise to instead apply two layers of 12.7 mm Type X gypsum protection. In the 5-ply floor test with one layer of gypsum exposed to the non-standard fire, when the gypsum board fell, the fire was at its peak temperature of around 1100°C. At this temperature, the exposed CLT caught fire and began to contribute to fire in the furnace. In a real construction, this type of building would require a sprinkler system; however in the instance of sprinkler failure, this type of scenario is possible, given that the non-standard fire used was based on a typical bedroom fuel load. In the experiment

the temperature was controlled by cooling the furnace with water, however, if this was not done, the exposed and flaming CLT would have continued to burn for much longer. It is likely that the CLT would have continued to burn until the floor structurally failed, even after the hypothetical "fuel load" in the furnace had been spent. The potential of continued burning and structural failure poses the threat of allowing the fire to spread to adjacent units in a building constructed of CLT. This scenario could be avoided by the application of two layers of 12.7 mm Type X gypsum to the construction. As demonstrated by the 3-ply panel exposed to the non-standard fire with two layers of gypsum, by the time both layers had fallen, the fire temperature had dropped to around 600°C from 1100°C and took around 80 minutes to do so. The decay phase of the non-standard fire in these experiments was exaggerated greatly and a real bedroom fire would likely be smouldering at far lower temperatures than 600°C, 80 minutes after steady burning in the room had finished. In that scenario, chances that both layers of gypsum will fall-off and the exposed panels would ignite are very low. Thus, if the fuel load in the bedroom was large enough to cause both gypsum boards to fail, by the time this happens, the exposed CLT is in a much less vulnerable position to catch fire and cause continued damage. The application of two layers of gypsum can reduce the potential risk of fire spread to adjacent compartments and possibly even prevent any damage on the CLT at all if the second layer does not fail.

Ply delamination plays an important role in the fire resistance rating of CLT. Aside from adding gypsum protection, further techniques of improving the fire resistance of CLT panels include the use of adhesives that fail at higher temperatures or do not fail at all

and simply char as solid timber, called thermosets. As well, increasing the thickness and number of plies in a panel will increase the fire resistance and reduce the frequency of a potential ply delamination. However, the use of thermoset adhesives, rather than thermoplastic adhesives, would have the effect of extending the fire resistance times of CLT by not allowing plies to delaminate [19]. This provides a twofold benefit in fire scenarios; it maintains the protective char layer that has accumulated, which insulates and slows the rate of heating and charring into the assembly, and prevents uncharred wood from becoming exposed and reigniting after a ply layer delaminates, which has been found to extend the duration of room fire [50].

With the use of the numerical model, these features can be adjusted and quickly assessed to determine the most effective way to achieve a specific desired fire resistance rating required by the building code.

8 References

[1] KLH UK, "Stadthaus, Murray Grove," Spoken Image, [Online]. Available: http://www.klhuk.com/portfolio/residential/stadthaus,-murray-grove.aspx. [Accessed 7 November 2012].

[2] Legislative Assembly of British Columbia, "Bill 9 - 2009 Wood First Act," Queen's Printer, Victoria, British Columbia, Canada, 2009. [Online]. Available: http://www.leg.bc.ca/39th1st/1st_read/gov09-1.htm. [Accessed 8 November 2012].

[3] NEWBuildS, "NEWBuildS Canada," Wood Science and Technology Centre / University of New Brunswick, 2012. [Online]. Available: http://newbuildscanada.ca/. [Accessed 9 November 2012].

[4] G. Hadjisophocleous and N. Bénichou, "Development of Performance-Based Codes, Performance Criteria and Fire Safety Engineering Methods," *International Journal on Engineering Performance-Based Fire Codes,* vol. 2, no. 4, pp. 127-142, 2000.

[5] Underwriters' Laboratories of Canada, "Standard Methods of Fire Endurance Tests of Building Construction and Materials," in *National Standard of Canada - CAN/ULC-S101-07*, vol. Fourth Edition, Ottawa, Underwriters' Laboratories of Canada, 2007.

[6] ASTM, "ASTM E119-05a Standard Test Methods for Fire Tests of Building Construction and Materials," in *Annual Book of ASTM Standards, Vol. 04.07,*

Philidelphia, ASTM, 2005, pp. 331-351.

[7] International Organization for Standardization, Fire-Resistance Tests - Elements of Building Construction, Geneve: International Organization for Standardization, 1999.

[8] A. H. Buchanan, Structural Design for Fire Safety, John Wiley & Sons Ltd, 2002.

[9] National Research Council Canada, "Floor Test Furnace," 9 December 2004. [Online]. Available: http://archive.nrc-cnrc.gc.ca/eng/facilities/irc/furnace.html. [Accessed 28 September 2012].

[10] K. A. Collette, "Comparison of Structural Designs in Fire," Worcester Polytechnical Institute, Worcester, 2007.

[11] D. Drysdale, An Introduction to Fire Dynamics - Second Edition, John Wiley & Sons, 2009.

[12] C. Bailey, "Parametric Fire Curves - Wickström's Model," University of Manchester, 2004. [Online]. Available: http://www.mace.manchester.ac.uk/project/research/structures/strucfire/Design/performance/fireModelling/parametricFireCurves/wickModel.htm. [Accessed 28 September 2012].

[13] C. Bailey, "Parametric Fire Curves - BSEN1991-1-2," University of Manchester, 2004.

[Online]. Available: http://www.mace.manchester.ac.uk/project/research/structures/strucfire/Design/performance/fireModelling/parametricFireCurves/bsen.htm. [Accessed 28 September 2012].

[14] Eurocode 5, "Part 1-2: General - Structural Fire Design," in *Eurocode 5 - Design of Timber Structures*, 2004.

[15] FPInnovations, "Fire Performance of Cross-Laminated Timber Assemblies," in *CLT Handbook*, Vancouver, FPInnovations, 2011.

[16] J. Schmid, K. J and K. J, "Fire-Exposed Cross-Laminated Timber - Modelling and Tests," *World Conference on Timber Engineering,* 2010.

[17] L. Osborne and C. Dagenais, "CLT Fire Resistance Testing Report," FP Innovations, Ottawa, 2012.

[18] CGC Inc., "CGC Fire Resistant SHEETROCK® FIRECODE® Type C & Type X," [Online]. Available: http://www.cgcinc.com/en/products/panels/interior-panels/fire-resistant/sheetrock%C2%AE-firecode%C2%AE-type-c--type-x.aspx?pType=DIY. [Accessed 4 October 2012].

[19] A. Frangi, M. Fontana, E. Hugi and R. Jobstl, "Experimental Analysis of Cross-Laminated Timber Panels in Fire," *Fire Safety Journal,* vol. 44, pp. 1078-1087, 2009.

[20] M. Fragiacomo, A. Menis and I. Clemente, "Finite Element Modelling of Cross-Laminated Timber Floors Exposed to Fire," in *Wood & Fire Safety*, Technická Univerzita, 2004, pp. 51-58.

[21] Dassault Systemes, "Abaqus Unified FEA," Dassault Systemes, 2012. [Online]. Available: http://www.3ds.com/products/simulia/portfolio/abaqus/overview/. [Accessed 30 November 2012].

[22] B. Kallsner and J. Konig, "Thermal and Mechanical Properties of Timber and Some other Materials used in Light Timber Frame Construction," in *CIB-W18*, Karlsruhe, Germany, 2000.

[23] University of Liege, "SAFIR," N-HiTec, 2007. [Online]. Available: http://www.argenco.ulg.ac.be/logiciels/SAFIR/index.html. [Accessed 20 November 2012].

[24] Canadian Standards Association, CAN/CSA-O86-01 Engineering Design in Wood, Mississauga: Canadian Standards Association, 2001.

[25] Forestry Products Laboratory, "Wood Handbook: Wood as an Enineering Material," Forestry Products Laboratory, Madison, WI, 2010.

[26] M. Tabaddor, "Thermal and Mechanical Finite Element Modeling of Wood-Floor Assemblies Subjected to Furnace Exposure," Underwriters Laboratories, Northbrook, 2008.

[27] N. Bénichou and M. A. Sultan, "Fire Resistance Performance of Lightweight Wood-Framed Assemblies," National Research Council Canada Institute for Research in Construction, Ottawa, 2000.

[28] H. Takeda and J. R. Mehaffey, "WALL2D: A Model for Predicting Heat Transfer through Wood-Stud Walls Exposed to Fire," *Fire and Materials,* vol. 22, pp. 133-140, 1998.

[29] T. T. Lie, "Structural Fire Protection," American Society of Civil Engineers, Manuals and Reports on Engineering Practice No.78, 1994.

[30] M. Janssens, "Modeling of the Thermal Degradation of Structural Wood Members Exposed to Fire," *Fire and Materials,* vol. 28, pp. 199-207, 2004.

[31] B. W. Gammon, Reliability Analysis of Wood-Frame Assemblies Exposed to Fire, Berkeley: University of California, Berkeley, 1987.

[32] R. Preusser, "Plastic and Elastic Behaviour of Wood Affected by Heat in Open Systems," *Holztechnologie,* vol. 9, no. 4, pp. 229-231, 1968.

[33] E. L. Schaffer, "Elevated Temperature Effect on the Longitudinal Mechanical Properties of Wood," University of Wisconsin, Madison, 1970.

[34] G. C. Thomas, "Fire Resistance of Light Timber Framed Walls and Floors," University of Canterbury, Canterbury, 1997.

[35] R. M. Knudson and A. P. Schniewind, "Performance of Structural Wood Members Exposed to Fire," *Forest Products Journal,* vol. 25, pp. 23-32, 1975.

[36] P. F. Cuerrier, "Development of a Two-Dimensional Fire Endurance Model for Gypsum-Board/Wood-Stud Walls," Forintek Canada Corporation, Ottawa, 1993.

[37] M. L. Janssens, "Thermo-Physical Properties for Wood Pyrolysis Models," *Pacific Timber Engineering Conference,* pp. 607-618, 1994.

[38] M. A. Sultan and A. Roy-Poirier, "Gypsum Board Fall-Off Temperature in Floor Assemblies Exposed to Standard Fires," Institute for Research in Construction National Research Council of Canada, Ottawa, 2007.

[39] I. Rahmanian and Y. Wang, "Thermal Conductivity of Gypsum at High Temperatures," Czech Technical University Publishing House, 2009.

[40] S. M. Cramer, O. M. Friday, R. H. White and G. Sriprutkiat, "Mechanical Properties of Gypsum Board at Elevated Temperatures," University of Wisconsin-Madison, Madison, 2003.

[41] S. H. Park, S. L. Manzello, D. P. Manzello and T. Mizukami, "Determining Thermal Properties of Gypsum Board at Elevated Temperatures," John Wiley & Sons Ltd, Gaithersburg, 2009.

[42] G. Thomas, "Thermal Properties of Gypsum Plasterboard at High Temperatures,"

Fire and Materials, no. 26, pp. 37-45, 2002.

[43] N. Bénichou, M. A. Sultan, C. MacCallum and J. Hum, "Thermal Properties of Wood, Gypsum and Insulation at Elevated Temperatures," Fire Risk Management Program, Institute for Research in Construction, National Research Council of Canada, Ottawa, 2001.

[44] Gypsum Association, "Fire Resistance Provided by Gypsum Board Membrane Protection (GA-610-02)," Gypsum Association, Hyattsville, 2002.

[45] Carlin Combustion Technology Inc., "Commercial Burners - Gas Fired," [Online]. Available: http://www.carlincombustion.com/products/201gburn.htm. [Accessed 1 October 2012].

[46] Nordic Engineered Wood, "X-Lam Cross-Laminated Timber," [Online]. Available: http://www.nordicewp.com/products/x-lam/. [Accessed 1 October 2012].

[47] Nordic Engineered Wood, "X-Lam Cross-Laminated Timber - Technical Note," 10 August 2012. [Online]. Available: http://www.nordicewp.com/literatures/T-S21_e-Properties.pdf. [Accessed 2 October 2012].

[48] Ontario Ministry of Municipal Affairs and Housing, Building Code Act, 1992 Ontario Regulation 350/06 Building Code, Ottawa: Service Ontario, 2012.

[49] Canadian Wood Council, Wood Design Manual, Mississauga: Canadian Standards

Association, 2005.

[50] C. McGregor, "Contribution of Cross-Laminated Timber Panels to Room Fires," Carleton University, Ottawa, 2012.

[51] M. A. Sultan, "Fire Resistance Furnace Temperature Measurements: Plate Thermometers vs Shielded Thermocouples," *Fire Technology,* vol. 42, pp. 253-267, 2006.

[52] U. Wickström, "The Plate Thermometer- A Simple Instrument for Reaching Harmonized Fire Resistance Tests," *Fire Technology,* no. 2nd Quarter, pp. 195-208, 1994.

[53] R. H. White and E. V. Nordheim, "Charring Rate of Wood for ASTM E 119 Exposure," *Fire Technology,* vol. 28, no. 1, pp. 5-30, 1992.

[54] Structurlam, "Cross Laminated Timber Design Guide," Structurlam, 2012. [Online]. Available: http://www.structurlam.com/product/images/CLT_Design_Guide_v4.pdf. [Accessed 22 October 2012].

[55] M. S. B. Frank Kreith, Principles of Heat Transfer 6th Edition, Brookes/Cole, 2001.

[56] S. L. Manzello, S.-H. Park, T. Mizukami and D. P. Bentz, "Measurement of Thermal Properties of Gypsum Board at Elevated Temperatures," in *Fifth International*

Conference on Structures in Fire, 2008.

[57] S. T. Craft, "Fire Performance of Cross-Laminated Timber Assemblies," in *CLT Handbook*, Ottawa, FPInnovations, 2010.

[58] Canadian Commission on Building and Fire Codes., National Building Code of Canada, 2005, Ottawa: Canadian Commission on Building and Fire Codes, 2005.

Appendix A Summary of Medium-Scale Results

# of Plys	3	3	3	5	5	5
Ply Thickness (mm)	35	35	35	35	35	
Type X Gypsum Protection	-	1x 5/8"	2x 1/2"	-	1x 5/8"	
Load Criteria	L/240	L/240	L/240	L/240	L/240	
Fire	CAN/ULC	CAN/ULC	CAN/ULC	CAN/ULC	CAN/ULC	
Load Applied from Jack	8.82kN	8.44kN	8.20kN	40.14kN	39.74kN	
Load Ratio	29%	29%	29%	48%	48%	
Test Ended	46min	74min	92min	99min	115min	
Face Gypsum Failure Time	-	-	51min	-	-	
Face Gypsum Failure Temp	-	-	275 C	-	-	
Face Gypsum Finish Rating	-	-	28min	-	-	
Base Gypsum Failure Time	-	47min	66min	-	37min	
Base Gypsum Failure Temp	-	363 C	275 C	-	300 C	
Base Gypsum Finish Rating	-	24min	55min	-	23min	
1st Ply Failure Time	64-65min	-	107-111min	58-70min	79-82min	
1st Ply Failure Temp	195-310 C	-	180-220 C	195-285 C	170-260 C	
2nd Ply Failure Time	-	-	-	87min +	115min +	
2nd Ply Failure Temp	-	-	-	205 C +	140 C +	
Center Deflection @ Stop Load	190mm	191mm	192mm	167mm	157mm	
Onset of Charring (min)	1.8min	40min	67min	1.5min	36min	
Overall Char Rate at 17.5mm	0.37	-	0.96	0.46	0.90	
Overall Char Rate at 35mm	0.57	-	0.81	0.57	0.74	
Overall Char Rate at 52.5mm	-	-	-	0.72	0.79	
Overall Char Rate at 70mm	-	-	-	0.76	0.77	
Overall Char Rate at 87.5mm	-	-	-	-	0.93	
Overall Char Rate	0.59	-	0.81	0.73	0.93	
Avg. Total Charring Rate	0.47	-	0.88	0.63	0.83	
Avg. Heated Zone (mm)	46	45	50	40	41	

Appendix B Summary of Full-Scale Results

# of Plies	3	3	5	5
Ply Thickness (mm)	35	38	35	35
Type X Gypsum Protection	1x 5/8"	2x 1/2"	Unprotected	1x 5/8"
Load Criteria	NBCC Office (> L/240)	L/240	L/240	NBCC (< L/240)
Fire	CAN/ULC	CAN/ULC	CAN/ULC	CAN/ULC
Load Applied	2.4 kPa	2.7 kPa	11.75 kPa	8.1 kPa
Load Ratio	62%	30%	47%	80%
Test Ended	*[a]86min	**77min	[a]96min	*[a]124min
Face Gypsum Failure Time	-	65min	-	-
Face Gypsum Failure Temp	-	690 C	-	-
Face Gypsum Finish Rating	-	15min	-	-
Base Gyp Failure Time	52min	>76min	-	26min
Base Gyp Failure Temp	700 C	510 C	-	~350 C
Base Gypsum Finish Rating	21min	46min	-	22min
1st Ply Failure Time	~80min	-	60-65min	75-81min
1st Ply Failure Temp	~200 C	-	195-220 C	190-210 C
2nd Ply Failure Time	-	-	92min +	107min +
2nd Ply Failure Temp	-	-	205 C +	200 C +
Center Deflect at Failure	195mm (74min) 403mm (86min)	**32mm	129mm	156mm
Onset of Charring (min)	25min	-	-	25min
Overall Char Rate at 17.5mm	0.43	0.59 (9.2mm)	0.52	0.55
Overall Char Rate at 35mm	0.42	-	0.55	0.42
Overall Char Rate at 52.5mm	0.62	-	0.64	0.53
Overall Char Rate at 70mm	-	-	-	0.59
Overall Char Rate at 87.5mm	-	-	-	-
Overall Char Rate	0.78	-	0.73	0.88
Avg. Total Charring Rate	0.56	-	0.61	0.59

[a] *Failed when flames were observed at one of the joints*

**Structurlam used SPF No.1/No.2 visually graded lumber instead of MSR lumber for spanning plies (E = 9500 MPa and f_b = 11.8 MPa)*

*** Test ended early due to safety concerns for laboratory equipment*

*** Nordic used SPF 1650F_b-1.5E MSR lumber instead of SPF 1950Fb MSR lumber for spanning plies (E = 10300 MPa and f_b = 23.9 MPa)*

Appendix C Summary of Numerical Model Results

# of Plys	3	3	3	5	5
Ply Thickness (mm)	35	35	35	35	35
Type X Gypsum Protection	-	1x 5/8"	2x 1/2"	-	1x 5/8"
Load Criteria	L/240	L/240	L/240	L/240	L/240
Fire	CAN/ULC	CAN/ULC	CAN/ULC	CAN/ULC	CAN/ULC
Load Applied from Jack	8.82kN	8.44kN	8.20kN	40.14kN	39.74kN
Load Ratio	29%	29%	29%	48%	48%
Test Ended	67min	96min	116min	104min	130min
Face Gypsum Failure Time	-	-	60min	-	-
Face Gypsum Failure Temp	-	-	550 C	-	-
Face Gypsum Finish Rating	-	-	17min	-	-
Base Gyp Failure Time	-	55min	76min	-	54min
Base Gyp Failure Temp	-	526 C	520 C	-	526 C
Base Gypsum Finish Rating	-	23min	47min	-	22min
1st Ply Failure Time	57min	86min	107min	55min	85min
1st Ply Failure Temp	210 C	210 C	210 C	210 C	210 C
2nd Ply Failure Time	-	-	-	90min	117min
2nd Ply Failure Temp	-	-	-	210 C	210 C
Center Deflect at Failure	87-429mm	92-429mm	93-428mm	133mm	133mm
Onset of Charring (min)	2.7min	31min	62min	2.5min	31min
Overall Char Rate at 17.5mm	0.66	0.59	0.84	0.69	0.60
Overall Char Rate at 35mm	0.54	0.54	0.66	0.56	0.55
Overall Char Rate at 52.5mm	0.80	0.81	0.96	0.82	0.82
Overall Char Rate at 70mm	-	-	-	0.75	0.76
Overall Char Rate at 87.5mm	-	-	-	0.87	0.88
Overall Char Rate	0.80	0.81	0.96	0.87	0.88
Avg. Total Charring Rate	0.67	0.65	0.82	0.74	0.72
Avg. Heated Zone (mm)	33	36	47	40	40

** Time when charring into the panel stopped; structural failure did not occur*

*** Time of highest temperature at the back of board; gypsum failure criteria was not met, however failure is likely*